

Composites of Indigenous Nanostructured Layered Materials

A Dissertation Submitted in Partial Fulfilment of the Requirement for the Degree of Doctor of Philosophy (Ph.D.) in Applied Chemistry and Chemical Engineering at University of Dhaka, Dhaka-1000, Bangladesh



SUBMITTED BY

Exam Roll: 120

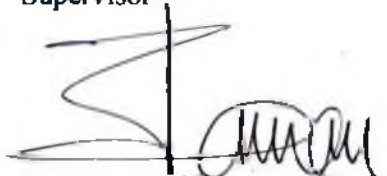
Registration No: 120/2012-2013

Session: 2012-2013

DECLARATION CERTIFICATE

It is herewith certified that **Exam Roll: 120, Registration No: 120/2012-2013, Session: 2012-2013**, Department of Applied Chemistry and Chemical Engineering, University of Dhaka, has carried out thesis work, Title: **“Composites of Indigenous Nanostructured Layered Materials”** in the Department of Applied Chemistry and Chemical Engineering, University of Dhaka, Dhaka-1000, Bangladesh. The candidate has successfully carried out her thesis research work under my supervision and is ready to present her dissertation, which is required in partial fulfillment of her **Doctor of Philosophy (PhD)** degree. This is an original study of the author and no part of the thesis has been submitted to any other institution for any degree.

Supervisor



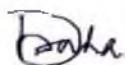
Dr. Md. Ashaduzzaman, Professor
Department of Applied Chemistry and Chemical Engineering
Faculty of Engineering and Technology
University of Dhaka, Dhaka-1000, Bangladesh

ACKNOWLEDGEMENTS

First and foremost, I am grateful to the Almighty for the good health and well-being that were necessary to complete this PhD research work. At this moment of accomplishment, I am greatly indebted to the people who mean a lot to me, my parents, for showing faith in me and giving me liberty to choose what I desired. I salute you all for the selfless love, care, pain and sacrifice you did to shape my life. I would first like to thank my PhD supervisor **Professor Dr. Md. Ashaduzzaman**, Department of Applied Chemistry and Chemical Engineering, University of Dhaka. The door of his office was always open whenever I ran into a trouble spot or had a question about my research or writing. He consistently steered me in the right the direction whenever he thought I needed it.

I express my profound regard to **Professor Dr. Ajoy Kumar Das** and **Professor Dr. A.M. Sarwaruddin Chowdhury**, co-supervisor of my research work, Department of Applied Chemistry and Chemical Engineering, University of Dhaka. I am particularly thankful to **Dr. Mithun Sarker** Assistant Professor and **Mr. Shaikat Chandra Dey**, Lecturer, Department of Applied Chemistry and Chemical Engineering, University of Dhaka, for their continuous motivation and support during this research. I am also thankful to **Mr. Md. Wahedur Rahman**, **Mr. Mithun Kumar Majumdar** and **Mrs. Afroza Alam** for their assistance in fabricating and characterizing the composites. I am also very grateful to Bangladesh Council for Scientific and Industrial Research (BCSIR) and Centre for Advanced Research in Sciences (CARS), University of Dhaka for partial analytical support. Getting through my dissertation required more than academic support, and I have many, many people to thank for listening to and, at times, having to tolerate me over the past few years.

Finally I would like to express my gratitude and appreciation to all of my department colleagues, students, friends and relatives for their support and friendship. I would like to extend my sincere thanks to all of them.



Dipti Saha
November, 2019

ঢাকা বিশ্ববিদ্যালয়
এম.ফিল./পিএইচ.ডি. থিসিস জমা দেওয়ার দরখাস্ত

বয়সসীমা,
পরীক্ষা নিয়ন্ত্রক
ঢাকা বিশ্ববিদ্যালয়
ঢাকা-১০০০।



ম্যানেজার, জনতা ব্যাংক
ঢাকা বিশ্ববিদ্যালয় (টি.এস.সি.) শাখা, ঢাকা
এম.ফিল./পিএইচ.ডি. থিসিসের ফিস্ বাবদ
টাকার পরিমাণ (.....) টাকা
টাকা গ্রহণ করা যাইতে পারে।

সেকশন অফিসার
পরীক্ষা নিয়ন্ত্রক অফিস

মহোদয়,
নিবেদন এই যে, আমি ঢাকা বিশ্ববিদ্যালয়ের ২নং বিজ্ঞান ভবন ৩ ফ্লোরে বিভাগের/ইনস্টিটিউটের
অধীনে এম.ফিল./পিএইচ.ডি. থিসিসের কাজ সম্পন্ন করিয়াছি। এক্ষেত্রে আমি থিসিস জমা দিতে ইচ্ছুক। তদুপরে, থিসিস জমা
দেওয়ার অনুমতি দিয়া বাধিত করিবেন।

গবেষকের নাম (ক) বাংলায় দীপ্তি সাহা
(খ) ইংরেজীতে DIPTI SAHA
(স্মার্টফিক্টেট অনুযায়ী বড় অক্ষরে)
স্থায়ী ঠিকানা ২২০ পাড়া, পো: পূর্বাত্তা নগর, ফুলশ্রী, নাগাবন্দর
এম.ফিল./পিএইচ.ডি. রেজিস্ট্রেশন নং ২২০ সেশন ২০২২-২৬ যোগদানের তারিখ ২০-৫-২৬
পুনঃরেজিস্ট্রেশন নং ২২০ সেশন ২০২২-২৬ যোগদানের তারিখ
গবেষণার শিরোনাম Composites of Indigenous Nano-structured Layered Materials
গবেষণার শিরোনাম বাংলায় হইলে উহার ইংরেজী :-

সুপারভাইজারের নাম ড. মো. আশাদুজ্জামান
অধ্যক্ষ-সুপারভাইজারের নাম (১) ড. মো. আশাদুজ্জামান
(যদি থাকে) (২) ড. মো. আশাদুজ্জামান

সুপারভাইজারের স্বাক্ষরিত হওয়া।
Dr. Md. Ashaduzzaman
Professor
Dept. of Applied Chemistry
and Chemical Engineering
University of Dhaka
Dhaka-1000, Bangladesh

তারিখ ২৪.৮.১৭
গবেষকের পূর্ণ নাম ও তারিখ ডীপ্তি সাহা
বর্তমান ঠিকানা ২নং বিজ্ঞান ভবন ৩ ফ্লোরে
২২০ পাড়া, পো: পূর্বাত্তা নগর, ফুলশ্রী, নাগাবন্দর

২০/৮/১৭
সুপারভাইজারের (দেব) সুপারিশসহ স্বাক্ষর
তারিখ ও সীলমোহর।
ফোন/মোবো: ০১৭৩১৩৬৮৮৬৭

মিস্ত্রী/সহকারী
২৭.০৮.১৭
মিস্ত্রী/সহকারী
২৭.০৮.১৭

তারিখ ২৪.৮.১৭
চেয়ারম্যান/পায়তোলাফের স্বাক্ষর
তারিখ ও সীলমোহর।
Dipti Saha
Professor & Chairman
Dept. of Applied Chemistry & Chemical Engineering
Faculty of Engineering & Technology
University of Dhaka, Dhaka-1000, Bangladesh

- ১। ৩ (চার) কপি থিসিস জমা দিতে হইবে।
- ২। (ক) থিসিসের শিরোনাম, সুপারভাইজারের (দেব) নাম ও থিসিস জমা দেওয়ার সময়-সীমা সম্বলিত রেজিস্ট্রারের অফিসের
ইস্রাকৃত কাগজপত্রের ফটোকপি দরখাস্তের সহিত জমা দিতে হইবে।
(খ) স্নাতকোত্তর (বা সমমান) পরীক্ষার "ইংলিশ অ্যান্ড" স্মার্টফিক্টেটের ফটোকপি জমা দিতে হইবে।
- ৩। থিসিস জমা দেওয়ার সময় উহার (থিসিসের) ২(দুই) কপি 'এ্যাবস্ট্রাক্ট' জমা দিতে হইবে। এ্যাবস্ট্রাক্টে থিসিসের
শিরোনাম, গবেষকের নাম ও বিভাগের/ইনস্টিটিউটের নাম উল্লেখ থাকিতে হইবে।
- ৪। পিএইচ.ডি. গবেষকদের ক্ষেত্রে তত্ত্বাবধায়ক ও বিভাগীয় একাডেমিক কমিটির সুপারিশসহ কমপক্ষে ২(দুই)টি বৈমনিয়র
রিপোর্ট জমা দিতে হইবে।
- ৫। থিসিসের সাথে উহার Soft Copy (CD) জমা দিতে হবে।
- ৬। উল্লিখিত কাগজপত্রসহ থিসিস পরীক্ষা নিয়ন্ত্রকের অফিসে দাখিল করার পর ব্যাংকে ফিস্ জমা দেওয়ার অনুমতি প্রদান
করা হইবে।

Abstract

Naturally occurring nanostructured layered materials are receiving increased attention from researchers in academia and industries owing to their unique characteristic features including naturally controlled nano-scale particle size, higher surface area, cheap, availability, biocompatibility etc. Surface modification of the nanomaterials with various natural and synthetic materials largely extends their applicability in various fields such as packaging, coating, water purification, antimicrobial agents, cancer nanotherapy etc. However, the potential of nanostructured kaolinite having layered aluminosilicate structure for diversified applications has largely been unexplored in Bangladesh although it is widely available in the country. In this doctoral research, we have thoroughly investigated the effect of the modification of kaolinite in terms of various physio-chemical properties. Here, we have prepared four different types of composites using different proportions of kaolinite with starch, choline chloride, poly(methylmethacrylate), and inorganic salt solutions separately. Firstly, we have successfully fabricated nanocomposite films through incorporating kaolinite into potato starch. Secondly, self-standing porous composite beads were prepared by modification of kaolinite with choline chloride. Thirdly, choline chloride-modified kaolinite was incorporated as fillers for preparing nanocomposite films using poly(methylmethacrylate) (PMMA) as a matrix. Finally, metal oxides [c.f. zinc oxide (ZnO), ferric oxide (Fe_2O_3)] were anchored onto kaolinite surface via heat treatment. In order to confirm the successful modification of kaolinite, we employed several analytical techniques such as attenuated total reflectance infra-red analysis (ATR-IR), x-ray diffraction (XRD), scanning electron microscopy (SEM), and energy-dispersive x-ray spectroscopy (EDX). Various useful mechanical properties of the films were investigated with a universal testing machine (UTM), whereas, thermogravimetric analysis (TGA) was performed to investigate the improvement in thermal stability.

We carefully observed that the incorporation of both virgin and modified kaolinite into natural and synthetic polymer dramatically improved thermal and mechanical properties of the films. These films are expected to find widespread applications in packaging industries. Modification of kaolinite with choline chloride led to the development of a novel self-standing porous composite bead, which displayed unique filtration ability for anionic azo dyes (Remazol Red) at alkaline pH. The dye filtration performance was continuously monitored using a UV-Vis spectrophotometer. We strongly believe that this advanced material might contribute significantly in treating effluents from textile industries. Lastly, metal oxide-loaded kaolinite showed significantly improved antibacterial action against selective bacteria (*Salmonella pullorum*, *Escherichia coli*, *Pseudomonas aeruginosa*) and cytotoxic effect against cancer cells (HeLa and BHK-21). Due to this promising performance, metal oxide-loaded kaolinite might find potential biomedical applications. In conclusion, we firmly state that this study would open new doors for the development of kaolinite-based technology for the advancement of materials science.

List of Figures

Sl. No.	Figure Name	Page No.
Figure 1.1	Synthesis approach with different application of polymer-clay composite.	2
Figure 1.2	Structure of clay materials	3
Figure 2.1	Extraction of starch from potato (a) potato chopped was blended, (b) settling, (c) washing, (d) screening and (e) dried starch powder.	12
Figure 2.2	Film solution of starch with glycerol (a) and gelatinized film of starch with glycerol (b).	12
Figure 2.3	Energy dispersive X-ray spectra, (b, c) SEM images of kaolinite at different magnifications obtained from Bijoypur, Bangladesh.	17
Figure 2.4	ATIR spectrum of (a) K ₀ SNC, (b) K ₅ SNC, (c) K ₁₀ SNC, (d) K ₁₅ SNC, (e) K ₂₀ SNC films and (f) Kaolinite recorded within the range of 500-4000 cm ⁻¹ .	18
Figure 2.5	XRD pattern of (a) K ₀ SNC, (b) K ₅ SNC, (c) K ₁₀ SNC, (d) K ₁₅ SNC, (e) K ₂₀ SNC and (f) Kaolinite recorded from powder of the sample after drying at 105°C for 12h.	19
Figure 2.6	Effect of kaolinite content on the tensile strength of the nanocomposite films produced from (a) K ₀ SNC, (b) K ₅ SNC, (c) K ₁₀ SNC, (d) K ₁₅ SNC and (e) K ₂₀ SNC films.	21
Figure 2.7	Effect of kaolinite content on the percentage elongation of the nanocomposite films produced from (a) K ₀ SNC, (b) K ₅ SNC, (c) K ₁₀ SNC, (d) K ₁₅ SNC and (e) K ₂₀ SNC films.	22
Figure 2.8	Effect of kaolinite content on the modulus of resilience, modulus of toughness of the nanocomposite films produced from (a) K ₀ SNC, (b) K ₅ SNC, (c) K ₁₀ SNC, (d) K ₁₅ SNC and (e) K ₂₀ SNC films.	23
Figure 2.9	Comparison of the effect of kaolinite content on the elastic and plastic reasons of the nanocomposite films produced from starch and 0, 5, 10, 15 & 20 % w/w of kaolinite.	23
Figure 2.10	Thermogravimetric graphs of (a) K ₀ SNC, (b) K ₅ SNC, (c) K ₁₀ SNC (d) K ₁₅ SNC, (e) K ₂₀ SNC and (f) a comparison chart of films.	26
Figure 2.11	TMA and DTMA curves for contraction analysis from thermal analysis of (a) K ₀ SNC, (b) K ₅ SNC, (c) K ₁₀ SNC (d) K ₁₅ SNC, (e) K ₂₀ SNC and (f) a comparison chart of films.	31
Figure 2.12	SEM images of the films produced from (a) K ₀ SNC, (b) K ₅ SNC, (c) K ₁₀ SNC (d) K ₁₅ SNC and (e) K ₂₀ SNC using kaolinite and starch.	33
Figure 3.1	Comparison of the physical features of the composite components and the composite bed. a) Free flowing kaolinite (K) in powder form supported in a syringe, b) a film of choline chloride (C), and c) self-standing composite bed of kaolinite and choline chloride (K-C bed).	45
Figure 3.2	a) FTIR spectra of kaolinite, choline chloride and the K-C composite bed. The green shaded box and the yellow shaded box in the spectra highlight the regions where the difference in peaks of the three materials are observed. b) Thermogravimetric curve for kaolinite and	46

	the K-C composite bed.	
Figure 3.3	Electron microscope (SEM) images of kaolinite (A), modified kaolinite (B), respectively.	48
Figure 3.4	a) SEM micrographs of the K-C composite bed at different magnification. The porous nature of the bed is evident from the images. b) XRD pattern of kaolinite and the K-C composite bed. The dashed lines in the patterns indicate the relative positions of the peaks for the (001) and (002) crystal planes in kaolinite and the K-C composite bed.	49
Figure 3.5	a) Photo of the setup for the aqueous Remazol Red treatment with the K-C composite bed. The thickness of the bed was 0.55 cm. b) UV/vis spectra of the treated solution at different time intervals. The time intervals represent the attainment of every 5 ml solution from the treatment with the K-C composite bed.	50
Figure 3.6	a) Surface of the K-C bed after Remazol Red from aqueous solution, and b) cross-sectional image of the bed after the dye removal. The images show all the removed dye is accumulated on the surface of the bed, rather than migrating in the bulk of the composite bed.	51
Figure 3.7	a) Setup of dye treatment with bare kaolinite powder supported on a syringe, b) solution of Remazol Red in a cuvette before treatment with kaolinite, and c) solution of Remazol Red in a cuvette after treatment with kaolinite.	51
Figure 3.8	a) Effect of concentration of RR to the time required for filtrate collection after the treatment with the K-C composite bed, b) effect of pH on the time required for filtrate collection after treatment of the RR solution with the K-C composite bed. The thickness of the bed was chosen to be 0.55 cm.	52
Figure 3.9	Degraded K-C composite bed upon treatment of Remazol Red solution at pH 7.	53
Figure 4.1	Schematic illustration for the fabrication of composite film from choline chloride modified kaolinite (CCMK) and PMMA.	63
Figure 4.2	Camera images of nanocomposite films before (A) and after drying (B).	64
Figure 4.3	A Attenuated total reflection infra-red (ATR-IR) spectra of films produced from nanocomposite of poly(methylmethacrylate) (PMMA) and choline chloride modified kaolinite (CCMK). (A) CK10PNC (B) CK5PNC, (C) CK3PNC, (D) CK1PNC and neat PMMA.	66
Figure 4.4	XRD patterns of CK ₀ PNC, CK10PNC. (A) Stress versus strain (%) curve. (B) The effect of modified kaolinite on the tensile strength (N/mm ²) of nanocomposite films. (C) The effect of CCMK on the elongation at break (%) of the PMMA/CCMK nanocomposite films (D).	67
Figure 4.5	Schematic illustrations of neat PMMA film and the composite films to show the impact on interface and crystallinity of modified kaolinite	69

Figure 4.6	Thermograms of neat PMMA film and nanocomposite films.	70
Figure 4.7	SEM images of virgin PMMA film (A) and the composites CK ₁ PNC (B), CK ₃ PNC (C), CK ₅ PNC (D), and CK ₁₀ PNC (E) films.	72
Figure 5.1	Schematic presentation of the synthetic route of metal oxide nanoparticles embedded kaolinite nanocomposites.	82
Figure 5.2	Shows the EDS spectral (EDAX) analysis of pure kaolinite and modified kaolinite with ZnSO ₄ and FeSO ₄ salts before (A, C, E) and after (B, D, F) calcination at 680°C respectively.	85
Figure 5.3	ATR-IR spectral analysis of pure kaolinite and modified kaolinite with ZnSO ₄ and FeSO ₄ salts before (A, C, E) and after (B, D, F) calcination at 680 °C respectively.	87
Figure 5.4	XRD pattern of pure kaolinite and modified kaolinite with ZnSO ₄ and FeSO ₄ salts before (A, C, E) and after (B, D, F) calcination at 680 °C respectively	88
Figure 5.5	Shows scanning electron microscope images of pure kaolinite and modified kaolinite with ZnSO ₄ and FeSO ₄ salts before and after calcination at 680°C.	90
Figure 5.6	Bar chart for the anti-microbial activity of pure kaolinite and modified kaolinite with ZnSO ₄ and FeSO ₄ salts before and after calcination at 680 °C against <i>E. coli</i> , <i>P. aeruginosa</i> , <i>S. pullorum</i> cells.	92
Figure 5.7	Schematic representation of the ROS generation, propagation and cell wall penetration of bacteria during interaction of pure kaolinite (A) and modified kaolinite (B).	94
Figure 5.8	Images recorded from an inverted light microscope after 24 hours of incubation for cytotoxicity test of cancer cell HeLa in presence of pure kaolinite, and modified kaolinite with ZnSO ₄ and FeSO ₄ salts before and after calcination at 680°C.	96
Figure 5.9	Magnified images produced from the images originated from an inverted light microscope after 24 hours of incubation for cytotoxicity test of cancer cells HeLa in presence of pure kaolinite, and modified kaolinite with ZnSO ₄ and FeSO ₄ salts before and after calcination at 680°C.	97
Figure 5.10	Images recorded from an inverted light microscope after 24 hours of incubation for cytotoxicity test of cancer cell BHK-21 in presence of pure kaolinite, and modified kaolinite with ZnSO ₄ and FeSO ₄ salts before and after calcination at 680°C.	99
Figure 5.11	Magnified images produced from the images originated from an inverted light microscope after 24 hours of incubation for cytotoxicity test of cancer cell BHK-21 in presence of pure kaolinite, and modified kaolinite with ZnSO ₄ and FeSO ₄ salts before and after calcination at 680°C.	100

List of Tables

Sl. No.	Table Name	Page No.
Table 2.1	Elemental analysis of kaolinite.	16
Table 2.2	Thermogravimetric analysis of different composites	24
Table 2.3	Summary of thermal mechanical analysis (TMA) and differential TMA	32
Table 3.1	Elemental composition of kaolinite-choline chloride composite bed determined through energy-dispersive X-ray spectroscopy (EDX).	47
Table 4.1	Compositional variation of nanocomposite films produced from poly (methylmethacrylate) (PMMA) and chloride modified kaolinite (CCMK).	62
Table 4.2	Thermogravimetric profile of pure PMMA and composite films recorded from thermographs.	71
Table 5.1	Elemental analysis of neat kaolinite and the modified kaolinite prepared at different conditions.	86
Table 5.2	Survival percentage of different microorganisms against the pure kaolinite and the modified kaolinite.	93
Table 5.3	Effect of concentration of kaolinite and modified kaolinite on percentage Hela Cell survival.	95
Table 5.4	Effect of concentration of kaolinite and modified kaolinite on percentage of BHK-21 Cell survival.	98

List of Abbreviations

Abbreviation	Meaning
K	Kaolinite
S	Starch
K-C	Kaolinite-Choline Chloride
CCMK	Choline Chloride Modified Kaolinite
A	Anatase
Q	Quartz
Z	ZnSO ₄
F	FeSO ₄
PMMA	Poly(methylmethacrylate)
RR	Remazol Red
DMSO	Dimethyl Sulfoxide
DMEM	Dulbecco's Modified Eagles' Medium
FBS	Fetal Bovine Serum
ROS	Reactive Oxygen Species
NC	Nanocomposite
PNC	Polymer Nanocomposite
TS	Tensile Strength
Eb	Elongation at Break
FTIR	Fourier Transform Infrared Spectroscopy
ATR-IR	Attenuated Total Reflection Infrared Spectroscopy
XRD	X-ray Diffraction
SEM	Scanning Electron Microscopy
FESEM	Field Emission Scanning Electron Microscopy
TGA	Thermogravimetric Analysis
TMA	Thermomechanical Analysis
EDX	Energy Dispersive X-ray Spectroscopy
UTM	Universal Testing Machine
UV-Vis	Ultraviolet Visible Spectroscopy

Table of Contents

SL. No.	Titles	Page No.
	Title Page	i
	Declaration Certificate	ii
	Acknowledgements	iii
	Abstract	iv
	List of Figures	v-vii
	List of Tables	viii
	List of Abbreviations	ix
	Table of Contents	x-xii
	Chapter One: Introduction	1-6
1.1	Introduction	2-4
1.2	Aim of this research	4
	References	5-6
	Chapter Two: Preparation and Properties Investigation of Potato-Starch Based Nanocomposite Films	7-38
	Abstract	8
1	Introduction	9-11
2	Experimental	11-14
2.1	Materials	11
2.2	Methods	11-33
2.2.1	Extraction of starch from potato	11-12
2.2.2	Film preparation	12
2.2.3	Composites film preparation	13
2.2.4	Characterization techniques	13-14
3	Results and discussion	14-33
3.1	Energy dispersive x-ray defraction spectroscopy (EDS)	16-17
3.2	Attenuated Total Reflection Infra-red (ATR-IR) Spectral Analysis	17-18
3.3	X-ray diffraction (XRD) analysis	19
3.4	Mechanical properties	20-23
3.4.1	Tensile strength of the nanocomposite films	20-21
3.4.2	Elongation of the nanocomposite films at break	21-23
3.5	Thermogravimetric Analysis (TGA)	23-29
3.6	Thermal Mechanical Analysis (TMA)	29-32
3.7	Studies of Surface morphology of films using SEM	32-33
	Conclusion	34

	References	35-38
Chapter Three: Fabrication of Kaolinite/Choline Chloride Self-Standing Porous Composite Bed for Filtration of Aqueous Dye Solution		
		39-56
	Abstract	40
1	Introduction	41-42
2	Experimental	42-43
2.1	Materials	42
2.2	Fabrication of self-standing bed structure	42-43
2.3	Characterization	43
3	Results and discussion	44-53
	Conclusion	54
	References	55-56
Chapter Four: Studies on Mechanical Properties of PMMA/Choline Chloride Modified Kaolinite Nanocomposite Films		
		57-76
	Abstract	58
1	Introduction	59-60
2	Experimental	61-65
2.1	Materials	61
2.2	Methods	61-65
2.2.1	Modification of Kaolinite by Choline Chloride	61
2.2.2	Fabrication of Poly(methylmethacrylate)/Choline Chloride Modified Kaolinite PMMA/CCMK Nanocomposite Films	61-64
2.2.3	Characterization	64-65
3	Results and discussion	65-72
3.1	ATR-IR Spectral Analysis	65-66
3.2	XRD Analysis	66-67
3.3	Studies of Mechanical Properties of Nanocomposite Films	67-69
3.3.1	Stress-Strain Relationship	68
3.3.2	Tensile Strength Measurement	68-69
3.3.3	Elongation at Break	69
3.4	Thermo Gravimetric Analysis (TGA)	70-71
3.5	Scanning Electron Microscope (SEM) Morphological Studies of Nanocomposites Films	71-72
	Conclusion	73
	References	74-76

	Chapter Five: Fabrication of Kaolinite/Metal Oxides Nanocomposites and Their Biological Applications	77-104
	Abstract	78
1	Introduction	79-81
2	Experimental	81
2.1	Materials	81
2.2	Methods	81-82
2.3	Characterization	82-83
2.4	Antimicrobial activity	83
2.5	Cytotoxic effect	83
3	Results and discussion	84-100
3.1	Preparation of kaolinite-metal oxides hybrid nanocomposites	84
3.2	Energy Dispersive X-Ray spectrophotometer (EDS)	84-86
3.3	Characterization of nanocomposites by spectral means	86-87
3.4	XRD analysis	87-88
3.5	Observation of Morphological by SEM	89-90
3.6	Antibacterial activity	91-93
3.7	Proposed mechanism for ROS generation	93-94
3.8	Cytotoxic effect against HeLa cells	95-97
3.9	Cytotoxic effect against BHK-21 cells	97-100
	Conclusion	101
	References	102-104
	Conclusion	105-107
	List of Publications from This Research	108
	Biography	109

Chapter: One

Introduction

Chapter One

1.1. Introduction

Composite materials can be defined as materials that consist of two or more chemically and physically different phases separated by a distinct interface.^{1,2} The two materials work together to give the composite unique properties. The individual components remain separate and distinct within the finished structure, differentiating composites from mixtures and solid solutions. When they are combined they create a material which is specialized to do a certain job, for instance to become stronger, lighter or resistant to electricity.³⁻⁵ The reason for their use is because they improve the properties of their base materials and are applicable in many situations.⁶ Composites also provide design flexibility because many of them can be moulded into complex shapes. By choosing an appropriate combination of matrix and reinforcement material, a new material can be made that exactly meets the requirements of a particular application.^{7, 8} Recently, researchers have been introducing actively different materials especially layered and Nano materials into composites.⁹

Nano composites are defined as a promising class of hybrid materials that is mixtures of organic polymers with inorganic solids (clays to oxides) at the nanometric scale.^{10, 11} Clay-polymer nanocomposites offer tremendous improvement in a wide range of physical and engineering properties for polymers with low filler loading.^{12, 13} This class of material uses smectite-type clays, such as hectorite, montmorillonite, and synthetic mica, as fillers to enhance the properties of polymers. Smectite-type clays have a layered structure. Each layer is constructed from tetrahedrally coordinated Si atoms fused into an edge-shared octahedral plane of either $\text{Al}(\text{OH})_3$ or $\text{Mg}(\text{OH})_2$.^{14, 15} According to the nature of the bonding between these atoms, the layers should exhibit excellent mechanical properties parallel to the layer direction. The layers have a high aspect ratio and each one is approximately 1 nm thick, while the diameter may vary from 30 nm

to several microns or larger. Hundreds or thousands of these layers are stacked together with weak van der Waals forces to form a clay particle.

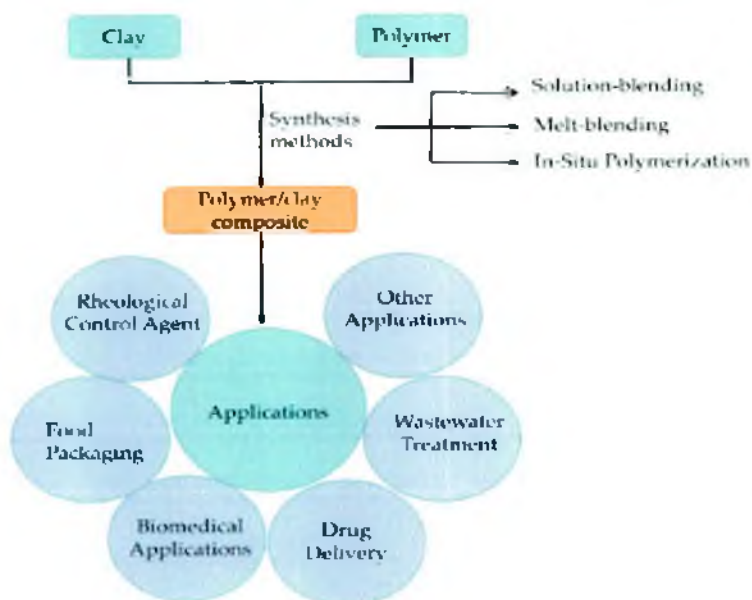


Figure 1.1: Synthesis approach with different application of polymer-clay composite.^{16, 17}

The essential nanoclay raw material is white clay, a doubled layered structure. White clay consists of 1 nm thick aluminosilicate layers surface- substituted with metal cations and stacked in 10 μm -sized multilayer stacks. Naturally occurring white clay is hydrophilic. In microcomposites, the polymer and clay remain immiscible (phase separation), resulting in agglomeration of the clay in the matrix and poor macroscopic properties of the material. Interaction between the layered silicates and polymer chains may produce two types of nanoscale composites. The intercalated nanocomposites result from the penetration of polymer into the interlayer region of the clay, resulting in an ordered multilayer structure with alternating polymer/inorganic layers at a repeated distance of a few nanometers.¹⁸ The exfoliated nanocomposites involve extensive polymer penetration, with the clay layers delaminated and randomly dispersed in the polymer matrix. It has been shown that for glycerol content above 10 % (w/w), the system leads to the formation of an intercalated structure with a clay interlayer spacing of 12 Å, corresponding mainly to glycerol intercalation.¹⁹ Consequently, these results have highlighted the great influence of plasticizers on the clay intercalation/ exfoliation process and hence on the properties of the resulting materials.

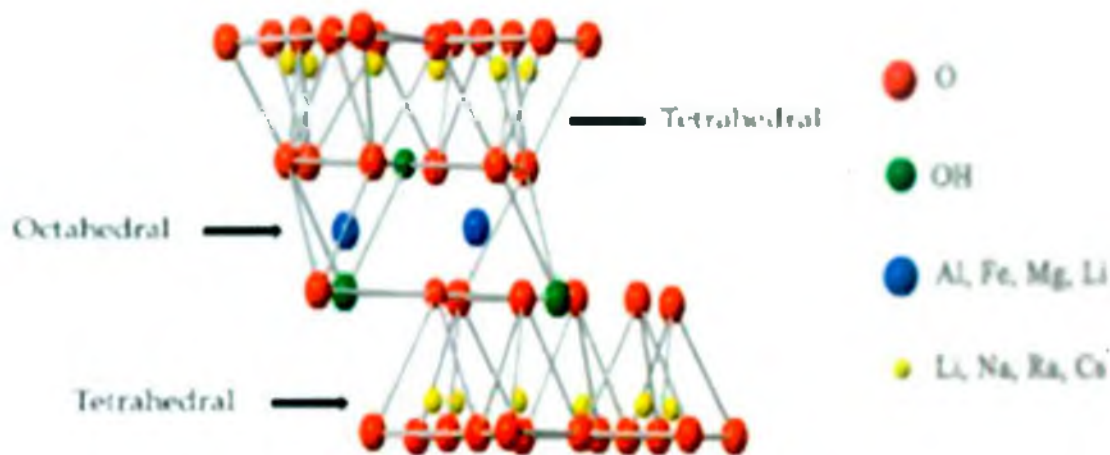


Figure 1.2: Structure of clay materials

To overcome the limitations induced by glycerol plasticizers, some authors have replaced these plasticizers with urea/formamide.²⁰ White clay dispersion into this glycerol plasticized starch matrices by a solvent or melt process leads to the formation of intercalated structures. The presence of nanoclay in polymer formulations increases the tortuosity of the diffusive path for a penetrating molecule, and changes the molecular mobility, which enhances the thermal and mechanical properties, confers stability to oxidation, and decreases the solvent absorption, amongst other advantages. It also allows the incorporation of multiple features such as color, aroma, or the ability to act as reservoirs for the controlled release of drugs or fungicides. The

incorporation of white clay in proportions below 20% also offers benefits such as low density, transparency, good flow, better surface properties and recyclability.²¹

Clays are classified into several types such as bentonite chlorite, hectorite, kaolinite, montmorillonite and pyrophyllite, based on their morphology and chemical composition.²² Among them Kaolinite is an important clay mineral, part of the group of industrial minerals with the chemical composition $\text{Al}_2\text{Si}_2\text{O}_5(\text{OH})_4$.²³ It is a layered silicate mineral, with one tetrahedral sheet of silica (SiO_4) linked through oxygen atoms to one octahedral sheet of alumina octahedra. Kaolinite has physical and chemical properties (favorable properties such as natural whiteness, fine particle size, non-abrasiveness, and chemical stability) which make it useful in a great number of applications.^{24, 25} One of the most important applications of kaolinite is coating and filling paper. Moreover, kaolinite filler improves the mechanical and electrical properties of polymer composites which is improve the performance of kaolinite-polymer composites.²⁶ Bijoypur clay, a type of locally available kaolinite clay, is used for the fabrication of biocomposite. The major phases present in Bijoypur clay are kaolinite, halloysite and quartz. Bijoypur clay has high content of SiO_2 (70.08 %), it also has significant amount of Al_2O_3 (27.24%) and relatively low amount of Fe_2O_3 (1.03%) and TiO_2 (1.65%).^{27, 28}

In this this research, we have attempted to fabricated different types of industrially valuable composites using kaolinite nanoclay.

1.2. Aim of this research

The major objectives of this study are:

- Preparation and properties investigation of potato-starch based nanocomposite films
- Fabrication of kaolinite/choline chloride self-standing porous composite bed for filtration of aqueous dye solution
- Studies on mechanical properties of PMMA/choline chloride modified kaolinite nanocomposite films
- Fabrication of kaolinite/metal oxides nanocomposites and their biological applications

References

1. Vasiliev, Valery V., and Evgeny V. Morozov. *Advanced Mechanics of Composite Materials and Structures*. Elsevier, 2018.
2. İsmal, Özlenen Erdem, and Roshan Paul. "Composite textiles in high-performance apparel." In *High-Performance Apparel*, pp. 377-420. Woodhead Publishing, 2018.
3. Narayana, K. Jagath, and Ramesh Gupta Burela. "A review of recent research on multifunctional composite materials and structures with their applications." *Materials Today: Proceedings* 5, no. 2 (2018): 5580-5590.
4. Sai, M. K. S. "Review of composite materials and applications." *International Journal of latest Trends in Engineering and Technology* 6, no. 3 (2016): 129-135.
5. Gay, Daniel. *Composite materials: design and applications*. CRC press, 2014.
6. Mallick, Pankar K. *Fiber-reinforced composites: materials, manufacturing, and design*. CRC press, 2007.
7. Mittal, Garima, Kyong Y. Rhee, Vesna Mišković-Stanković, and David Hui. "Reinforcements in multi-scale polymer composites: Processing, properties, and applications." *Composites Part B: Engineering* 138 (2018): 122-139.
8. Al-Oqla, Faris M., and S. M. Sapuan. "Natural fiber reinforced polymer composites in industrial applications: feasibility of date palm fibers for sustainable automotive industry." *Journal of Cleaner Production* 66 (2014): 347-354.
9. Gibson, Ronald F. "A review of recent research on mechanics of multifunctional composite materials and structures." *Composite structures* 92, no. 12 (2010): 2793-2810.
10. Wahid, Fazli, Taous Khan, Zohaib Hussain, and Hanif Ullah. "Nanocomposite scaffolds for tissue engineering; properties, preparation and applications." In *Applications of Nanocomposite Materials in Drug Delivery*, pp. 701-735. Woodhead Publishing, 2018.
11. Siró, István, and David Plackett. "Microfibrillated cellulose and new nanocomposite materials: a review." *Cellulose* 17, no. 3 (2010): 459-494.
12. Gao, Fengge. "Clay/polymer composites: the story." *Materials today* 7, no. 11 (2004): 50-55.
13. Sengupta, R., S. Chakraborty, S. A. Bandyopadhyay, S. Dasgupta, R. Mukhopadhyay, K. Auddy, and A. S. Deuri. "A short review on rubber/clay nanocomposites with emphasis on mechanical properties." *Polymer Engineering & Science* 47, no. 11 (2007): 1956-1974.
14. Ray, Suprakas Sinha, and Masami Okamoto. "Polymer/layered silicate nanocomposites: a review from preparation to processing." *Progress in polymer science* 28, no. 11 (2003): 1539-1641.
15. Haider, Safia, Ayesha Kausar, and Bakhtiar Muhammad. "Overview of various sorts of polymer nanocomposite reinforced with layered silicate." *Polymer-Plastics Technology and Engineering* 55, no. 7 (2016): 723-743.
16. Guo, Feng, Saman Aryana, Yinghui Han, and Yunpeng Jiao. "A review of the synthesis and applications of polymer–nanoclay composites." *Applied Sciences* 8, no. 9 (2018): 1696.

17. Kim, Deuk Ju, Min Jae Jo, and Sang Yong Nam. "A review of polymer–nanocomposite electrolyte membranes for fuel cell application." *Journal of Industrial and Engineering Chemistry* 21 (2015): 36-52.
18. Park, Hwan-Man, Xiucuo Li, Chang-Zhu Jin, Chan-Young Park, Won-Jei Cho, and Chang-Sik Ha. "Preparation and properties of biodegradable thermoplastic starch/clay hybrids." *Macromolecular Materials and Engineering* 287, no. 8 (2002): 553-558.
19. Slavutsky, Anibal Marcelo, Maria Alejandra Bertuzzi, and Margarita Armada. "Water barrier properties of starch-clay nanocomposite films." *Brazilian Journal of Food Technology* 15, no. 3 (2012): 208-218.
20. Pareta, R., and M. J. Edirisinghe. "A novel method for the preparation of starch films and coatings." *Carbohydrate polymers* 63, no. 3 (2006): 425-431.
21. Park J. S., Yang J. H., Kim D. H., Lee D. H.: Degradability of expanded starch/PVA blends prepared using calcium carbonate as the expanding inhibitor. *Journal of Applied Polymer Science*, 93, 911–919, 2004.
22. Bergaya, F. B. K. G., and G. Lagaly. "General introduction: clays, clay minerals, and clay science." In *Developments in Clay Science*, vol. 5, pp. 1-19. Elsevier, 2013.
23. Miranda-Trevino, Jorge C., and Cynthia A. Coles. "Kaolinite properties, structure and influence of metal retention on pH." *Applied Clay Science* 23, no. 1-4 (2003): 133-139.
24. Murray, Haydn H. "Industrial applications of kaolin." *Clays and Clay Minerals* 10, no. 1 (1961): 291-298.
25. Theng, B. K. G. "Some practical applications of the clay–polymer interaction." In *Developments in Clay Science*, vol. 4, pp. 153-199. Elsevier, 2012.
26. Tawfik, Magda, Nivin Ahmed, and Azza Ward. "Characterization of kaolin-filled polymer composites."
27. Mousharraf, Adnan, Md Sazzad Hossain, and Md Fakhru Islam. "Potential of locally available clay as raw material for traditional-ceramic manufacturing industries." *Journal of Chemical Engineering* 26 (2011): 34-37.
28. Zaker, Y.; Hossain, M.A.; Islam, T.S.A. Adsorption kinetics of methylene blue onto clay fractionated from Bijoypur soil. *Bangladesh Res. J. Chem. Sci.* 2013, 3, 65–72.

Chapter: Two

Preparation and Properties Investigation of Potato-starch Based Nanocomposite Films

Chapter Two

Abstract: Environmental friendly advanced materials are promising candidates for engineering of nanoscience and technology. Here, starch-kaolinite self-assembled nanocomposite films were prepared using potato starch and indigenous layered materials, kaolin. The film consists of kaolinite and the matrix which was prepared by disruption and plasticization of starch granules with water and glycerine. Nanocomposite self-assembled films with 0, 5, 10, 15, 20 % w/w of kaolinite were obtained by casting and evaporating the mixture from homogeneous aqueous suspension at 95°C. The thickness of the film about 200 µm was controlled by predesigned glass frame. The resulting films were conditioned before testing and the effect of accelerated ageing in moist atmosphere was investigated. The films were characterized using attenuated total reflection infra-red (ATR-IR) for interaction of moieties via function groups, X-ray diffraction (XRD) for crystallinity change, universal testing machine (UTM) for tensile strength Young's modulus and elongation at break investigation. Thermal stability of the films using thermogravimetric analysis (TGA) and effect of temperature on contraction behaviors using thermal mechanical analysis (TMA) were carried. Distribution of kaolin into the matrix and morphology of the self-assembled films were observed from SEM images. Developed nanocomposite materials from indigenous sources would play vial role in the field of foods and packaging industries in Bangladesh.

1. Introduction

There is a growing interest in developing bio-based products and innovative processing technologies which offer sustainability and mitigation of the dependence on fossil fuel. Because for centuries, scientific community has been searching for effective substitutes for the natural coatings of foods, in order to keep them fresh and isolated from physical, chemical and/or microbiological contaminants. For many years, the packaging industry has used materials produced from various petroleum-derived monomers to elaborate various types of plastic, which have very good functional properties but also produce serious pollution problems¹. The growing interest in the environmental impact of discarded plastics, a new series of materials of biological origin (plant, animal and microbial) have been developed, whose main advantages are that they are fully degradable and even edible in some cases. Among biopolymers, starch is one of the most promising renewable bioresources due to its versatility, competitiveness in price, and applicability to various industries.²⁻⁵ Through destructurezation by the introduction of mechanical and heat energy or by incorporation of a plasticizing agent (e.g., water, amide, and/or polyols), starch can be processed into thermoplastic materials. Currently, biodegradable plastics are primarily used in food packaging films, shopping bags, and flushable sanitary product backing material.⁶⁻⁸ The use of starch-based materials is greatly hindered by its intractable nature, brittleness, water-sensitivity, and poor mechanical strength.⁸⁻¹¹ It has been found that using reinforcing materials in a starch matrix is an effective method to obtain high-performance starch-based biocomposites.¹²

Nanocomposites are hybrid nanostructured materials. A widely studied type of nano-composite is a class of hybrid materials composed of organic polymer matrices and nanoclay fillers. The essential nanoclay raw material is white clay, a doubled layered structure. White clay consists of 1 nm thick aluminosilicate layers surface- substituted with metal cations and stacked in 10 μm -sized multilayer stacks. Naturally occurring white clay is hydrophilic. In microcomposites, the polymer and clay remain immiscible (phase separation), resulting in agglomeration of the clay in the matrix and poor macroscopic properties of the material. Interaction between the layered silicates and polymer chains may produce two types of nanoscale composites. The intercalated nanocomposites result from the penetration of polymer into the interlayer region of the clay, resulting in an ordered multilayer structure with alternating polymer/inorganic layers at a

repeated distance of a few nanometers¹³. The exfoliated nanocomposites involve extensive polymer penetration, with the clay layers delaminated and randomly dispersed in the polymer matrix. It has been shown that for glycerol content above 10 % (w/w), the system leads to the formation of an intercalated structure with a clay interlayer spacing of 12 Å, corresponding mainly to glycerol intercalation¹⁴. Consequently, these results have highlighted the great influence of plasticizers on the clay intercalation/ exfoliation process and hence on the properties of the resulting materials. To overcome the limitations induced by glycerol plasticizers, some authors have replaced these plasticizers with urea/formamide¹⁵. White clay dispersion into this glycerol plasticized starch matrices by a solvent or melt process leads to the formation of intercalated structures. The presence of nanoclay in polymer formulations increases the tortuosity of the diffusive path for a penetrating molecule, and changes the molecular mobility, which enhances the thermal and mechanical properties, confers stability to oxidation, and decreases the solvent absorption, amongst other advantages. It also allows the incorporation of multiple features such as color, aroma, or the ability to act as reservoirs for the controlled release of drugs or fungicides. The incorporation of white clay in proportions below 20% also offers benefits such as low density, transparency, good flow, better surface properties and recyclability¹⁶.

Biodegradable polymers such as starch have attracted considerable attention in the packaging industry. Starch is a promising raw material because of its annual availability from many plants, its rather excessive production with regard to current needs and its low cost. It is known to be completely degradable in soil and water and can promote the biodegradability of a non-biodegradable plastic when blended. Starch is commonly pretreated with a plasticizer to make it thermoplastic thus enabling melt-processing.

The present work sets out to prepare and characterize starch–clay nanocomposites with clays that can act as hosts at a range of volume fractions and to compare the results with similar clays that do not host starch¹⁷. However, thermoplastic starch (TPS) alone often cannot meet all the requirements of a packaging material and an environmentally acceptable filler is called for to improve the properties of TPS in such applications. Clay is a potential filler; itself a naturally abundant mineral that is toxin-free and can be used as one of the components for food, medical, cosmetic and healthcare recipients. TPS reinforced by clay has recently been investigated. To

the authors' knowledge, there are just four publications describing this new class of materials, i.e. TPS–clay nanocomposites¹⁸. Starch is hydrophilic and forms nanocomposites with natural clays and conventional composites with kaolinite. It has been shown that the tensile strength of TPS was increased from 2.5 to 3.9 MPa with the presence of 5 wt% white clay, while the elongation at break was increased from 0.01 to 0.26%. Also the relative water vapour diffusion coefficient of TPS was decreased to 65% and the temperature at which the composite lost 50% mass was increased from 305 to 336.8°C. Interesting preliminary results were also obtained for starch nanocrystals reinforced starch plasticized by glycerine. It was shown that the reinforcing effect of starch nanocrystals can be attributed to strong fillers/filler and filler/matrix interactions due to the establishment of hydrogen bonding. the presence of starch nanocrystal also led to slow down the recrystallization of the matrix during aging the humid atmosphere¹⁹.

2. Experimental

2.1. Materials

White clay was collected from Bijoypur and is known as kaolinite, having layered structured. It was used after acid (dilute HCl) treatment to remove foreign inorganic minerals. Potato was purchased from local market and was processed to extract starch from it (extraction technique has been discussed in later section). Glycerol (99.5%) was purchased from Sigma-Aldrich and was used as received. Prescribed design of glass frame was prepared from glass-ware shop and was used after wrapping with Teflon ribbon.

2.2. Methods

2.2.1. Extraction of starch from potato

Extraction of potato was performed according to the following procedure.

1. Grate about 100 g potatoes. The potatoes do not need to be peeled, but it should be clean.
2. Put the potato into the blending machine and add about 100 mL distilled water. Grind the potato carefully.
3. Pour the liquid off through the tea strainer into the beaker, leaving the potato behind in the mortar. Add 100 mL water, grind and strain twice more.
4. Leave the mixture to settle in the beaker for 10 minutes.

5. Decant water from the beaker, leaving behind the white starch which should have settled in the bottom. Add about 100 mL distilled water to the starch and stir gently leave to settle again and then filtered through a cloth, leaving the starch behind (Figure 2.1).

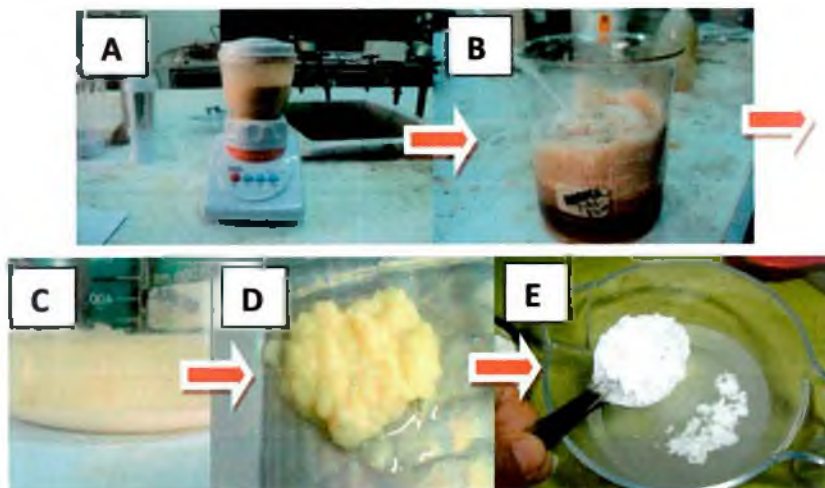


Figure 2.1: Extraction of starch from potato (a) potato chopped was blended, (b) settling, (c) washing, (d) screening and (e) dried starch powder.

2.2.2. Film Preparation

A quantity of 3 g of a mixture of starch and glycerol (2:1) was first dispersed in 35 mL of distilled water (Figure 2.2a). Then the mixture was heated at 95°C for 15 minutes under mechanical stirring. Gelatinized starch was cast and stored in a non-ventilated oven at 40 °C for 24 h (Figure 2.2b).

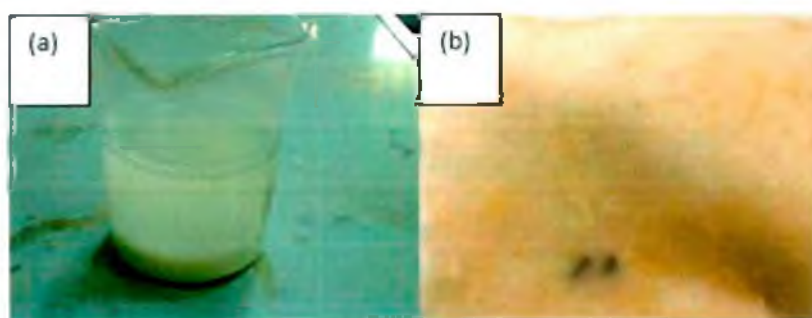


Figure 2.2: Film solution of starch with glycerol (a) and gelatinized film of starch with glycerol (b).

2.2.3. Composites Film Preparation

Starch (2 g) was first dispersed in distilled water (35 mL). Besides, kaolinite (0, 5, 10 15 and 20% w/w of starch) were homogeneously dispersed in 1 g of glycerol and agglomeration was prevented by sonication for 10 minutes. Then the two mixtures were added together and stirred mechanically while the solution was heated at 95°C for 15 minutes. The mixture was further stirred and sonicated for 10 min to remove micro-bubbles before casting onto the surface of glass frame wrapped with Teflon sheet. The film was dried by atmospheric evaporation at 25°C and then dried at 40°C in a non-ventilated oven for 24 h.

2.2.4. Characterization Techniques

2.2.4.1. Energy dispersive x-ray defraction spectroscopy (EDS): Pure kaolinite was subjected to analyze using energy dispersive X-ray spectroscopy (EDS) for elemental analysis

2.2.4.2. Attenuated Total Reflection Infra-red (ATR-IR) Spectral Analysis: ATR-IR spectra were measured on a FT-IR 8400S spectrophotometer (Shimadzu Corporation, Japan) in the range of 4000–400 cm^{-1} , resolution: 4 cm^{-1} ; no. of scans: 16 times.

2.2.4.3. X-ray diffraction (XRD): The x-ray powder diffraction (XRPD) patterns of the samples were recorded by a x-ray defractometer (Ultima IV, Rigaku Corporation, Japan) at room temperature. Prior to XRD analysis the samples were ground into fine powders using mortar-pestle. Nickel (Ni) filtered Cu $K\alpha$ radiation ($\lambda=0.154\text{nm}$), from a broad focus Cu tube operated at 40 kV and 40 mA, was applied to the samples for measurement. The XRD patterns of the samples were measured in the continuous scanning mode with scan speed of 3°/min and in the scan range of 5 to 100°. Bragg's law was used to compute the basal spacing (d_{001}) of the crystalline samples.

2.2.4.4. Universal Testing machine (UTM): Mechanical properties (Tensile strength, elongation break, Young's modulus) were investigated using UTM.

2.2.4.5. Thermal Characterization: The thermograms of samples were recorded by thermo gravimetric analyzer (TGA-50, Shimadzu, Japan) with alumina cell under nitrogen atmosphere at the rate of 5°C/minute. In order to understand the thermal behavior, thermograms were recorded in the temperature range of 30-600°C.

2.2.4.6. Thermal Mechanical Analysis (TMA) or Dilatometry: Thermomechanical analysis was conducted using dilatometry.

2.2.4.7. Scanning electron microscope (SEM): The morphology of the samples were analyzed by an analytical scanning electron microscope (JEOL JSM-6490LA, Tokyo, Japan) operated at an accelerating voltage of 20 kV in the back-scattered electron mode.

3. Results and Discussion

At first the starch was extracted from potato and the yield was obtained about 18% w/w. It is revealed that the content of starch in potato is relatively higher which was aged for several months in cold storage. The higher yield of starch and low cost of potato indicate that it can be a potential source of raw material for pharmaceutical and starch based industries. A white cotton fabric (cloth) was used for separation of starch by filtration. Therefore, a portion of starch was trapped into the mass of blended potato. The yield of production of starch may be increased by using an alternative and efficient sieving technique.

Biopolymers are usually hydrophilic and thus, water is the solvent used most often to dissolve to obtain film forming solutions. Instead of water some other solvents with or without water can be used to dissolve biopolymers. Usually, heating with solvent is needed to disrupt the native structure of the biopolymer to obtain a film forming solution. Plasticizer is added to the film forming solution at a convenient stage of the process to obtain flexible and elastic films which are often desired. There are various biomaterial film forming processes such as casting, spraying, extrusion and thermo-molding. The most common process to produce films on a laboratory scale is casting, which was used to produce films for testing here. In this process, a film forming solution was cast on a non-adhesive surface of glass frame covered with Teflon ribbon. Water i.e solvent was evaporated from the solution in order to form the film. As a result of solvent evaporation, biopolymer was increased and the basic film structure was developed by hydrogen bonding. Environmental properties, such as temperature and air relative humidity, during the evaporation stage could be used to control some of the film properties.

It is well known that the functional properties of biodegradable films and coatings depend on the characteristics of the film forming material²⁰. The biopolymers used in film formulations are polysaccharides, proteins and lipids. Lipids have good barrier properties against moisture, but little mechanical resistance and a waxy taste. Their ability to reduce the transfer of water is due to their hydrophobic characteristics and highly compact nature²¹. Films based on polysaccharides and proteins have been reported as effective barriers to gas transport (O₂, CO₂), although they present high water vapor permeability. The main functional properties (mechanical and barrier properties) of these hydrophilic materials depend on their water content. This is due to strong water vapor interactions with the polymer matrix, affecting the structure²². Nanotechnology focuses on the characterization, manufacture and manipulation of biological and non-biological structures smaller than 100 nm²³. The design of the internal structures on a micro-scale or nano-scale can improve the functional properties, morphology and stability of the polymer matrices used in edible films and coatings. Currently, the application of nanotechnology in this area is limited and is therefore a wide-open field for scientific research.

Addition of crystalline segment into starch biopolymer would dramatically change the film properties in terms of mechanical and chemical points of views. Thus to increase the clay/ matrix affinity, different quantities (0, 5, 10, 15 and 20 % w/w of starch) of white clay namely bijoypur clay and glycerol have been incorporated. Some plasticizers such as urea or urea/formamide/glycerol, has also been produced great results in the production of exfoliate nanocomposites but these compounds are eco-toxic and cannot be used to elaborate safe biodegradable "green" materials.

There are five nanocomposite films with varying quantities of kaolinite were prepared to investigate its mechanical properties. The self-assembled nanocomposite films were designed as KSNC for kaolinite starch nanocomposite. The different composition of the films was represented as K₀SNC, K₅SNC, K₁₀SNC, K₁₅SNC and K₂₀SNC for 0, 5, 10, 15 and 20% w/w of kaolinite present in the self-assembled nanocomposite films respectively.

3.1. Energy dispersive x-ray defraction spectroscopy (EDS)

Pure kaolinite was subjected to energy dispersive X-ray spectroscopy (EDS) for elemental analysis. The spectrum of the (Figure 2.3A) shows only three peaks of O, Al and Si elements which is the identity of the Kaolinite. The percentage of Al, Si and O in terms of mass and atoms in the kaolinite is presented in Table 2.1. The SEM images of kaolinite with different magnifications in Figures 2.3 (B, C) show that the morphology of the particle looks like a grain of rice. The size of the kaolinite was estimated to be around 250 nm.

Table 2.1: Elemental analysis of kaolinite

Element	(keV)	Mass%	Error%	Atoms	K
O	0.525	60.42	0.19	72.45	52.0661
Al	1.486	18.47	0.11	13.13	23.2418
Si	1.739	21.11	0.14	14.42	24.6921
Total		100.00		100.00	

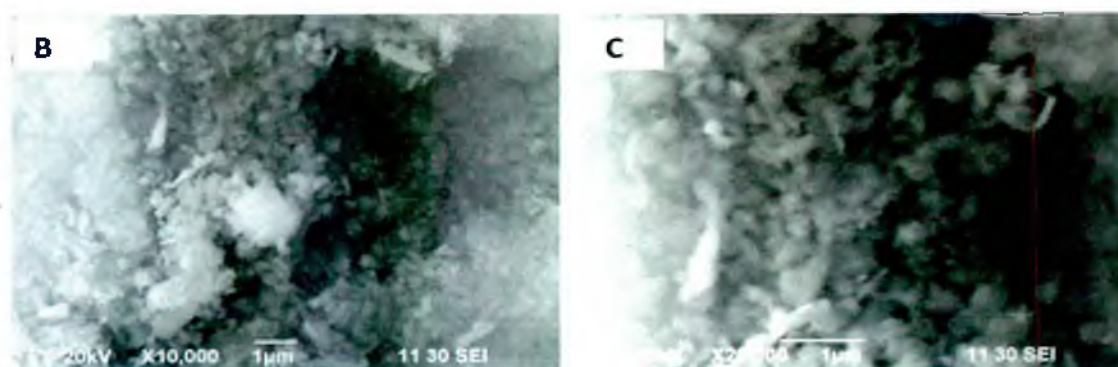
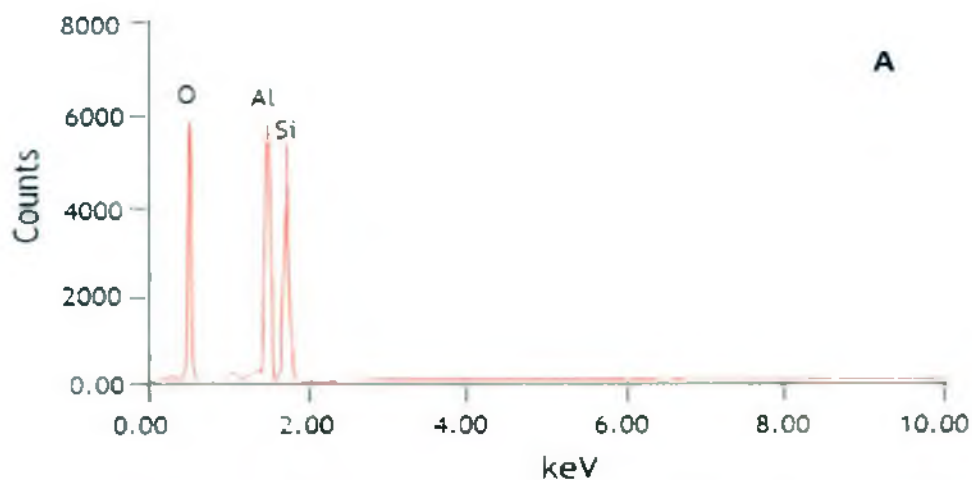


Figure 2.3: Energy dispersive X-ray spectra, (b, c) SEM images of kaolinite at different magnifications obtained from Bijoypur, Bangladesh.

3.2. Attenuated Total Reflection Infra-red (ATR-IR) Spectral Analysis

The functional groups and interaction of starch/clay self-assembled nanocomposites were analyzed by ATR-IR spectroscopy. The main bands for distinctive functional groups were identical in pure starch film which makes observation of many modifications in these bands difficult. However, intensive changes in the modes below 800 cm^{-1} were observed, more specifically at 578 and 528 cm^{-1} . These bands are due to skeletal modes, low frequency vibrations of the ring, etc²⁴. The appearance of a new band at $2,850\text{ cm}^{-1}$, attributed to CH_2 groups and the increase of intensity of the band at $1,463\text{ cm}^{-1}$, arising from OCH and CH_2 groups²⁵. **Figure 2.4** shows the ATR-IR spectra of (a) K_0SNC , (b) K_5SNC , (c) K_{10}SNC , (d) K_{15}SNC , (e) K_{20}SNC and (f) kaolinite recorded within the range of $500\text{-}4000\text{ cm}^{-1}$. The ATR-IR

spectrum of kaolinite showed the characteristic absorption bands of the inorganic moiety. These were $1,036.8\text{ cm}^{-1}$ (ν Si-O), 913.1 cm^{-1} (ν Al-OH), 819.5 cm^{-1} (ν Al-O), and 523.4 cm^{-1} (ν Al-O-Si)²⁶. The band at $3,600\text{-}3700\text{ cm}^{-1}$ relates to free OH stretching. These bands are existing in spectra of Kaolinite. OH stretching band of K₀SNC moved toward the higher frequency from 3294 to 3410 cm^{-1} which were induced from Kaolinite band. All nanocomposites gave sharp peaks at around 2922 cm^{-1} starch Starch/Kaolinite patterns show a band at $1,647\text{ cm}^{-1}$ relate to OH bending and the peak at $1,100 - 1,200\text{ cm}^{-1}$ indicated that the Si-O-C bond which may be associated with an H-bonded Si-OH group is produced from the interaction between starch and silicate phase of clay.

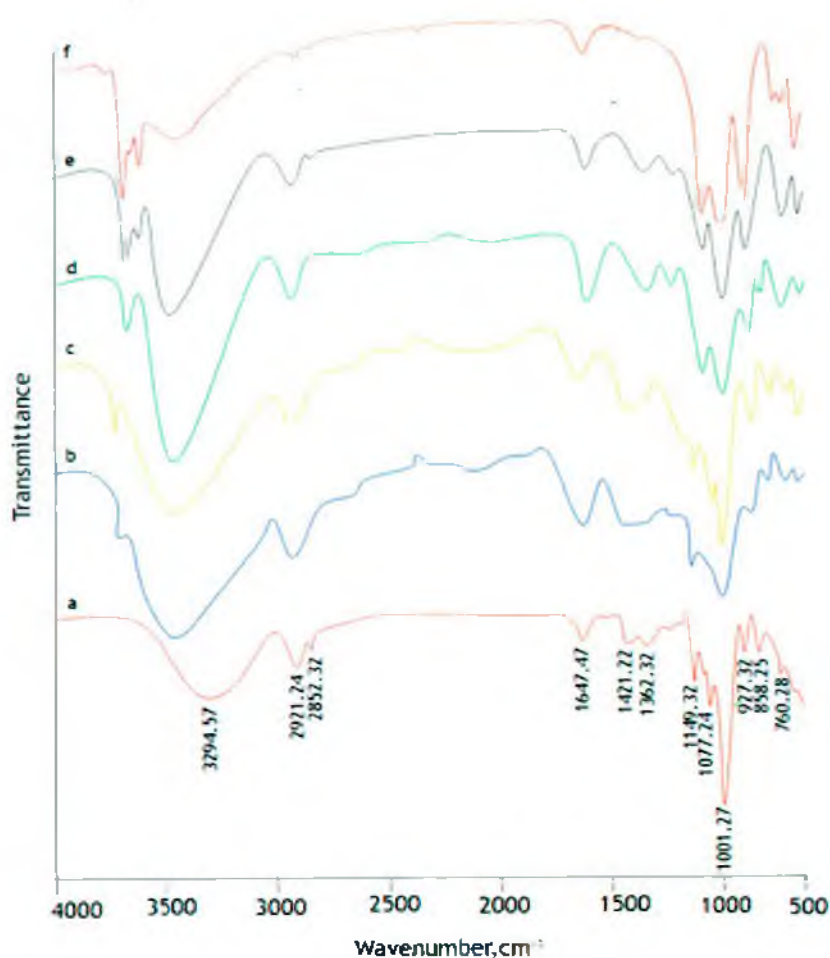


Figure 2.4: ATIR spectrum of (a) K₀SNC, (b) K₅SNC, (c) K₁₀SNC, (d) K₁₅SNC, (e) K₂₀SNC films and (f) Kaolinite recorded within the range of $500\text{-}4000\text{ cm}^{-1}$.

3.3. X-ray diffraction (XRD) analysis

XRD pattern of the films K₀SNC, K₅SNC, K₁₀SNC, K₁₅SNC, K₂₀SNC and kaolinite were depicted in Figure 2.5. Here it is evident that the peaks around at 12° recorded from the composite films were not shifted which indicates there was no intercalation of starch molecules in the kaolinite occurred²⁷. Whereas, the characteristic peaks at around 20° were gradually sharp as the addition of kaolinite was increased in the composite films.

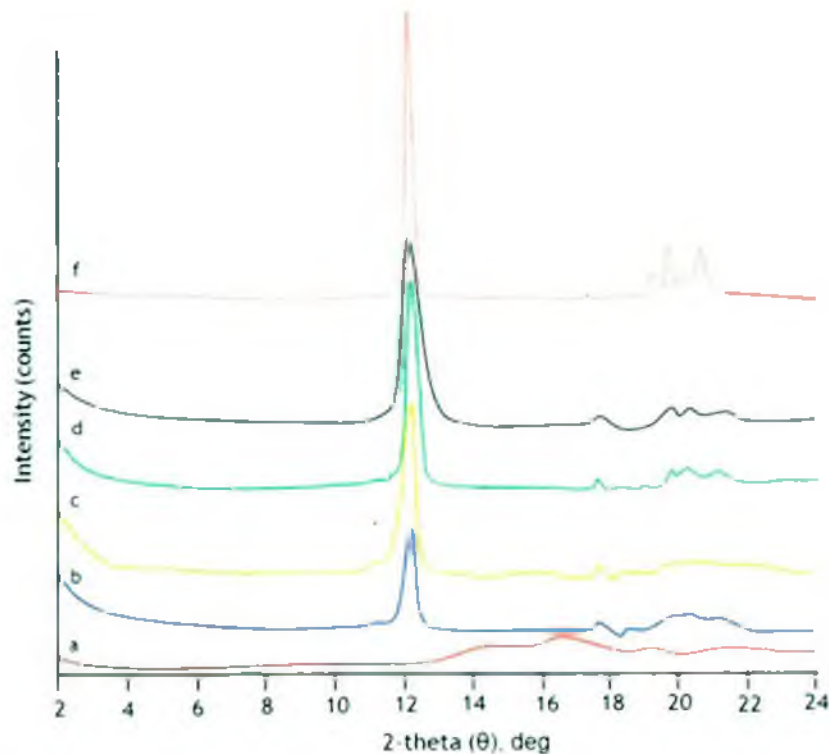


Figure 2.5: XRD pattern of (a) K₀SNC, (b) K₅SNC, (c) K₁₀SNC, (d) K₁₅SNC, (e) K₂₀SNC and (f) Kaolinite recorded from powder of the sample after drying at 105°C for 12h.

UTM provided data to discuss on tensile strength, elongation at break and modulus of resilience. Henceforth, UTM data has been analyzed carefully and discuss the film properties to understand the effect of kaolinite.

3.4. Mechanical Properties

Mechanical properties of the samples were studied in terms of tensile strength and percentage elongation at break.

3.4.1. Tensile strength of the nanocomposite films

As the film thickness (200 μm) and maximum force (15 N) exerted onto the films were unchanged, the experiment was run to measure the ability of a film to withstand a longitudinal stress, expressed as the greatest stress that the film can stand without breaking. The Figure 2.6 shows a relation between tensile strength of the self-assembled nanocomposite film and the variable content of kaolinite. At zero kaolinite content film, K_0SNC , gave tensile strength at 2.5 MPa, whereas, the maximum tensile strength (8.33 MPa) was found from the K_{20}SNC film. The overall trend of the line is straight with positive slope which indicates that the tensile strength increases with the increase of the amount of kaolinite²⁸. At 10 % w/w, there was an experimental error or the film K_{10}SNC was not perfectly prepared (may be the film was not homogeneous); therefore the value obtained (4.3 MPa) was slightly lower than that of the average values of the trend line. The explanation for this effect is ascribed to the formation of a rigid network of nanofillers, the mutual entanglement between the nanofiller (kaolinite) and the matrix, and the efficient stress transfer from the matrix to the nanofiller²⁹. Mathew et al. in 2002, proposes an increase in the overall crystallinity of the system resulting from the nucleating effect in the composite can be beneficial for mechanical properties.³⁰

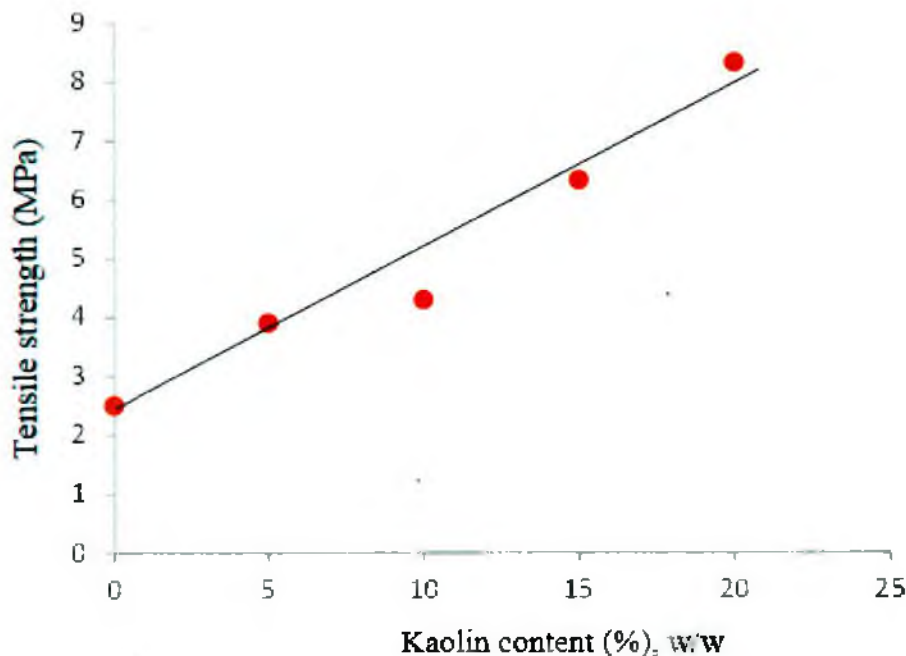


Figure 2.6: Effect of kaolinite content on the tensile strength of the nanocomposite films produced from (a) K₀SNC, (b) K₅SNC, (c) K₁₀SNC, (d) K₁₅SNC and (e) K₂₀SNC films.

3.4.2. Elongation of the nanocomposite films at break

Elongation at break, also known as fracture strain, is the ratio between changed length and initial length after breakage of the nanocomposite film. It expresses the capability of the film to resist changes of shape without crack formation. The **Figure 2.7** represents the effect of kaolinite content on the enlargement of nanocomposite film before the appearance of crack formation. It is revealed that the film K₀SNC without kaolinite showed very little elongation at break, this could be due to the lack of weak interaction of the starch molecules. Besides, as the kaolinite content increased from 5 to 20 % w/w the magnitude of the value decreased linearly²⁸. It can be explained that at K₅SNC film the interaction of starch molecules and the kaolinite was remarkably strong due to the ratio of matrix (starch) and kaolinite crystalline segment, where the surface of the kaolinite was fully covered by the starch biopolymers, and sufficient polymer between kaolin interfaces makes the film soft and less stiff. The K₂₀SNC film showed the lowest elongation, where the availability of soft segment (biopolymer) was decreased and the hard

crystalline kaolinite part was increased, as a result the thin starch film between the kaolinite particles gradually loses the expanding ability.

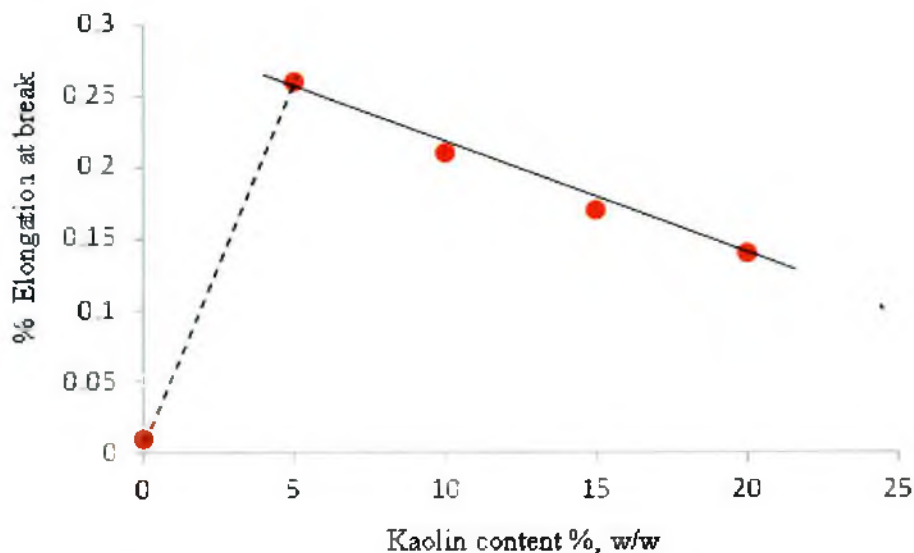


Figure 2.7: Effect of kaolinite content on the percentage elongation of the nanocomposite films produced from (a) K_0 SNC, (b) K_5 SNC, (c) K_{10} SNC, (d) K_{15} SNC and (e) K_{20} SNC films.

In **Figure 2.8**, stress (MPa) vs % strain was plotted and the effect of kaolinite on the elastic and plastic behaviors was depicted. K_0 SNC shows only modulus of resilience which is represented with green zone but when the Kaolinite was added with the starch then the film showed dual characteristic including plastic behavior. It indicates that kaolinite reinforced to incorporate brittle nature in the film. Interestingly, with the variation of kaolinite content from 5 to 20 % w/w in the film, the change of rheology in terms of elastic and plastic characteristics are explained more clearly from the **Figure 2.9**. It is evident that the maximum modulus of resilience was found for K_{15} SNC film which is about 5 times higher than that of K_0 SNC film. This could be due to the fact that the distribution of Kaolinite in the self-assembled film was homogeneous and perfect proportionate. Besides, initially the maximum plastic region was found for the film produced K_5 SNC materials which as decreased in case of K_{15} SNC film and further increased for K_{20} SNC film. In the K_{20} SNC film nanoparticles agglomerations were detected and the modulus of resilience resulted worse than that of the others composites. This can be easily explain that 20 % w/w Kaolinite content film suffered from agglomeration and lack of sufficient starch matrix to

carry out the flow properties of the film.

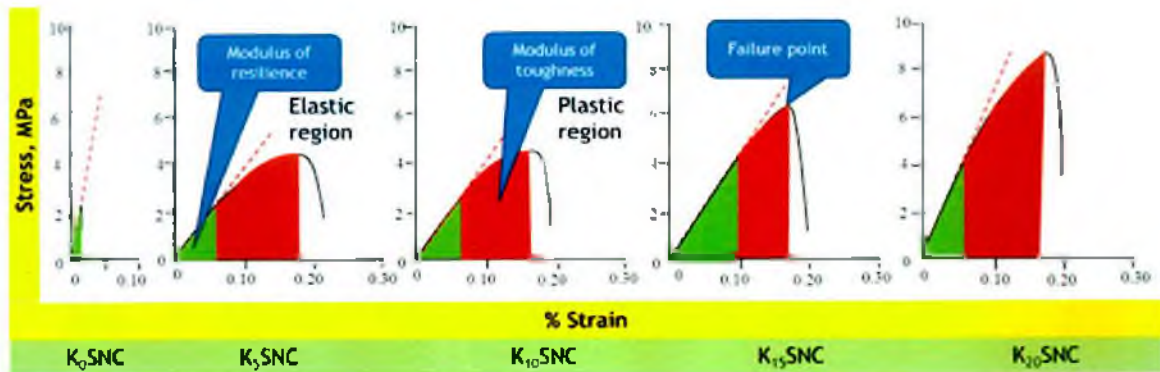


Figure 2.8: Effect of kaolinite content on the modulus of resilience, modulus of toughness of the nanocomposite films produced from (a) K₀SNC, (b) K₅SNC, (c) K₁₀SNC, (d) K₁₅SNC and (e) K₂₀SNC films.

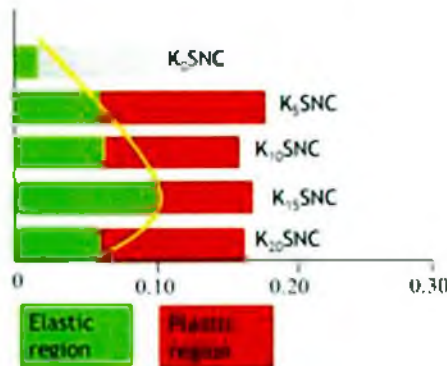


Figure 2.9: Comparison of the effect of kaolinite content on the elastic and plastic reasons of the nanocomposite films produced from starch and 0, 5, 10, 15 & 20 % w/w of kaolinite.

3.5. Thermogravimetric Analysis (TGA)

In **Figure 2.10** thermogravimetric characterization of the films designated as K₀SNC, K₅SNC, K₁₀SNC, K₁₅SNC and K₂₀SNC produced from 0, 5, 10, 15 and 20% w/w of kaolinite (by weight of starch) self-assembled nanocomposite respectively are showed. Approximately, 10 mg of sample was subjected to run the experiment using an aluminum pan over 30 to 600°C where the temperature was increased at a rate 5°C/min. Each graph shows three tracing curves, one for thermogravimetry which deals with the weight loss of sample due to moisture removal and decomposition of nanocomposite film materials are shown at the top. The second curve (at the

middle) represents differential thermal analysis (DTA) which is corresponding to the heat absorption and phase transition, crystallization due to endothermic and exothermic oxidative reactions. The third curve shows the degradation rate of nanocomposite films as shown at the bottom. In Figure 2.10A, the TG curve (top) shows that the initial weight loss (10%) occurs at about 120°C due to the removal of free moisture and the onset decomposition occurs at 270.6°C (about 12% weight loss) where more 2% weight loss were recorded may be due to the loss of bound or trapped water (moisture). Decomposition of starch with 66% of weight was escaped at 344°C showed a linearly decreased of line leaving 12.5% starch weight. Later the decomposed residue was further completely burned and the ash was found 0.6% approximately. Besides, the energy profile with heat absorption and desorption was described from middle curve and was found that at 80 and 176 °C, the initially heat gained by moisture, leads to downward the tracing line whereas, during combustion the heat produced from the system shows the exothermic reaction at approximately 300 °C. Later the line goes downward which indicates the endothermic reaction for further absorption of heat for complete combustion. The bottom graph shows that the highest rate of degradation (17.12 µg/°C) of starch films was occurred at 290.5°C with a sharp peak. Weight loss due to removal of free and bound water also leads a small broad peak at around 74 and 174°C with the rate 5.2 and 3.5 µg/°C respectively. Similar experiments were performed for a series of nanocomposite films prepared using 5 to 20% w/w kaolinite for the comparison of the properties stated.

Table 2.2: Thermogravimetric analysis of different composites

Sample ID	Top			Middle	Bottom curve
	T_{Onset} , °C	$T_{Decom. completed}$, °C	% Decom -position	Reaction pattern*	T_{peak} (°C) & $R_{Max. decom position}$ (µg/°C)
K ₀ SNC	270	334	76	Endo, Exo	290 & 17
K ₅ SNC	279	320	65	Endo, Exo	300 & 22
K ₁₀ SNC	280	336	61	Endo, Exo	312 & 22
K ₁₅ SNC	280	333	56	Endo, Exo	314 & 30
K ₂₀ SNC	284	338	54	Endo, Exo	316 & 36

*Endo-Endothermic and Exo-Exothermic

Table 2.2 shows a summary of thermogravimetric analysis of five samples, K₀SNC, K₅SNC, K₁₀SNC, K₁₅SNC and K₂₀SNC in terms of onset temperature, temperature at which decomposition completed, the amount of composite decomposed in percentage, type of reaction occurred and the temperature at which the maximum decomposition rate recorded. It is clear from the onset temperatures envisaged in the Table 1 that after addition of 5% kaolinite the change of temperature was significant i.e. 9°C was increased whereas from 5 to 20% increased of kaolinite lead 5°C more tolerance at 284°C for onset decomposition. This phenomenon indicates that kaolin plays crucial role to stabilize the composites against temperature. The films without kaolinite decomposed completely at 334°C but except K₅SNC and K₁₅SNC all films showed little higher temperatures. But it was not remarkably high compared to K₀SNC film. Decomposition amount from K₀SNC to K₂₀SNC films within the temperature range from onset to complete decomposition were gradually decreased from 76 to 54%. It is noticed from the data that there is an inverse relationship between decomposition quantity and kaolinite content. As the content of kaolinite increased in the composite films, the amount of decomposition was decreased, since the residue was gradually increased. The reactions involved with the whole temperature profile from 30 to 600°C are endothermic and exothermic due to heat absorption by moisture and the starch biopolymer and later desorption of heat occur by burning of starch for char formation. Interestingly, it is found that the rate of decomposition was increased with the increase of kaolinite content in the films. At 290°C the rate of maximum decomposition (R_{max}) was 17 $\mu\text{g}/^\circ\text{C}$ for K₀SNC film. A slightly higher decomposition rate 22 $\mu\text{g}/^\circ\text{C}$ were found for K₅SNC and K₁₀SNC films at 300 and 312°C. Besides, K₁₅SNC film gave drastically increased decomposition rate 30 $\mu\text{g}/^\circ\text{C}$ at 314°C which is lower than that obtained from K₂₀SNC, $R_{max} = 36 \mu\text{g}/^\circ\text{C}$, at $T_{peak} = 316^\circ\text{C}$, indicates that the K₂₀SNC film is more thermally unstable than K₁₅SNC film.

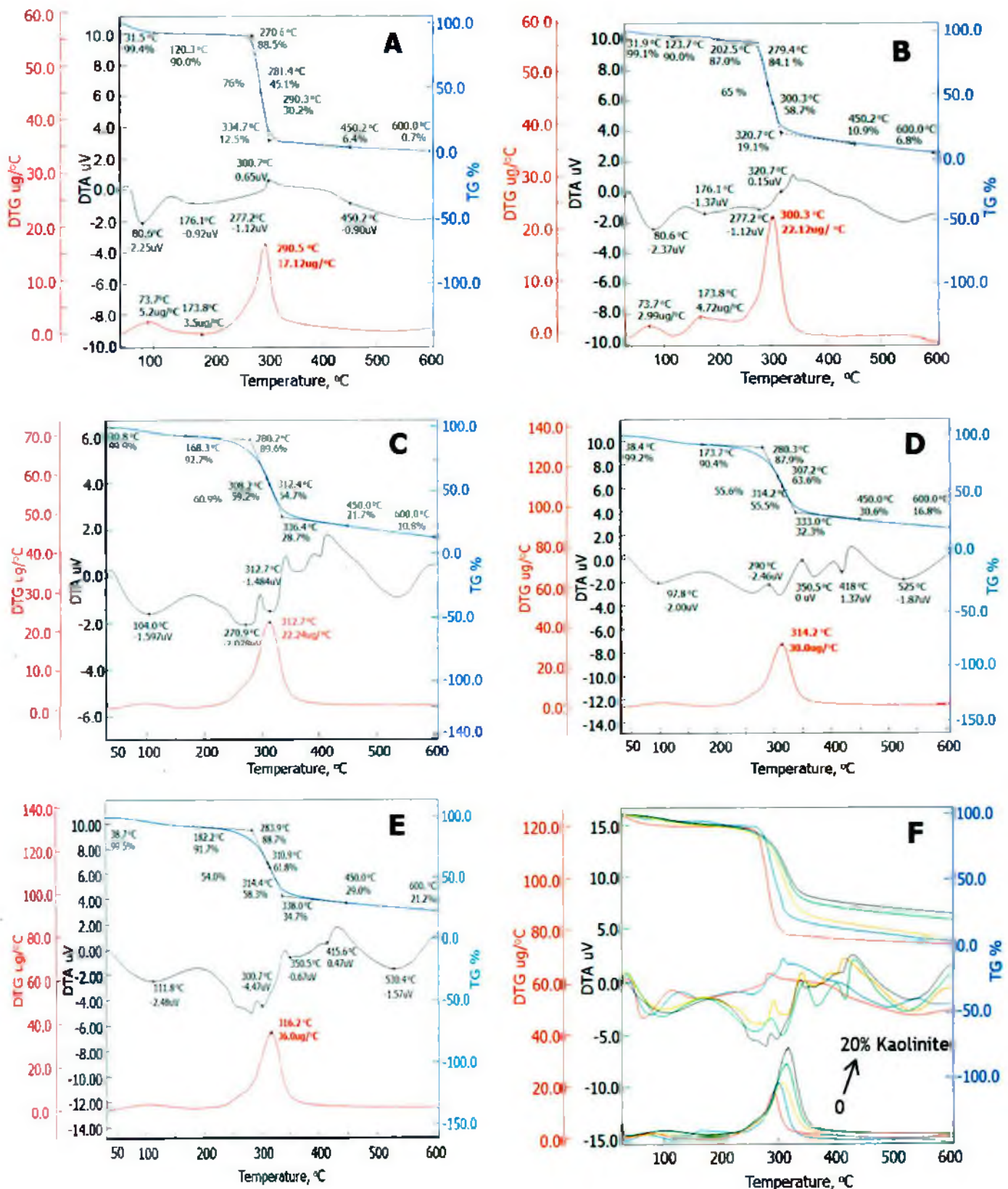


Figure 2.10: Thermogravimetric graphs of (a) K₀SNC, (b) K₅SNC, (c) K₁₀SNC (d) K₁₅SNC, (e) K₂₀SNC and (f) a comparison chart of films.

There are some research articles already published regarding thermogravimetric analysis performed on numerous synthetic polymer nanocomposite showed that many polymers filled with clay, specially montmorillonite exhibited improved thermal stability (*i.e.*, a higher temperature for the onset of thermal degradation), such as in the case of poly(methyl methacrylate) (PMMA)³¹, poly(dimethylsiloxane) (PDMS)³², polyamide (PA)^{33,34} and polypropylene (PP) systems³⁵. It is usually well accepted that in the case of polymer–clay nanocomposites the improved thermal stability of the polymer nanocomposite is mainly due to the formation of a char which hinders the out-diffusion of the volatile decomposition products, as a direct result of the decrease in permeability, usually observed in exfoliated nanocomposites³⁶. Despite this, the exact degradation mechanism is currently not clear; such behavior is probably associated with the morphological changes in proportion relative to exfoliated and intercalated species with the clay loading. At low clay loading (*ca.* 1 wt.%), exfoliation dominates but the amount of exfoliated nanoclay is not enough to enhance the thermal stability through residue formation³⁷. In addition, in air atmosphere, clay may slow down oxygen diffusion and thus produce thermo-oxidative reactions. On the other hand, the effect of clay on thermal stability in nitrogen is system dependent; therefore, there is no scientific evidence that there is an increase in thermal stability due to a decrease in permeability. When increasing the clay concentration (2 wt %–4 wt %), much more exfoliated clay is formed, char forms more easily and effectively and, consequently, promotes the thermal stability of the nanocomposites. At even higher clay loading level (up to 10 wt %), the intercalated structure is the dominant population and, even if char is formed in high quantity, the different morphology of the nanocomposite probably does not allow the maintaining of a high thermal stability. However, it is known that the chemical nature of the polymers, the type of clays and their modification route play an important role in the degradation behavior of polymer nanocomposite. TGA measurement could also give indirect information about the amount of exfoliated nanoclay in the self-assembled nanocomposite. However, char formation could not affect thermal stability since it is obtained at the very end of the decomposition. Two important works review the thermal properties and degradation processes of nanocomposites based on different polymer matrices.^{36,38} They discuss the basic changes in thermal behavior of different synthetic polymer matrices (polyolefins, polyamides (PA), styrene containing polymers, poly(methyl methacrylate) (PMMA), poly(vinyl chloride) (PVC),

polyesters, polyimides (PI), epoxy resins, polyurethanes (PU), ethylene-propylene-diene terpolymer (EPDM), poly(vinyl alcohol) (PVA), and polylactide (PLA) upon addition of montmorillonite, with special focus on the influence of montmorillonite on the kinetics of the degradation process and the formation of condensed/volatile products in oxidative and pyrolytic conditions. The results of recent research reported in the mentioned reviews^{36,39} indicate that the introduction of layered silicates into polymer matrix causes an increase in thermal stability. Due to the characteristic structure of layers in a polymer matrix and their shape and dimensions close to molecular level, several effects have been observed that can explain the changes in thermal properties. Experimental results have shown that layers of MMT are impermeable to gases, meaning that both intercalated and exfoliated structure can create a labyrinth for gas penetrating the polymer bulk. Thus, the effect of a “labyrinth” limits the oxygen diffusion inside the nanocomposite during thermal degradation. Similarly, in the samples exposed to a high temperature, the kaolinite layers restrain the diffusion of gasses evolved during degradation, contributing to keep the neat polymer in contact with a non-oxidizing environment. Moreover, kaolinite layers are thought to reduce heat conduction. In the presence of kaolin layers, strongly interacting with polymer matrix, the motions of polymer chains are limited. This effect brings additional stabilization in the case of polymer/kaolinite nanocomposites. The heat barrier effect could also provide superheated conditions inside the polymer melt leading to extensive random scission of a polymer chain and the evolution of numerous chemical species which, trapped between clay layers, have more opportunity to undergo secondary reactions. As a result, some degradation pathways could be promoted leading to enhanced charring. It is also suggested that the effect of more effective char production during thermal decomposition of polymer-clay nanocomposites may be derived from a chemical interaction between the polymer matrix and the clay layer surface during thermal degradation. Some authors indicated that catalytic effect of nanodispersed clay is effective in promoting char-forming reactions. Nanodispersed MMT layers were also found to interact with polymer chains in a way that forces the arrangement of macrochains and restricts the thermal motions of polymer domains^{38,39}. Generally, the thermal stability of polymeric nanocomposites containing MMT is related to the organoclay content and dispersion. Specifically, the onset decomposition temperature, T_{onset} , and the temperature of maximum weight loss rate, T_{peak} , are higher in the nanocomposites. For example, Ge *et al.*³⁹

found that 5 wt % MWNT addition caused a 24°C shift in T_{onset} as compared to that of the neat PAN. A number of mechanisms have been suggested. Dispersed nanotubes might hinder the flux of degradation products and thereby delay the onset of degradation. Polymers near the nanotubes might degrade more slowly, which would shift T_{peak} to higher temperatures. Another possible mechanism attributes the improved thermal stability to the effect of higher thermal conductivity in the nanotube/polymer composites that facilitates heat dissipation within the composite⁴⁰.

3.6. Thermal Mechanical Analysis (TMA)

Figure 2.11 shows TMA and differential thermal mechanical analysis (DTMA) graphs obtained from 0 to 20% kaolinite containing starch films. TMA is a highly sensitive technique for the measurement of expansion and contraction of cross-linked or filled materials, including nanocomposites⁴¹. There are many research groups have already used TMA to measure the coefficient of thermal expansion (CTE) of nanocomposite materials⁴²⁻⁴⁶ where montmorillonite was only incorporated into the composites. In general, the extent of CTE reduction depends on the particle rigidity and on the dispersion of the clay platelets in the matrix and also on an efficient stress transfer to clay layers. It is believed that the retardation of chain segmental movement through incorporation of organically modified clays also leads to decrease in the CTE⁴⁷. PA-6 modified with organo-MMT was found to exhibit lower values of CTE than pure polymer in the direction parallel to the melt flow during injection molding⁴³, while increased values of CTE were measured in the direction normal to the melt flow. TMA results may indirectly provide information about the spatial orientation of MMT layers in nanocomposite materials. TMA can be also used to measure the glass transition, in terms of change in the CTEs, as the polymer turns from glass to rubber state with a dramatic change in free molecular volume. Thus, T_g can be determined from the thermal expansion curve. In the Figure 2.11, the top curve is for DMA and the bottom curve is for DTMA were obtained for K_0SNC film. The TMA curve shows that the first onset of contraction occurs at 37°C, the value of which is 0.38µm and second onset of contraction occurs at 93.5°C, the value of which is 9.64µm. DTMA curve also shows two stages of contraction occurs at a rate of 0.068µm/°C at 31.7°C, and at a rate of 0.196µm/°C at 98.5°C. There is also an expansion occurs at 47.3°C with 0.21µm contraction. Similar data were acquired from the kaolinite self-assembled starch nanocomposite films. The

Table 2.3 represents the two-phase contractions within the range 30 to 100°C. First onset contraction of nanocomposite occurs within the temperature range 37-38°C, but the deformation was significantly varies from 0.38µm to 1.86µm for K₀SNC and K₂₀SNC films respectively. It indicates that the kaolinite assisted to contract the film more strongly within the temperature range 37-38°C. Interestingly, at higher temperature (93.5°C) contraction was increased dramatically from 0.38 to 9.64µm for K₀SNC.

Temperature increases plastic flow of starch matrix originated from loosening entanglement of polymer chain the reason why the contraction increases. Whereas, in case of K₅SNC film, contraction was changed from 0.56 to 6.34µm which indicates kaolinite plays crucial role as a crystalline phase to prevent expansion by increasing interfacial interaction with the soft polymer matrix. It is evident that the contraction of K₅SNC film was the lowest in magnitude compared to other nanocomposites produced using kaolinite. Interestingly, the contraction was increased gradually upto 8.19µm for K₂₀SNC film from 6.34µm for K₅SNC film. DTMA shows the contraction rate at two different temperatures. Initially, at around 31°C the contraction rate decreased to 0.037µm/°C when 5% kaolinite was added, after further addition of kaolinite contraction rate maintains almost steady (~0.08µm/°C) upto 20% kaolinite content. Likewise, at the films within the range 94-98°C shows similar pattern, initially decreased from 0.196 to 0.086µm/°C then increased to 0.154µm/°C of contraction rate which indicates that the K₂₀SNC film was more unstable than other K₁₀SNC and K₁₅SNC films.

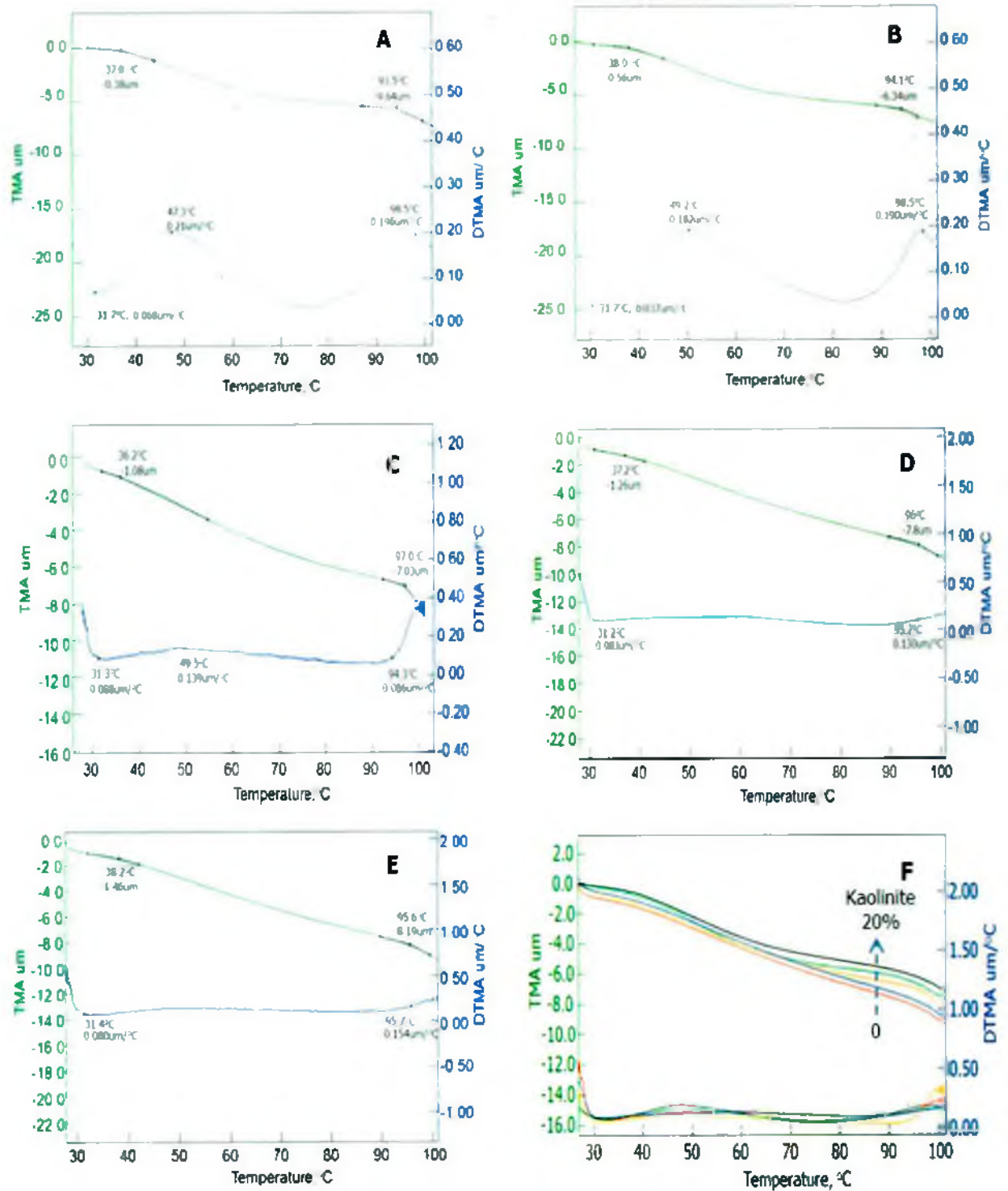


Figure 2.11: TMA and DTMA curves for contraction analysis from thermal analysis of (a) K₀SNC, (b) K₅SNC, (c) K₁₀SNC (d) K₁₅SNC, (e) K₂₀SNC and (f) a comparison chart of films.

Table 2.3: Summary of thermal mechanical analysis (TMA) and differential TMA

Sample ID	Onset contraction (Top curve) TMA				DTMA (Bottom curve)			
	°C	µm	°C	µm	°C	µm/°C	°C	µm/°C
K ₀ SNC	37.0	0.38	93.5	9.64	31.7	0.068	98.5	0.196
K ₅ SNC	38.0	0.56	94.1	6.34	31.7	0.037	98.5	0.190
K ₁₀ SNC	36.2	1.08	97.0	7.03	31.3	0.088	94.3	0.086
K ₁₅ SNC	37.2	1.26	96.0	7.8	31.2	0.083	95.2	0.130
K ₂₀ SNC	38.2	1.86	95.6	8.19	31.4	0.080	95.7	0.154

3.7. Studies of Surface morphology of films using SEM

A scanning electron microscope (SEM) is a type of electron microscope that produces images of a sample by scanning it with a focused beam of electrons. The composite films were subjected to probe its morphological structure using SEM. In **Figure 2.12**, SEM images are inserted and it is seen that **Figure 2.12A**, represent the image of film produced without kaolinite. The arrow indicates the dark spot of the film where a porous structure was found. The pore was distributed almost homogeneously in the film. The porosity was decreased after addition of kaolinite as shown in **Figure 2.12 (B-D)**. A least number of pores were observed from K₁₅SNC film indicate the homogeneous distribution of kaolinite in the film. Besides, the surface of K₂₀SNC film looks rough due to the agglomeration of excess kaolinite is depicted in **Figure 2.12E**.

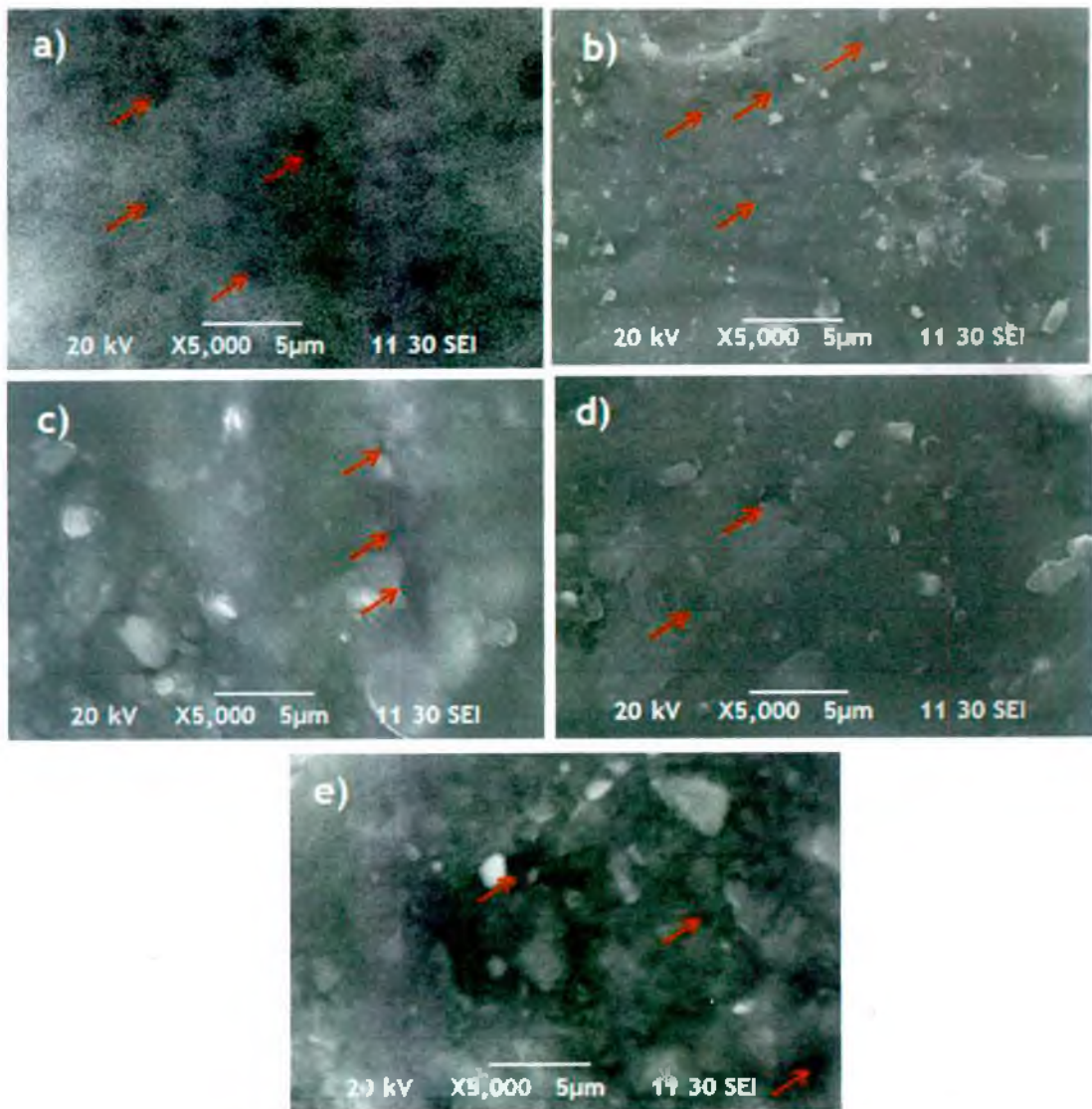


Figure 2.12: SEM images of the films produced from (a) K₀SNC, (b) K₅SNC, (c) K₁₀SNC (d) K₁₅SNC and (e) K₂₀SNC using kaolinite and starch.

Conclusion: In this report, we have successfully prepared nano-composite films of kaolinite dispersed and self-assembled in starch biopolymer. ATR-IR spectrum shows the presence of the functional groups of starch and kaolinite in the nanocomposite films. The self-assembled nanocomposite film produced from 15% w/w kaolinite and starch exhibited moderate mechanical strength (stress 6.3 MPa) at break but showed the highest workable mechanical strength (stress 4.3 MPa) within the area of modulus of resilience. Thermal stability of composites were increased with the addition of kaolin but the optimum stability was found for K₁₅SNC film with $T_{Onset} = 280^{\circ}\text{C}$, Maximum rate of decomposition $R_{max} = 30 (\mu\text{g}/^{\circ}\text{C})$ and $T_{peak} = 314^{\circ}\text{C}$. Contraction of all K₍₅₋₂₀₎SNC nanocomposite films at around 95°C were found lower in magnitude compared to K₀SNC film. SEM images proved that the nanofiller kaolinite reduces the porosity of the film and the minimum number of pore was envisaged in the K₁₅SNC film. Such nanocomposite advanced materials produced from starch biopolymer and indigenous layered materials would play crucial role in the field of nanoscience and technology.

References:

1. Pushpadass, Heartwin A., Ajay Kumar, David S. Jackson, Randy L. Wehling, Joseph J. Dumais, and Milford A. Hanna. "Macromolecular changes in extruded starch-films plasticized with glycerol, water and stearic acid." *Starch-Stärke* 61, no. 5 (2009): 256-266.
2. Yang, Ke-Ke, Xiu-Li Wang, and Yu-Zhong Wang. "Progress in nanocomposite of biodegradable polymer." *Journal of Industrial and Engineering Chemistry* 13, no. 4 (2007): 485-500.
3. Edlund, Ulrica, and A-C. Albertsson. "Degradable polymer microspheres for controlled drug delivery." In *Degradable aliphatic polyesters*, pp. 67-112. Springer, Berlin, Heidelberg, 2002.
4. Pandey, Jitendra K., A. Pratheep Kumar, Manjusri Misra, Amar K. Mohanty, Lawrence T. Drzal, and Raj Palsingh. "Recent advances in biodegradable nanocomposites." *Journal of Nanoscience and Nanotechnology* 5, no. 4 (2005): 497-526.
5. John, Maya Jacob, and Sabu Thomas. "Biofibres and biocomposites." *Carbohydrate polymers* 71, no. 3 (2008): 343-364.
6. Liu, Dagang, Tuhua Zhong, Peter R. Chang, Kaifu Li, and Qinglin Wu. "Starch composites reinforced by bamboo cellulosic crystals." *Bioresource technology* 101, no. 7 (2010): 2529-2536.
7. Rhim, Jong-Whan. "Potential use of biopolymer-based nanocomposite films in food packaging applications." *Food Science and Biotechnology* 16, no. 5 (2007): 691-709.
8. Kelfkens, M., and R. J. Hamer. "Agronomic factors related to the quality of wheat for the starch industry. Part II: Nitrogen fertilisation and overall conclusions." *Starch-Stärke* 43, no. 9 (1991): 344-347.
9. Liu, Dagang, and Lina Zhang. "Structure and properties of soy protein plastics plasticized with acetamide." *Macromolecular Materials and Engineering* 291, no. 7 (2006): 820-828.
10. Kumar, Rakesh, Dagang Liu, and Lina Zhang. "Advances in proteinous biomaterials." *Journal of Biobased Materials and Bioenergy* 2, no. 1 (2008): 1-24.
11. Liu, Dagang, Qinglin Wu, Huihuang Chen, and Peter R. Chang. "Transitional properties of starch colloid with particle size reduction from micro-to nanometer." *Journal of Colloid and Interface Science* 339, no. 1 (2009): 117-124.
12. Cao, Xiaodong, Yun Chen, Peter R. Chang, Mark Stumborg, and Michel A. Huneault. "Green composites reinforced with hemp nanocrystals in plasticized starch." *Journal of Applied Polymer Science* 109, no. 6 (2008): 3804-3810.
13. Park, Hwan-Man, Xiucuo Li, Chang-Zhu Jin, Chan-Young Park, Won-Jei Cho, and Chang-Sik Ha. "Preparation and properties of biodegradable thermoplastic starch/clay hybrids." *Macromolecular Materials and Engineering* 287, no. 8 (2002): 553-558.
14. Wilhelm, H-M., M-R. Sierakowski, G. P. Souza, and Fernando Wypych. "Starch films

reinforced with mineral clay." *Carbohydrate Polymers* 52, no. 2 (2003): 101-110.

- 15 Pareta, R., and M. J. Edirisinghe. "A novel method for the preparation of starch films and coatings." *Carbohydrate polymers* 63, no. 3 (2006): 425-431.
- 16 Park, Jong-Shin, June-Ho Yang, Dae-Hyun Kim, and Dae-Hoon Lee. "Degradability of expanded starch/PVA blends prepared using calcium carbonate as the expanding inhibitor." *Journal of applied polymer science* 93, no. 2 (2004): 911-919.
- 17 Schwach, Emmanuelle, and Luc Averous. "Starch-based biodegradable blends: morphology and interface properties." *Polymer International* 53, no. 12 (2004): 2115-2124.
- 18 Stepto, R. F. T. "Understanding the processing of thermoplastic starch." In *Macromolecular Symposia*, vol. 245, no. 1, pp. 571-577. Weinheim: WILEY-VCH Verlag, 2006.
- 19 Tomasik, Piotr, and Christopher H. Schilling. "Chemical modification of starch." *Advances in carbohydrate chemistry and biochemistry* 59 (2004): 175-403.
- 20 Chen, Biqiong, and Julian RG Evans. "Thermoplastic starch-clay nanocomposites and their characteristics." *Carbohydrate polymers* 61, no. 4 (2005): 455-463.
- 21 Mani, R., J. Tang, and Mrinal Bhattacharya. "Synthesis and characterization of starch-graft-polycaprolactone as compatibilizer for starch/polycaprolactone blends." *Macromolecular Rapid Communications* 19, no. 6 (1998): 283-286.
- 22 McGlashan, Stewart A., and Peter J. Halley. "Preparation and characterisation of biodegradable starch-based nanocomposite materials." *Polymer International* 52, no. 11 (2003): 1767-1773.
- 23 Moraru, Carmen I., Chithra P. Panchapakesan, Qingrong Huang, Paul Takhistov, Sean Liu, and Jozef L. Kokini. "Nanotechnology: a new frontier in food science." (2003).
- 24 Vasko, P. D., J. Blackwell, and J. L. Koenig. "Infrared and raman spectroscopy of carbohydrates.: Part II: Normal coordinate analysis of α -D-glucose." *Carbohydrate Research* 23, no. 3 (1972): 407-416.
- 25 Bellamy L. J. *Advanced in infrared group frequencies*. Methuen and Co. Ltd, Great Britain, 1998.

- 26 Liao, Hsin-Tzu, and Chin-San Wu. "Synthesis and characterization of polyethylene-octene elastomer/clay/biodegradable starch nanocomposites." *Journal of applied polymer science* 97, no. 1 (2005): 397-404.
- 27 Namazi, Hassan, and Mohsen Mosadegh. "Preparation and properties of starch/nanosilicate layer/polycaprolactone composites." *Journal of Polymers and the Environment* 19, no. 4 (2011): 980-987.
- 28 Matsuda, Daniel KM, Ana ES Verceheze, Gizilene M. Carvalho, Fabio Yamashita, and Suzana Mali. "Baked foams of cassava starch and organically modified nanoclays." *Industrial Crops and Products* 44 (2013): 705-711.
- 29 Kaushik, Anupama, Mandeep Singh, and Gaurav Verma. "Green nanocomposites based on thermoplastic starch and steam exploded cellulose nanofibrils from wheat straw." *Carbohydrate Polymers* 82, no. 2 (2010): 337-345.
- 30 Mathew, Aji P., and Alain Dufresne. "Morphological investigation of nanocomposites

- from sorbitol plasticized starch and tunicin whiskers." *Biomacromolecules* 3, no. 3 (2002): 609-617.
- 31 Blumstein, Alexandre. "Polymerization of adsorbed monolayers. II. Thermal degradation of the inserted polymer." *Journal of Polymer Science Part A: General Papers* 3, no. 7 (1965): 2665-2672.
 - 32 Burnside, Shelly D., and Emmanuel P. Giannelis. "Synthesis and properties of new poly (dimethylsiloxane) nanocomposites." *Chemistry of materials* 7, no. 9 (1995): 1597-1600.
 - 33 Qin, Huaili, Quansheng Su, Shimin Zhang, Bin Zhao, and Mingshu Yang. "Thermal stability and flammability of polyamide 66/montmorillonite nanocomposites." *Polymer* 44, no. 24 (2003): 7533-7538.
 - 34 Ide, Fumio, and Akira Hasegawa. "Studies on polymer blend of nylon 6 and polypropylene or nylon 6 and polystyrene using the reaction of polymer." *Journal of applied polymer science* 18, no. 4 (1974): 963-974.
 - 35 Zanetti, M.; Camino, G.; Peichert, P.; Mülhaupt, R. Thermal behaviour of poly(propylene) layered silicate nanocomposites. *Macromol. Rapid Commun.* 22, 176-180, 2001.

 - 36 Leszczyńska, A.; Njuguna, J.; Pielichowski, K.; Banerjee, J.R. Polymer/montmorillonite nanocomposites with improved thermal properties: Part I. Factors influencing thermal stability and mechanisms of thermal stability improvement. *Thermochim. Acta* 453, 75-96, 2007.

 - 37 Alexandre, Michael, and Philippe Dubois. "Polymer-layered silicate nanocomposites: preparation, properties and uses of a new class of materials." *Materials Science and Engineering: R: Reports* 28, no. 1-2 (2000): 1-63.
 - 38 Leszczyńska, A., James Njuguna, Krzysztof Pielichowski, and J. R. Banerjee. "Polymer/montmorillonite nanocomposites with improved thermal properties: Part II. Thermal stability of montmorillonite nanocomposites based on different polymeric matrixes." *Thermochimica Acta* 454, no. 1 (2007): 1-22.
 - 39 Ge, Jason J., Haoqing Hou, Qing Li, Matthew J. Graham, Andreas Greiner, Darrell H. Reneker, Frank W. Harris, and Stephen ZD Cheng. "Assembly of well-aligned multiwalled carbon nanotubes in confined polyacrylonitrile environments: electrospun composite nanofiber sheets." *Journal of the American Chemical Society* 126, no. 48 (2004): 15754-15761.
 - 40 Huxtable, Scott T., David G. Cahill, Sergei Shenogin, Liping Xue, Rahmi Ozisik, Paul Barone, Monica Usrey et al. "Interfacial heat flow in carbon nanotube suspensions." *Nature materials* 2, no. 11 (2003): 731.
 - 41 Krump, H., A. S. Luyt, and I. Hudec. "Effect of different modified clays on the thermal and physical properties of polypropylene-montmorillonite nanocomposites." *Materials Letters* 60, no. 23 (2006): 2877-2880.
 - 42 Yoon, P. J., T. D. Fornes, and Donald R. Paul. "Thermal expansion behavior of nylon 6

- nanocomposites." *Polymer* 43, no. 25 (2002): 6727-6741.
- 43 Shen, Liang, Yijian Lin, Qiangguo Du, and Wei Zhong. "Studies on structure–property relationship of polyamide-6/attapulgite nanocomposites." *Composites Science and Technology* 66, no. 13 (2006): 2242-2248.
- 44 Krump, H., A. S. Luyt, and I. Hudec. "Effect of different modified clays on the thermal and physical properties of polypropylene-montmorillonite nanocomposites." *Materials Letters* 60, no. 23 (2006): 2877-2880.
- 45 Liang, Zhu-Mei, Jie Yin, Jian-Hua Wu, Zi-Xue Qiu, and Fei-Feng He. "Polyimide/montmorillonite nanocomposites with photolithographic properties." *European polymer journal* 40, no. 2 (2004): 307-314.
- 46 Fu, Huei-Kuan, Shiao-Wei Kuo, Ding-Ru Yeh, and Feng-Chih Chang. "Properties enhancement of PS nanocomposites through the POSS surfactants." *Journal of Nanomaterials* 2008 (2008): 46.
- 47 Asif, A., V. Lakshmana Rao, V. Saseendran, and K. N. Ninan. "Thermoplastic toughened layered silicate epoxy ternary nanocomposites—Preparation, morphology, and thermomechanical properties." *Polymer Engineering & Science* 49, no. 4 (2009): 756-767.

Chapter: Three

Fabrication of Kaolinite/Choline Chloride Self-standing Porous Composite Bed for Filtration of Aqueous Dye Solution

Chapter Three

Abstract: Design and Engineering of composites from indigenous functional materials and synthetic biodegradable matrix are present demand to create a sustainable environment due to their outstanding applications in the field of advanced materials science and separation technology. Here, a pH induced self-standing composite porous bed have been fabricated from kaolinite and choline chloride and aqueous solutions of textile dyes (c.f. remazol red and methylene blue) have been treated. The composite bed was characterized using attenuated total reflectance infra-red (ATR-IR), x-ray diffraction (XRD), elemental analysis (EA), Thermogravimetric analysis (TGA) and scanning electron microscopy (SEM). It is revealed that the eluent collected after treating remazol red solution was absolutely free from dye whereas, methylene blue was passed through the bed from the very beginning. The effect of the thickness of bed on filtration was merely observed, but at lower pH (9.5) and higher pH (11.5), the bed shows very slow and almost steady flow rate respectively. Development of such technology from eco-friendly materials with satisfactory performance would play vital role in separation science in near future.

1. Introduction

Efficient removal of azo dyes from industrial effluents has been a long-standing technological challenge for the scientific community. Numerous researchers and their coworkers have employed several methods including physical, chemical, and biological approaches including coagulation,¹ membrane filtration,² ion-exchange,³ adsorption⁴ photo-degradation,⁵ enzymatic degradation⁶ etc. for the effective treatment of these recalcitrant dyes. To date, fixed-bed column adsorption has been one of the most widely used methods for separating hazardous pollutants from wastewater via filtration.⁷ Fixed-bed adsorption is advantageous over batch studies since large volume of wastewater can be continuously treated in this method using a small quantity of adsorbent.⁸ On the contrary, batch equilibrium experiments are applicable only in laboratory scale for treating small quantity of wastewater.⁹ The data obtained from fixed-bed adsorption experiments can be used as a benchmark to scale up for industrial applications.¹⁰

Different types of substrates have been used in fixed-bed column for isolation of toxic pollutants from wastewater such as activated carbon,¹¹ natural zeolites,⁷ chitosan-glutaraldehyde,⁹ *Eucalyptus sheathiana* bark,¹² chitin,¹³ chitosan,¹⁴ eggshells,¹⁵ sawdust,¹⁶ pine cone,¹⁷ carbon-alumina composite¹⁸ etc. However, major attention has been given on activated carbon since the commercial activated carbon has high surface area, porous structure, and good adsorption capacity.¹¹ However, the high cost for preparation and the difficulty in regeneration limits the industrial applications of activated carbon.⁹ Therefore, focus has been shifted towards cost-effective alternate materials.¹² In this regard, naturally occurring clay minerals appear as attractive candidate for detoxification of industrial hazards. The low cost, availability, high surface area, lack of toxicity, potential for ion-exchange, a variety of surface and structural properties, molecular (organic) adsorption-desorption properties and chemical and mechanical stability make ground for the widespread application of clay minerals in fixed-bed column.¹⁹⁻²² Srivastava et al. reported the removal of nitrate from drinking water by bentonite using fixed-bed column.²³ Baskan et al. reported the efficient adsorption of arsenic in fixed-bed column using natural and modified clinoptilolite.²⁴ The separation of copper in fixed-bed column from aqueous solution by chitosan-immobilized bentonite was studied by Futralan et al.²⁵ However, to the best of our knowledge, there is no report on the application of kaolinite based materials in fixed-bed column for separation of textile dyes from aqueous solution.

The free-flowing nature of powdered kaolinite restricts itself to be used in fixed-bed column for filtration purpose. Therefore, porous and channeled architecture should be made from kaolinite by appropriate modification with other materials. Here, choline chloride could be used as a suitable modifier, since it has already drawn attention from researchers for adsorption purpose. Wartelle et al. reported the adsorption of chromate ion by choline chloride modified agricultural by-products.²⁶ Karachalios et al. studied the removal of nitrate from water by quaternized pine bark using choline chloride based ionic liquid analogue.²⁷ The quaternary structure of choline helps adsorb various ionic pollutants from wastewater. Therefore, modification with choline chloride could greatly alter the surface chemistry of kaolinite for adsorption purpose.

The objective of this study was to successfully fabricate a self-standing porous composite bed for the filtration of textile dyes from aqueous solution. Here, we report that the negatively charged functionalities of the fabricated filter bed perfectly restricted the penetration of a model azo dye (anionic) at alkaline pH. The effect of various process parameters such as initial dye concentration, and solution pH were thoroughly investigated for proper evaluation of the filtration performance. We highly expect that the fabricated filter bed will draw commercial interest for applications in removal of hazardous dyes from the effluents of textile, paint, food, leather, pharmaceutical, printing, cosmetic, and other industries.

2. Experimental

2.1. Materials

Locally available kaolinite clay and choline chloride, purchased in dissolved form, were utilized in this study for the fabrication of porous filter bed. Purified sodium hydroxide pellets and ethanol were supplied by Active Fine Chemicals Limited (Dhaka, Bangladesh). The dye removal performance of the fabricated bed was investigated with an aqueous solution of Remazol Red. This model anionic azo dye was collected from a local textile industry in Bangladesh in an air-tight container.

2.2 Fabrication of self-standing bed structure

0.95 g of kaolinite was suspended in 25 ml distilled water in a beaker and stirred at room temperature (25 °C) for 4 hours. 2.5 ml of choline chloride with 0.38 g/ml density was gradually dropped into the kaolinite suspension in order to maintain 1:1 ratio (w/w) of kaolinite to choline

chloride solution. The resulting suspension was stirred in a magnetic stirrer for 4 hours. After 4 hours of stirring, the suspension was finely dispersed in a sonicator for 50 minutes. A syringe was cleaned properly with detergent, ethanol and distilled water and then dried. A small portion of cotton was put at the bottom of the syringe tube. The syringe was then filled with 20 ml co-solvent of 15% NaOH (w/w) and 95% ethanol (v/v) in a volume ratio of 4:1. The kaolinite-choline chloride liquid suspension was added dropwise through a dropper. The composite bed was thus formed in the syringe. The cotton in the bottom of the syringe was then removed and the co solvent solution was also discharged from the bed. The composite bed in syringe was dried at 100 °C for 8 hours until the bed was completely dry. It is to be noted that care was taken when preparing the bed so that there was no gap between the sidewall of the syringe and the bed.

2.3. Characterization

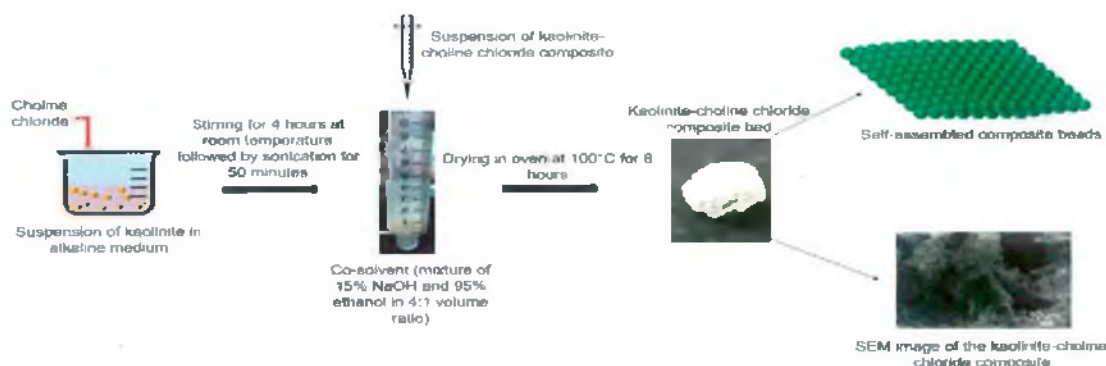
FTIR spectra of samples were recorded on a FTIR 8400S spectrophotometer (Shimadzu Corporation, Japan) in the wavenumber range of 4000–400 cm^{-1} ; the resolution was 4 cm^{-1} and the number of scans were 30. Approximately 1 mg of samples was ground with 100 mg KBr by agate mortar and then pellets were made from the mixture by applying pressure. The thermal degradation profiles (thermograms) of the samples were recorded on a thermogravimetric analyzer (TGA-50, Shimadzu, Japan). The samples were heated from room temperature to 800°C under nitrogen atmosphere at the flow rate of 10 ml/minute and at the heating rate of 10°C/minute using alumina cell. The weight of the samples varied from 4 to 10 mg. Total hold time at 800°C was 5 minutes. The elemental composition of the samples was determined by taking the EDS spectra of the material (EDS with the FESEM model JEOL JSM 7600F). Finally, the filtration performance of the samples was investigated by a UV-VIS spectrophotometer UV-2100PC (Human Lab Instrument Co., Korea). The morphology of the samples was analyzed by an analytical scanning electron microscope (JEOL JSM-6490LA, Tokyo, Japan) operated at an accelerating voltage of 20 kV in the back-scattered electron mode. XRD patterns of the samples were recorded by an x-ray diffractometer (Ultima IV, Rigaku Corporation, Japan) at room temperature. Cu K α radiation ($\lambda = 0.154\text{nm}$), from a broad focus Cu tube operated at 40 kV and 40 mA, was applied to the samples for the measurement. The XRD patterns of the samples were measured in the continuous scanning mode with scan speed of 3°/minute and in the scan range of 10 to 70°.

3. Results and Discussion

Chemically and thermally stable porous materials with interconnected channeled structures draw tremendous attention for potential applications in separation science due to their improved filtration efficiency. The dropwise and controlled addition of kaolinite/choline chloride mixture into a highly alkaline media in air resulted in the formation of composite beads (Scheme 3.1). The strong alkaline environment accelerated the breakdown of choline chloride and exposed the positive nitrogen terminal of the choline chloride. Performing the reaction in an aerated environment would also lead to the decomposition of the hydroxyl group of choline chloride (Reaction 1), as reported by Ramprasad et al.²⁸



The ensuing electrostatic chemical interaction between the positively charged N terminal of choline chloride and negatively charged surface of kaolinite resulted in the formation of the beads in the syringe. The newly formed composite beads settled to the bottom, where they came in contact with other beads resulting in self-assembled densely porous bed structures. In this fabrication process, the inner diameter of the syringe and cotton support at the bottom precisely controlled the shape of the fabricated filter bed. Hereafter, the composite bed will be denoted as K-C composite bed. Kaolinite in itself is a free flowing powder and cannot be molded into a self-standing bed while choline chloride can be synthesized in a strong film (Figure 3.1a and Figure 3.1b). The photo of the as synthesized self-standing K-C composite bed is reported in Figure 3.1c which showed the self-standing nature of the material.



Scheme 3.1: Fabrication process of kaolinite-choline chloride composite bed.

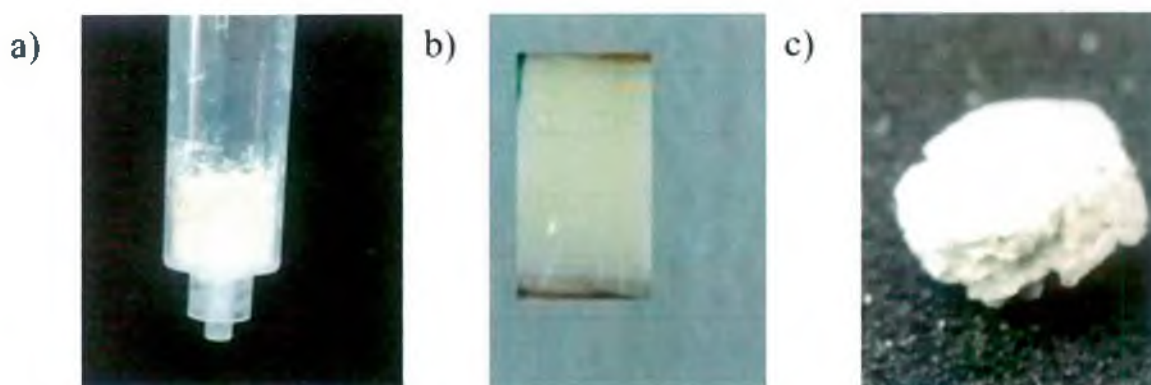


Figure 3.1: Comparison of the physical features of the composite components and the composite bed. a) Free flowing kaolinite (K) in powder form supported in a syringe, b) a film of choline chloride (C), and c) self-standing composite bed of kaolinite and choline chloride (K-C bed).

Figure 3.2a shows the FTIR spectra of kaolinite, choline chloride, and the K-C composite bed. The broad band in the green shaded region in the spectrum for choline chloride can be assigned for $\nu_{as} \text{OH}$.²⁹ Interestingly, this peak was absent in the K-C composite bed. This provided evidence that the OH group of choline chloride ($[\text{Me}_3\text{NCH}_2\text{CH}_2\text{OH}]^+\text{Cl}$) had decomposed, most probably through the reaction route provided in **Reaction 1**. The band in the yellow shaded region at around 1478 cm^{-1} in the FTIR spectrum for choline chloride (**Figure 3.2a**) could be assigned for ρCH_3 .²⁹ This particular vibration was still present in the K-C

composite bed. Hence, this proved the presence of choline chloride in the K-C composite bed and the lack of peak in the green shaded region was not just because of the absence of choline chloride in the final material. It also indicated that the CH_3 bond of the choline chloride remained unchanged during the fabrication of the composite bed. We further analyzed the pristine K-C composite bed through thermogravimetric analysis (Figure 3.2b). We included the thermogravimetric curve of kaolinite as a reference in order to pinpoint the contribution of the constituents towards the mass loss of the K-C composite bed during thermal analysis. From Figure 3.2b, the weight loss up to 100°C can be attributed to the loss of adsorbed water which accounted for about 7.8% of the total mass. There was a sharp weight loss (47.7%) from about less than 200°C till 386°C . This weight loss was mainly due to the decomposition of the choline chloride from the K-C composite bed. The remaining mass was due to the inorganic kaolinite phase (44.5%). It must be mentioned here that we synthesized the K-C composite bed with 1:1 ratio of kaolinite and choline chloride.

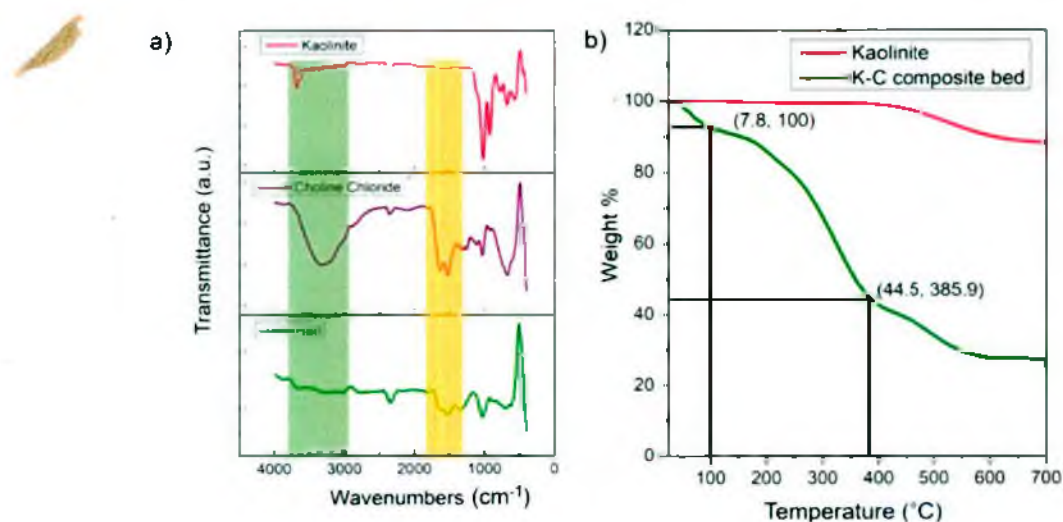


Figure 3.2: a) FTIR spectra of kaolinite, choline chloride and the K-C composite bed. The green shaded box and the yellow shaded box in the spectra highlight the regions where the difference in peaks of the three materials are observed. b) Thermogravimetric curve for kaolinite and the K-C composite bed.

As the amount of choline chloride and kaolinite almost had the same weight ratio, thermogravimetric analysis provided evidence that the composite bed was synthesized with the intended ratio of kaolinite and choline chloride. A full elemental composition of the K-C composite bed as determined from the energy dispersive X-ray spectroscopy (EDS) is provided in **Table 3.1**.

Table 3.1: Elemental composition of kaolinite-choline chloride composite bed determined through energy-dispersive X-ray spectroscopy (EDX).

Element	Mass (%)	Atom (%)
C	78.09	72.20
N	1.63	1.76
O	18.99	23.39
Na	0.3	0.53
Al	0.53	1.10
Si	0.45	0.97
Cl	0.02	0.06
Total	100.00	100.00

Figure 3.3 shows images of kaolinite and choline chloride modified kaolinite respectively. It is quite clear from the image of kaolinite that there were sharp edges and grains, denoted by arrows, due to its crystalline structures. When the kaolinite was modified with choline chloride, it lost sharpness and was covered by the soft, polymeric thin film, and displayed swollen wool like structures.

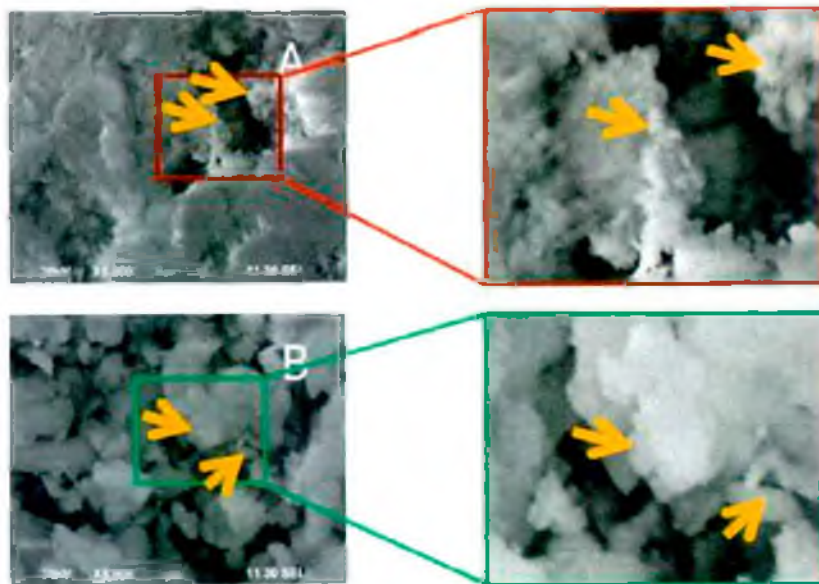


Figure 3.3: Electron microscope (SEM) images of kaolinite (A), modified kaolinite (B), respectively.

Figure 3.4a shows the SEM micrographs of the pristine K-C composite bed. The porous nature of the composite bed is evident from the images with average particle size being bigger than $10\mu\text{m}$. On the other hand, kaolinite itself has much smaller particle size with low porosity. The porous nature of the composite bed makes it an ideal candidate to be utilized as a medium for dye separation from aqueous solutions. XRD patterns of the K-C composite bed and kaolinite is reported in **Figure 3.4b**. The diffraction peaks at about 12° and 25° can be indexed to (001) and (002) crystal planes, respectively. The diffraction patterns of the composite bed closely resemble that of the kaolinite. However, a close inspection of the peaks of the two materials would reveal that there was a slight shift of the diffraction peaks towards the lower angle side for the composite material, meaning that the d spacing of the composite material is larger than the constituent kaolinite. This provided us evidence that rather than being a mere physical mixture of kaolinite and choline chloride, the constituents had a chemical interaction with each other in the final composite material. This slight shifting towards lower angle supports that choline chloride could be partially intercalated inside the galleries of kaolinite thereby forming a highly stable

composite bed structure. It has been widely reported in literature that intercalated composites display improved performance compared to the conventional composites.³⁰

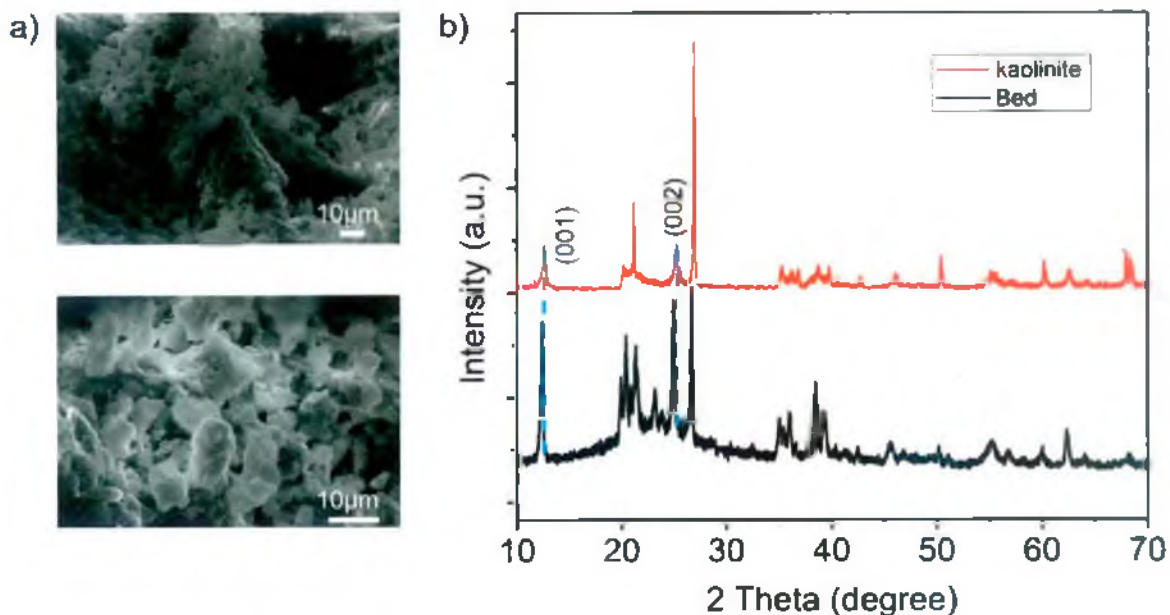


Figure 3.4: a) SEM micrographs of the K-C composite bed at different magnification. The porous nature of the bed is evident from the images. b) XRD pattern of kaolinite and the K-C composite bed. The dashed lines in the patterns indicate the relative positions of the peaks for the (001) and (002) crystal planes in kaolinite and the K-C composite bed.

Due to the porous nature of the K-C composite bed with a negatively charged choline functionality ($\text{Me}_3 \text{N}^+ \text{CH}_2 \text{CO}_2^-$), we hypothesized that the composite bed might facilitate to repulsive force for removal of anionic azo dyes from their aqueous solutions. This would provide an environmentally friendly solution of treating industrial effluent containing the hazardous azo dyes before it is discharged into the environment. In order to prove our hypothesis, we treated an aqueous solution of Remazol Red (RR), an anionic azo dye with the K-C composite bed. We treated a 50 ml 20 ppm aqueous solution of RR with the composite bed at a pH of 11.7. The justification of the chosen operating conditions is provided later. A setup similar to the one in **Figure 3.5a** was built in order to assess the efficiency of the K-C composite bed in removing RR from its aqueous solution. **Figure 3.5b** shows the UV/vis spectra of the dye solution before treatment with the bed and also for every 5 ml solutions after treatment with the bed. As can be

seen from the spectra, the aqueous solution of RR shows a peak at around 533 nm (**Figure 3.5b**). However, the solutions after treatment with the composite bed did not show any peak at all. This proves the efficient removal of RR from its aqueous solution. The absorbance of the treated solutions was equivalent to the background absorbance which signifies that almost all the RR dye was removed from the solution. The absorbance of all the treated solutions was close to the absorbance of water, further justifying our statement.

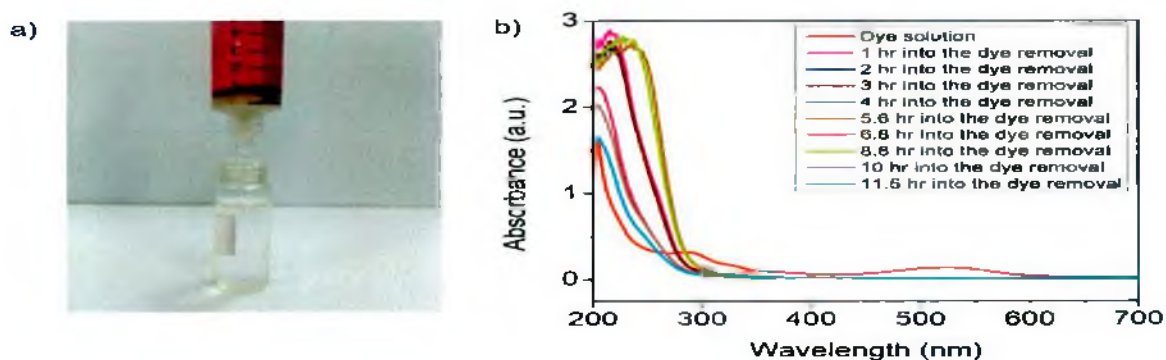


Figure 3.5: a) Photo of the setup for the aqueous Remazol Red treatment with the K-C composite bed. The thickness of the bed was 0.55 cm. b) UV/vis spectra of the treated solution at different time intervals. The time intervals represent the attainment of every 5 ml solution from the treatment with the K-C composite bed.

The highly efficient dye separation capability of the composite bed was exemplified by the accumulation of the removed RR on the surface of the composite bed (**Figure 3.6**). The efficient removal of anionic azo dye from the solution means that the dye is almost completely deposited just by the surface of the composite bed (**Figure 3.6a**) and the bulk of the bed was no further needed to remove the dye from the solution (**Figure 3.6b**). Thus, the efficiency of dye removal is independent of the bed thickness.

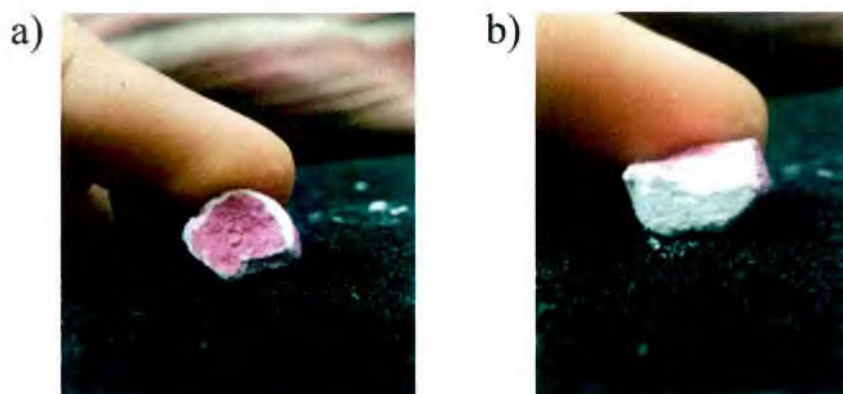


Figure 3.6: a) Surface of the K-C bed after Remazol Red from aqueous solution, and b) cross-sectional image of the bed after the dye removal. The images show all the removed dye is accumulated on the surface of the bed, rather than migrating in the bulk of the composite bed.

This must be noted here that we further attempted to remove the dye from its solution using kaolinite only (**Figure 3.7**). However, kaolinite was not as efficient as the K-C composite bed to remove dye from the solution and the loosely packed powder nature of kaolinite means that the dye solution would just flow right through it. Meanwhile, the choline chloride film was too firm and non porous for any solution to pass through it.

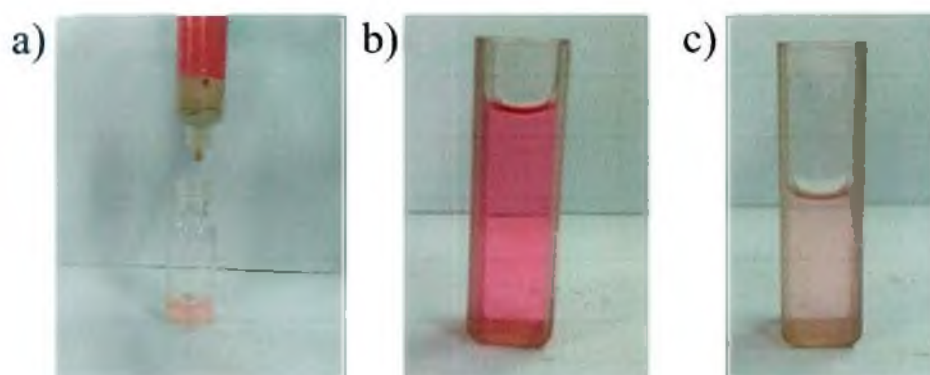


Figure 3.7: a) Setup of dye treatment with bare kaolinite powder supported on a syringe, b) solution of Remazol Red in a cuvette before treatment with kaolinite, and c) solution of Remazol Red in a cuvette after treatment with kaolinite.

To find out the optimum condition for efficient dye separation from its aqueous solution, the effect of dye concentration and pH on the time required for the dye solution to pass through the bed was studied. The thickness of the bed was chosen to be 0.5 cm. **Figure 3.8a** shows the influence of RR concentration on time required for collecting every 5 ml of treated solution. The pH of all the solutions were kept constant at 11.7. As can be seen from the figure, the time required for the dye removal increased as a function of increasing concentration. We suspect that at higher concentration, the accumulated dye on the surface of the composite bed would be blanketing the pores, making the passage of the solution progressively harder, hence requiring longer time. **Figure 3.8b** shows the influence of pH on the time required for collecting every 5 ml of the treated solution with the composite bed. The concentration of the RR solution was 20 ppm. The least time required among the two pH reported was at 11.7. At pH 9.1, the time required for collecting the solution increased significantly after a total collection of 15 ml solution and increased slowly thereafter. However, at pH 11.7, the time required for collecting every 5 ml solution was significantly lower than pH 9.1 and the time remained more or less the same throughout the dye removal operation. We did not perform the study beyond pH 11.7 because the highly alkaline solutions at a pH higher than 11.7 would pose an environmental threat in itself which would go against the overall goal of our research.

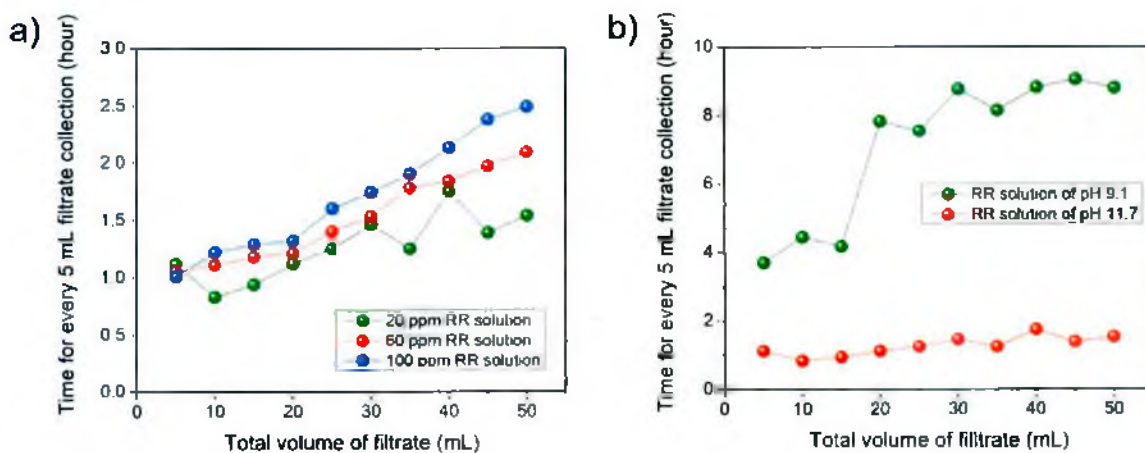


Figure 3.8: a) Effect of concentration of RR to the time required for filtrate collection after the treatment with the K-C composite bed, b) effect of pH on the time required for filtrate collection

after treatment of the RR solution with the K-C composite bed. The thickness of the bed was chosen to be 0.55 cm.

Moreover, the bed was ineffective at pH 7 or lower as the physical integrity of the bed was severely compromised (**Figure 3.9**). We suspect that the physical cohesion of the bed at lower pH is the underlying reason behind the observed trend in time required for collecting the solutions. The bed was synthesized in an alkaline condition. Hence, at lower pH, the bed might have a tendency to disintegrate, most probably through a hydrolysis reaction. This translates into having less porous structure at pH 9.1 and physical breakdown of beads at pH 7 to a film. Hence, pH values higher than 9.7 is best suited for efficient application of this composite. However, one does not need to go beyond pH 11.7 because at this pH, the dye removal was 100% and the speed of solution passing through the bed was also reasonably fast.

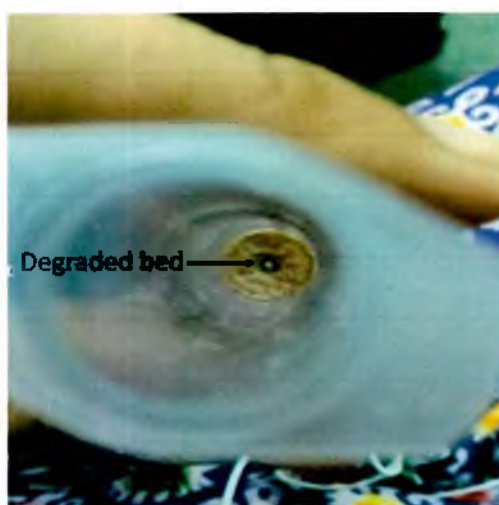


Figure 3.9: Degraded K-C composite bed upon treatment of Remazol Red solution at pH 7.

Conclusion: A self-standing and porous composite bed of kaolinite and choline chloride was synthesized with 1:1 w/w ratio of the constituents. Choline chloride and kaolinite had a chemical interaction with each other as determined through XRD and FTIR. The bed was highly efficient in removing RR dye from its aqueous solution. A 20 ppm aqueous solution at pH 11.7 was treated with the composite bed and the efficiency of dye removal was measured. It was found that the bed removed the dye from its solution with 100% efficiency. Due to the readiness of the dye removal at 20 ppm concentration by the composite bed, all the dye was removed by the surface of the bed and the bulk of the bed was not required to participate in the process. Hence, we found that the dye removal for this particular concentration was independent of bed thickness. Thus, we believe a competent bed for dye removal such as this would go a long way in answering the long lasting issues of water pollution due to textile industrial waste effluents.

References

1. Tang, Lipeng, Feng Xiao, Qunshan Wei, Yanbiao Liu, Yubin Zou, Jianshe Liu, Wolfgang Sand, and Christopher Chow. "Removal of active dyes by ultrafiltration membrane pre-deposited with a PSFM coagulant: Performance and mechanism." *Chemosphere* 223 (2019): 204-210.
2. Chen, Wensong, Jiahao Mo, Xing Du, Zhien Zhang, and Wenxiang Zhang. "Biomimetic dynamic membrane for aquatic dye removal." *Water research* 151 (2019): 243-251.
3. Hisada, Misaki, Yuriko Tomizawa, and Yoshinori Kawase. "Removal kinetics of cationic azo-dye from aqueous solution by poly- γ -glutamic acid biosorbent: Contributions of adsorption and complexation/precipitation to Basic Orange 2 removal." *Journal of Environmental Chemical Engineering* 7, no. 3 (2019): 103157.
4. M. M. Rahman, A. M. Zakaria, S. C. Dey, M. Ashaduzzaman and S. M. Shamsuddin, *Int. Lett. Chem. Phys. Astron.*, 2017, **75**, 25-36.
5. Z. Lu, G. Chen, W. Hao, G. Sun and Z. Li, *RSC Adv.*, 2015, **5**, 72916-72922.
6. A. N. Kagalkar, R. V. Khandare and S. P. Govindwar, *RSC Adv.*, 2015, **5**, 80505-80517.
7. Markovska, Liljana, Vera Meshko, and Vladimir Noveski. "Adsorption of basic dyes in a fixed bed column." *Korean Journal of Chemical Engineering* 18, no. 2 (2001): 190-195.
8. Gopal, N., M. Asaithambi, P. Sivakumar, and V. Sivakumar. "Continuous fixed bed adsorption studies of Rhodamine-B dye using polymer bound adsorbent." (2016).
9. López-Cervantes, Jaime, Dalia I. Sánchez-Machado, Reyna G. Sánchez-Duarte, and Ma A. Correa-Murrieta. "Study of a fixed-bed column in the adsorption of an azo dye from an aqueous medium using a chitosan–glutaraldehyde biosorbent." *Adsorption Science & Technology* 36, no. 1-2 (2018): 215-232.
10. Chakraborty, Sourja, Sirshendu De, Sunando DasGupta, and Jayanta K. Basu. "Adsorption study for the removal of a basic dye: experimental and modeling." *Chemosphere* 58, no. 8 (2005): 1079-1086.
11. N. Mohanraj, P. Mohanraj, S. Bhuvaneshwari and J. A. Ebinesar, (2018). *Chem. Eng. Processing: Process Intensification.*, 2018, **130**, 160-168.
12. Afroze, Sharmeen, Tushar Kanti Sen, and H. M. Ang. "Adsorption performance of continuous fixed bed column for the removal of methylene blue (MB) dye using *Eucalyptus sheathiana* bark biomass." *Research on Chemical Intermediates* 42, no. 3 (2016): 2343-2364.
13. McKay, G., H. S. Blair, and J. R. Gardner. "The adsorption of dyes onto chitin in fixed bed columns and batch adsorbers." *Journal of Applied Polymer Science* 29, no. 5 (1984): 1499-1514.
14. AL-THARWANI, INTIDHAR JABIR IDAN. "REMOVING REACTIVE AND ACID DYES FROM SINGLE AND BINARY SOLUTIONS BY ADSORPTION ON QUATERNIZED KENAF CORE FIBERS." (2017).
15. M. Chafi, S. Akazdam, C. Asrir, L. Sebbahi, B. Gourich, N. Barka and M. Essahli, *Int. J. Chem. Mol. Nucl. Mater. Metall. Eng.*, 2015, **9**, 1242-1248.
16. S. K. Singh, D. Katoria, D. Mehta and D. Sehgal, *Int. J. Adv. Res.*, 2015, **3**, 521-529.

17. Yagub, Mustafa T., Tushar Kanti Sen, Sharmeen Afroze, and Ha Ming Ang. "Fixed-bed dynamic column adsorption study of methylene blue (MB) onto pine cone." *Desalination and Water Treatment* 55, no. 4 (2015): 1026-1039.
18. Dutta, M., and J. K. Basu. "Fixed-bed column study for the adsorptive removal of acid fuchsin using carbon–alumina composite pellet." *International Journal of Environmental Science and Technology* 11, no. 1 (2014): 87-96.
19. Adeyemo, Aderonke Ajibola, Idowu Olatunbosun Adeoye, and Olugbenga Solomon Bello. "Adsorption of dyes using different types of clay: a review." *Applied Water Science* 7, no. 2 (2017): 543-568.
20. Y. M. Chen, T. M. Tsao and M. K. Wang, *Int. Conf. Environ. Sci. Eng.*, 2011, *IPCBE*, 8, 252-254.
21. Gürses, A., Ç. Dođar, M. Yalçm, M. Açıkyıldız, R. Bayrak, and S. Karaca. "The adsorption kinetics of the cationic dye, methylene blue, onto clay." *Journal of Hazardous Materials* 131, no. 1-3 (2006): 217-228.
22. Murray, Haydn H. "Traditional and new applications for kaolin, smectite, and palygorskite: a general overview." *Applied clay science* 17, no. 5-6 (2000): 207-221.
23. A. Srivastava, P. K. Singh, *Int. J. Eng. Res. Technol.*, 2017, 6, 390-394.
24. Baskan, Meltem Bilici, and Aysegul Pala. "Batch and fixed-bed column studies of arsenic adsorption on the natural and modified clinoptilolite." *Water, Air, & Soil Pollution* 225, no. 1 (2014): 1798.
25. Futralan, Cybelle Morales, Chi-Chuan Kan, Maria Lourdes Dalida, Chelo Pascua, and Meng-Wei Wan. "Fixed-bed column studies on the removal of copper using chitosan immobilized on bentonite." *Carbohydrate polymers* 83, no. 2 (2011): 697-704.
26. Wartelle, Lynda H., and Wayne E. Marshall. "Chromate ion adsorption by agricultural by-products modified with dimethyloldihydroxyethylene urea and choline chloride." *Water research* 39, no. 13 (2005): 2869-2876.
27. Karachalios, Antonis, and Mahmoud Wazne. "Nitrate removal from water by quaternized pine bark using choline based ionic liquid analogue." *Journal of Chemical Technology & Biotechnology* 88, no. 4 (2013): 664-671.
28. Dorai Ramprasad, W. Eamon Carroll, Francis J. Waller and Thomas Mebrahtu, in *8th Conference on Catalysis of Organic Reactions*, Charleston, SC, 2000.
29. Du, Cuiling, Binyuan Zhao, Xiao-Bo Chen, Nick Birbilis, and Haiyan Yang. "Effect of water presence on choline chloride-2urea ionic liquid and coating platings from the hydrated ionic liquid." *Scientific reports* 6 (2016): 29225.
30. Bhattacharya, Mrinal. "Polymer nanocomposites—a comparison between carbon nanotubes, graphene, and clay as nanofillers." *Materials* 9, no. 4 (2016): 262.

Chapter: Four

Studies on Mechanical Properties of PMMA/Choline Chloride Modified Kaolinite Nanocomposite Films

Chapter Four

Abstract: Composites materials produced from indigenous nano-scale particles and synthetic polymers have created demand in the field of nanoscience and technology. Layered silicates are a potential candidate for reinforcing the properties of composites. Here, we report the fabrication of nanocomposites using poly (methylmethacrylate, PMMA) as matrix and bijoypur clay known as kaolinite (200-250 nm) as filler via solution casting. Kaolinite was first modified using choline chloride to prepare core-shell particle through precipitation technique and was used for self-assembled nano-composite film preparation. A series of nano-composites films using 0, 1, 3, 5 and 10% w/w modified kaolinite was prepared. The neat PMMA and nanocomposites films were characterized by attenuated total reflection infra-red (ATR-IR), X-ray diffraction (XRD). The mechanical properties, thermal stability and morphology of the films were investigated using universal testing machine (UTM), thermal gravimetric analysis (TGA) and scanning electron microscope (SEM). The nanocomposite films exhibited better mechanical properties and thermal stability than neat PMMA film. Development of such nano-composites materials from naturally occurring nano-scale particles would play crucial role in the field of materials science for packaging applications and separation technology.

1. Introduction

Nanoscale indigenous layered material and polymer composites are of great interest to the researchers due to the environmental considerations¹⁻⁵. Nanostructured layered silicates incorporate higher mechanical, thermal stability, and barrier properties in the composite materials at relatively low filler contents compared to those of conventional composites⁶⁻¹⁰. The available naturally occurring nanostructures are montmorillonite, clay, silica and calcium carbonate. Kaolinite is composed of white, soft, and highly refractory clay particles¹¹. Hydrated kaolinite maintains aluminosilicate with a 1:1 layered structure consisting of an octahedral aluminum hydroxide sheet and a tetrahedral silica sheet¹². Due to the inherent rigid characteristic of a layered structure, kaolinite is not susceptible to interactions with functional polymers. Chemically modified kaolinite incorporates interfacial properties which can promote the compatibility and dispersion of the particles into a polymer matrix. Treatment of particles with epoxy functional silane coupling agent has been extensively used to examine the properties of calcined kaolinite (CKao), TiO₂ in polyethylene terephthalate (PET) composites¹³⁻¹⁶. Polymer/clay nanocomposites is an interesting and very promising research area due to cost effectiveness, their high specific surface area, and their ease of availability from natural resources¹⁷⁻¹⁹. Recently work has been focused on developing polymer/clay nanocomposites using various polymers, such as polypropylene (PP), polyamide, polyimide, nylon, polystyrene (PS), ethylene vinyl acetate copolymer, polyethylene terephthalate, polyurethane, low density polyethylene (LDPE), high density polyethylene (HDPE), epoxy, PS/HDPE, PP/HDPE, and PP/LDPE²⁰⁻²⁵. A number of clay types have been used, including kaolinite, Illite, Bentonite, Chlorite, and Montmorillonite^{26,27}. On the other hand, considering the outstanding mechanical properties, thermal capability and electric performance, poly(methylmethacrylate) (PMMA) has been widely used as the matrix. Many potential applications²⁸ of PMMA have evoked intense interest in PMMA based composites. As a result, many composites of PMMA-clay have been prepared by suspension polymerization, emulsion polymerization, and bulk polymerization, etc.²⁹⁻³¹. But PMMA-choline chloride modified kaolinite composites are rare.

In the last few years, researchers have begun to fabricate PMMA based composites. In 2015, Kumar, et al.³² reported nanocomposites consisting of poly(methyl methacrylate) (PMMA)/clay

with different compatibilizers (PP-g-MA, PE-g-MA and PS-g-MA), with 5 wt % nanoclay. Poly(methyl methacrylate) (PMMA) and montmorillonite (MMT), modified with 15–35 wt % octadecylamine and 0.5–5 wt % aminopropyltriethoxysilane, and different compatibilizers, such as polypropylene-grafted maleic anhydride (PP-g-MA), polyethylene-grafted maleic anhydride (PE-g-MA), and polystyrene-block-poly(ethylene-ran-butylene)-block-polystyrene-graft-maleic anhydride (PS-g-MA) were used. In 2014, Nabirqudri, et al.³³ developed composites films using poly(methyl methacrylate) and cocoamphodipropionate modified montmorillonite. In 2006, Hani, et al.³⁴ reported nanocomposites of dehydrogenated tallow quaternary ammonium modified montmorillonite clay and poly(methylmethacrylate), and also described the effect of nanoclay on mechanical properties. Besides, in 2012, Modak, et al.³⁵ reported a well-dispersed poly(methylmethacrylate) (PMMA)–bentonite clay composite by emulsion polymerization using methyl methacrylate (MMA) monomer and 3% sodium carbonate treated bentonite clay. Hydrophilic kaolinite surface is thermodynamically incompatible with most hydrophobic and thermoplastic polymers of commercial importance, such as poly(methylmethacrylate) (PMMA), polypropylene³⁶, and polyethylene³⁷. For favorable thermodynamic interactions at the molecular level of a specific polymer with kaolinite, organic modification of the kaolinite is required. Therefore, for the first time, we have used choline chloride as the modifying agent to prepare a new composite material. Choline chloride contains amino (–NH₂) and hydroxyl (–OH) functional groups, which can serve as coordination and reaction sites, and as a result it is used as an adsorbent. Negatively charged kaolinite is electrostatically interacted with by protonated amine groups (–NH₃) of choline chloride to form a choline chloride modified kaolinite. In this article, we have fabricated PMMA/choline chloride modified, kaolinite nanocomposite, self-assembled films by solution casting. This film would show improved mechanical properties and thermal stability, and can be used for advanced applications in the field of frontier science and technology.

2. Experimental

2.1. Materials

Kaolinite was collected from Bijoypur (Netrokona, Bangladesh). It was white crystalline powder. Poly(methylmethacrylate), (PMMA) (Mw 1,20,000) was procured from Sigma-Aldrich (Stockholm, Sweden). Choline chloride solution (40% w/w) was procured from Puyer (Nantong) BioPharma Co., LTD., Nantong, China. NaOH was supplied by Active Fine Chemicals Limited, Dhaka, Bangladesh. Ethanol and chloroform (CH₃Cl) were purchased from Merck KGaA, 64271 Darmstadt, Germany.

2.2. Methods

2.2.1. Modification of Kaolinite by Choline Chloride

In the present study, choline chloride modified kaolinite was prepared by adsorption onto the negatively charged kaolinite with protonated choline chloride. 0.95 gm pure kaolinite was suspended in 25 mL distilled water in a beaker and it was stirred at room temperature. Then 2.5 mL choline chloride was gradually dropped into the kaolinite suspension where the ratio (w/w) of kaolinite and choline chloride solution was maintained at 1:1. The resulting suspension was stirred with a hot plate with magnetic stirrer for 4 h. After 4 h, the resulting suspension was agitated by a sonicator for 50 min. Then the suspension was sprayed drop wise through a dropper at a constant rate into the 20 mL co-solvent of aqueous sodium hydroxide (15%) and ethanol (95%) (4:1) to maintain a pH of about 10. Then the composite was separated by filtration. The formed composite bead was washed with deionized water until the solution became neutral. The composite bead was dried in the oven at 60°C for 10 h. This way the modification of kaolinite by choline chloride was done.

2.2.2. Fabrication of Poly(methylmethacrylate)/Choline Chloride Modified Kaolinite PMMA/CCMK Nanocomposite Films

Five films with different weight ratios of choline chloride modified kaolinite (CCMK) and poly(methylmethacrylate) (PMMA) were prepared as shown in **Table 4.1**.

Table 4.1: Compositional variation of nanocomposite films produced from poly(methylmethacrylate) (PMMA) and choline chloride modified kaolinite (CCMK).

Composite Identity	PMMA % (w/w)	CCMK % (w/w)	PMMA:CCMK
CK ₀ PNC	100	0	100:0
CK ₁ PNC	99	1	99:01
CK ₃ PNC	97	3	97:03
CK ₅ PNC	95	5	95:05
CK ₁₀ PNC	90	10	90:10

At first, 3 mL solution of PMMA in chloroform (CH₃Cl) was taken in each five different small glass vials. Then after leaving one vial (without addition of CCMK), 10, 30, 50 and 100 mg of CCMK were charged into the vials containing PMMA solution and stirred for 5 min. The resulting suspensions were sonicated with the help of a microprocess controlled bench-top ultrasound cleaner (sonicator) for 5 min and the sonicated mixtures were allowed to stir for 5 min again to make a homogenous suspension. The clear suspensions were then cast onto five glass frames (length and width of the glass plates were 7.62 cm and 2.54 cm respectively) and then the suspensions were turned into films via atmospheric drying for 48 h as shown in **Figures 4.1** and **Figure 4.2**. The dried films were then pulled out from the glass frame and cut into desired pieces for different purposes of use. Each of the sample films were subjected to analysis, and twice fabricated from the three batches of each composition.

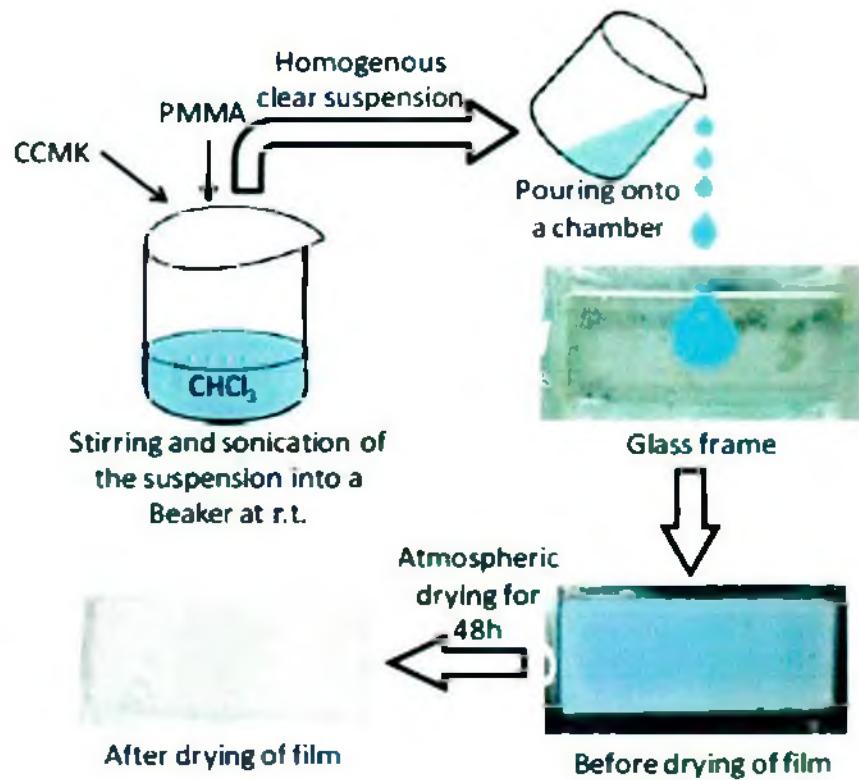


Figure 4.1: Schematic illustration for the fabrication of composite film from choline chloride modified kaolinite (CCMK) and PMMA.

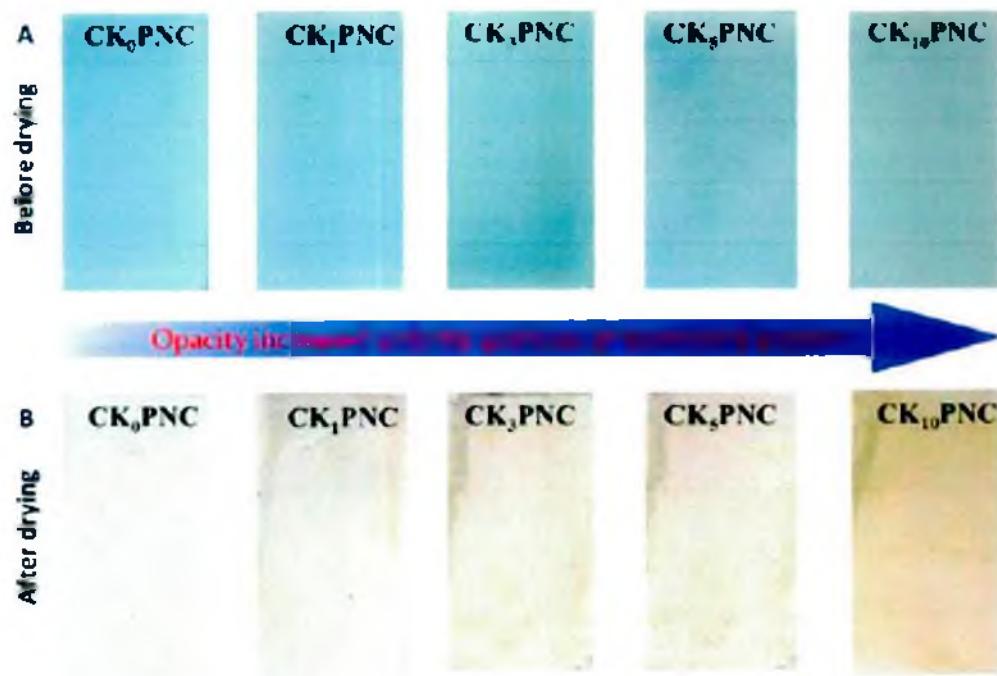


Figure 4.2: Camera images of nanocomposite films before (A) and after drying (B).

2.2.3. Characterization

ATR-IR spectra of samples were recorded on a FT-IR Shimadzu IR Prestige 21 (Shimadzu, Corporation, Kyoto, Japan) in the wave number range of 4000–400 cm^{-1} ; resolution: 4 cm^{-1} ; scan number 30. The samples were examined by an x-ray diffractometer (Ultima IV, Rigaku Corporation, Tokyo, Japan) at room temperature. At first, the samples were ground into fine powders using a mortar and pestle. Cu K α radiation ($\lambda = 0.154 \text{ nm}$), from a broad focused Cu tube operated at 40 KV and 40 mA, was applied to the samples for measurement. The XRD patterns of the samples were measured in the continuous scanning mode with a scan speed 5°/min and in the scan range of 10 to 60°. Bragg's law was used to compute the basal spacing of the crystalline samples. The thermogravimetric analyses of the samples were recorded on a thermogravimetric analyzer TGA-50H (Shimadzu, Kyoto, Japan). The samples were heated from room temperature to 700°C under a nitrogen atmosphere at the flow rate of 19 mL/min and at the heating rate of 10°C/min using an alumina cell. The weight of the samples was taken to be 10 mg for the experiment. Total hold time at 700°C was 5 min. The mechanical properties, tensile strength (TS), and elongation at break (Eb) of the nanocomposite films were examined with a universal strength tester machine (Titan, model 1410-Titan5, Shanghai, China). The film length and width used were 50 mm and 20 mm, respectively. Dry films with an average thickness of around 150 μm were obtained by measuring with a Phynix digital micrometer. All the test samples were conditioned at 20°C and 50% relative humidity. All the tests were carried out under the same conditions. The following equations were used to measure the tensile properties.

$$\text{Tensile strength, TS (MPa)} = \frac{\text{Load}}{\text{Thickness} \times \text{Width}} \text{ and Elongation at break, Eb (\%)} = \frac{\text{Displacement}}{\text{Gauze Length}}$$

The morphology of the samples was analyzed by an analytical scanning electron microscope (JEOL JSM-6490LA, Tokyo, Japan) operated at an accelerating voltage of 20 kV. In order to get further insight into the morphology, microstructures of the samples were examined at the 5 μm scale with 500 magnifications without coating, and using an only partial vacuum.

3. Results and Discussion

3.1. ATR-IR Spectral Analysis

A comparison of the ATR-IR spectrum of nanocomposites produced using 1, 3, 5, and 10% (w/w) modified choline chloride kaolinite, self-assembled in PMMA and neat PMMA is shown in **Figure 4.3**. The band around 3690 cm^{-1} assigned for kaolinite was absent in the nanocomposite film fabricated using 1% w/w CCMK (curve D in **Figure 4.3**), but the peak gradually appeared as the kaolinite content increased, as shown in the curves A–C in **Figure 4.3**. The absorption band at 1730.15 cm^{-1} is the characteristic peak at PMMA polymer which denotes the $>\text{C}=\text{O}$ group present in the PMMA polymer (curve E in **Figure 4.3**). The band at 943.19 cm^{-1} is the $-\text{C}-\text{H}$ bending vibration together with the bands at 1028.06 cm^{-1} and 852.54 cm^{-1} in the acrylate group in PMMA³². The band at 1452.40 cm^{-1} can be attributed to the bending vibration of the $\text{C}-\text{H}$ bonds of the $-\text{CH}_3$ group. The two bands at 2931.80 cm^{-1} and 2872.01 cm^{-1} were assigned to the $\text{C}-\text{H}$ bond stretching vibrations of the $-\text{CH}_3$ and $-\text{CH}_2-$ groups, respectively. Furthermore, there was another weak absorption band at 3446.79 cm^{-1} which was attributed to the $-\text{OH}$ group stretching of physisorbed moisture³⁸. The absorption bands at 1107.14 cm^{-1} , 1161.15 cm^{-1} , and 1247.87 cm^{-1} were attributed to the $\text{C}-\text{O}-\text{C}$ stretching vibration. The two bands at 1381.03 cm^{-1} and 763.81 cm^{-1} were attributed to the methyl group vibrations. The characteristic absorption band at 1730.15 cm^{-1} represents stretching vibration of $\text{C}=\text{O}$ of pure PMMA. In all composite films, the stretching vibration of carbonyl group ($\text{C}=\text{O}$) group appearing at the frequency of 1730.15 cm^{-1} for pure PMMA moves to lower positions at 1720 cm^{-1} . Furthermore, the absorption peak at 3446.79 cm^{-1} assigned for OH stretching in PMMA was also shifted to 3393 cm^{-1} . In addition, the absorption band at 1166 cm^{-1} for the $\text{C}-\text{O}-\text{C}$ stretching vibration of PMMA was shifted to 1150–1161 cm^{-1} in nanocomposites films. That result proves that there was an interaction between CCMK and PMMA molecular chains³⁹.

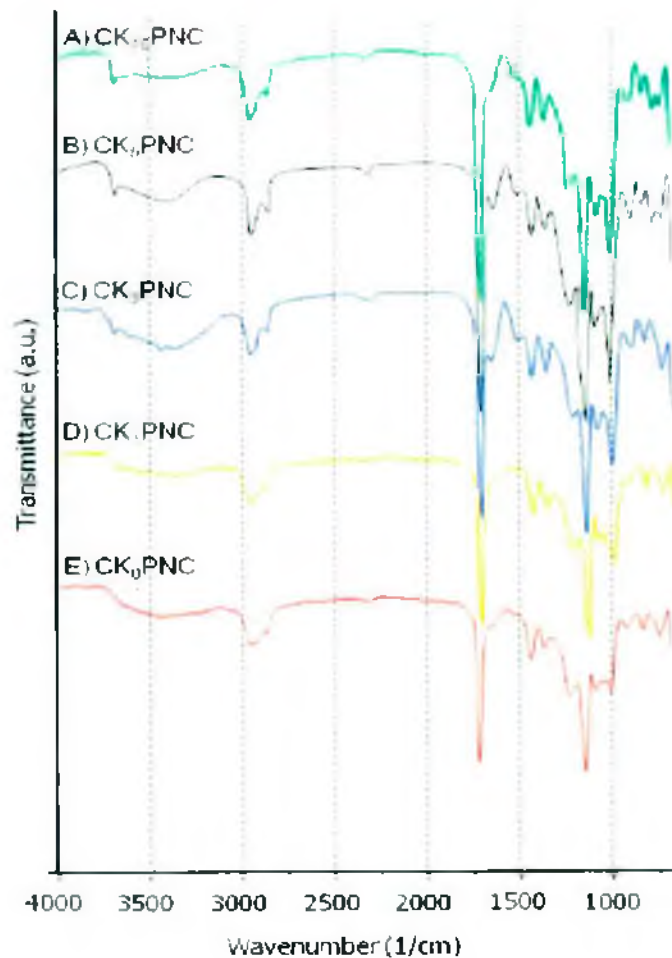


Figure 4.3: A Attenuated total reflection infra-red (ATR-IR) spectra of films produced from nanocomposite of poly(methylmethacrylate) (PMMA) and choline chloride modified kaolinite (CCMK). (A) CK₁₀PNC (B) CK₅PNC, (C) CK₃PNC, (D) CK₁PNC and neat PMMA.

3.2. XRD Analysis

In the **Figure 4.4A** the broad peak at the position (2θ) with d-spacing was found for the crystalline segment of PMMA in neat film which was almost unchanged in the nanocomposite films of CK₁₀PNC. Furthermore, the sharp peaks in the nanocomposite films indicate the presence of kaolinite, and these peaks were in the similar positions of pure kaolinite. The non-variable and

non-shifting of peak position clearly indicates that the nanocomposites consisted of un-intercalated nor adhered kaolinite, due to the electrostatic interaction.

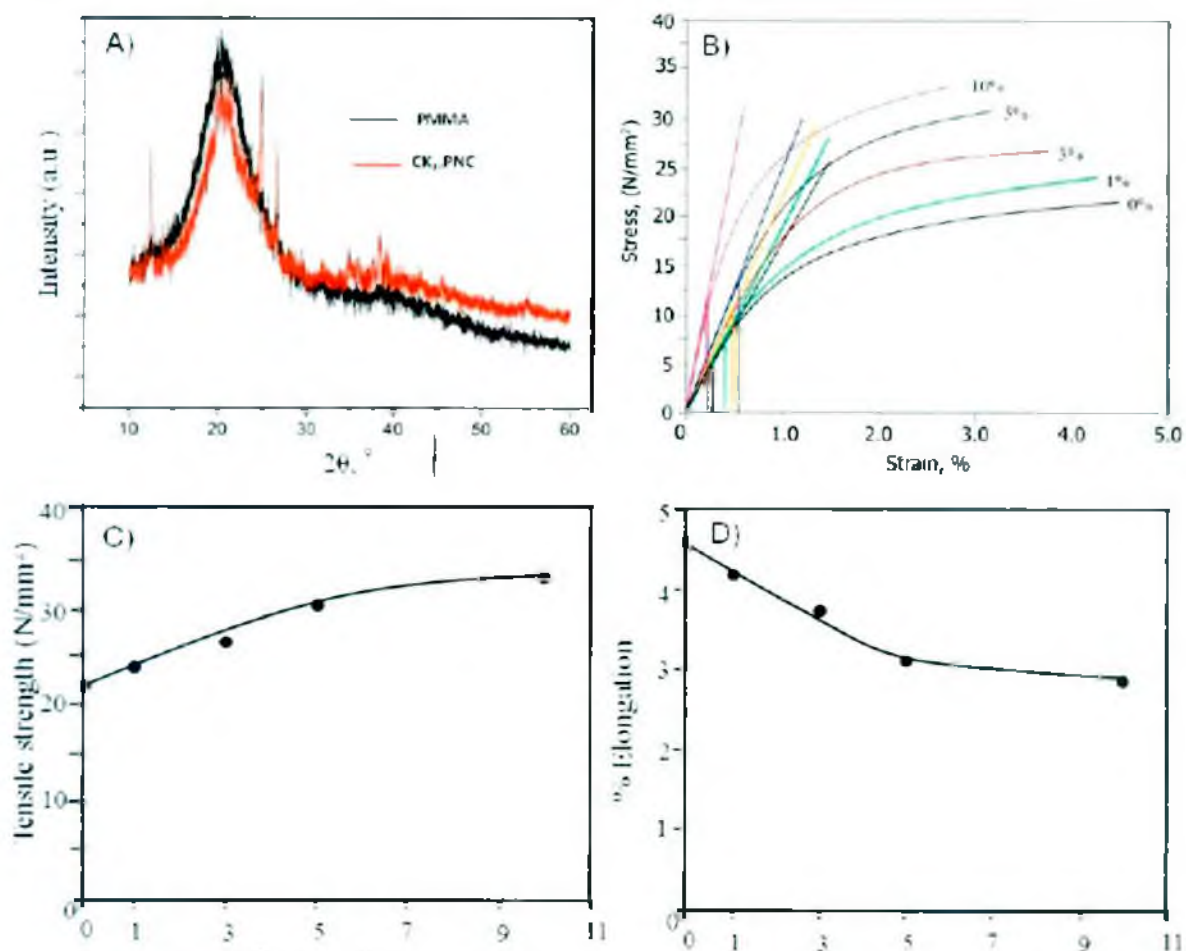


Figure 4.4: XRD patterns of CK₀PNC, CK₁₀PNC. (A) Stress versus strain (%) curve. (B) The effect of modified kaolinite on the tensile strength (N/mm^2) of nanocomposite films. (C) The effect of CCMK on the elongation at break (%) of the PMMA/CCMK nanocomposite films (D).

3.3. Studies of Mechanical Properties of Nanocomposite Films

Films fabricated from neat PMMA and choline chloride modified kaolinite composites were subjected to various kinds of stress in order to study the mechanical properties for determining the performance of the structural materials^{40,41}. With the view of these objectives, strain-stress

relationships of the fabricated films has been investigated, first with the **Figure 4.4B**, later with the tensile strength and elongation at break of films plotted as a function of the choline chloride modified kaolinite contents and CK5PNC, as shown in **Figure 4.4.(C,D)** for deep discussion.

3.3.1. Stress–Strain Relationship

Figure 3.4B shows the engineering stress–strain relationship curve (tensile) for self-assembled nanocomposite films with different quantities of CCMK. The tensile property of a material is shown by its stress–strain curve. Strain at yield was found to increase linearly with applied stress. It reaches maximum and then falls down. The curves have two regions—one is elastic region and another is plastic region. From the **Figure 4.4B**, it was found that composites deform elastically and then plastic deformation starts. The vertical lines parallel to the y-axis from the strain at yield point separate elastic and plastic zones of corresponding engineering stress versus strain curve; the area in the left zone is called elastic zone, where the reversible deformation occurs, and the right zone is where the permanent deformation occurs up to the break or failure. The film produced from neat PMMA (0%) shows the minimum elasticity and maximal plastic behavior; it indicates that the reversible deformation occurs within a very short range of 0.25% strain at yield. As the addition of modified kaolinite increased from 0 to 10% w/w, the strain at yield was first increased from 0.25 to 0.60% for CK₅PNC films, and then decreased to 0.20% for CK₁₀PNC. It means that the matrix PMMA was sufficient to cover the CCMK particles and to form a kaolinite cored, PMMA-thick, shell-based homogeneously dispersed film produced from CK₅PNC. But in case of CK₁₀PNC film, the PMMA matrix was not sufficient to cover in that manner, as was the case for the CK₁PNC to CK₅PNC films formed. Therefore, the particles were agglomerated, and the soft insufficient polymeric phase became hard and brittle. As a result, CK₅PNC film shows higher tensile strength (stress) than that of CK₁₀PNC film.

3.3.2. Tensile Strength Measurement

The tensile strength of the fabricated films was measured and plotted against the modified kaolinite content, as shown in the **Figure 4.4C**. It is observed that the tensile strength of the nanocomposite was increased with the increase of choline chloride modified kaolinite content, up to 5% w/w, and then it was slowed down. The tensile strength of the neat PMMA film

CMKNC was 22 N/mm². However, for CMK₅NC film, the tensile strength was 31 N/mm² and for CMK₁₀NC film, the tensile strength was 33 N/mm². It is clear that the rate of increment of tensile strength up to 5% was higher than the rate within the range of 5 to 10% modified kaolinite.

3.3.3. Elongation at Break

The influence of choline chloride modified kaolinite in nanocomposites films on the elongation at

break is shown in **Figure 4.4D**. It is evident that elongation at break rapidly declined with the increase of CCMK down to 5% by weight but very slowly decreased after 5% CCMK content in nanocomposites films. The elongation of break of neat PMMA film (CK₀PNC) was about 4.6%. However, at 5% CCMK containing film (CK₅PNC), the elongation at break of the film was decreased drastically to 2.9%. **Figure 4.5** shows the schematic illustration, starting from the left with neat PMMA film, denoted as CK₀PNC, possess polymeric crystalline phase only. In the absence of CCMK (fillers), polymer film becomes very soft. With the addition of CCMK, the crystalline phase was increased in the nanocomposite film. Therefore, due to the choline chloride shell of CCMK, the PMMA matrix attached strongly with the interface and controlled the thickness of the layer (steyn or boundary layer) around the CCMK, as evident on the right of **Figure 4.5**. Since sufficient PMMA matrix remained in the CK₁PNC film, the elastic and plastic behavior did not change remarkably when compared to neat PMMA (CK₀PNC) film. The film CK₅PNC contained 5% CCMK; the whole PMMA matrix was used to cover the interface equally, and self-assembled stable CCMK incorporated better mechanical properties.

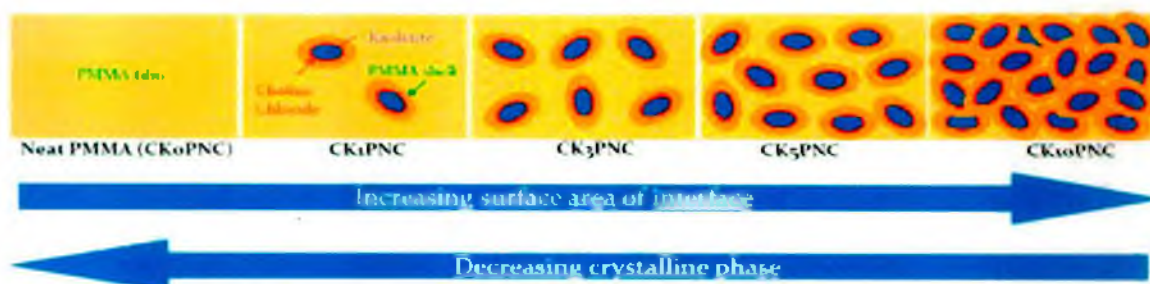


Figure 4.5: Schematic illustrations of neat PMMA film and the composite films to show the impact on interface and crystallinity of modified kaolinite.

3.4. Thermo Gravimetric Analysis (TGA)

The TGA thermogram of neat PMMA showed the weight loss profile at various temperatures, as shown in Figure 4.6. The first weight loss step was seen in the temperature range of 22–100 °C, corresponding to the weight loss of moisture (around 6%). Under nitrogen flow, a non-oxidative thermal degradation occurs in pure PMMA, which was observed in the temperature range of 280–430°C, indicating the de-propagation to the end of PMMA chain, first order termination of the PMMA chain, vaporization, and elimination of volatile products⁴². The degradation of PMMA is accelerated above 280°C owing to the formation of crosslinked and cyclic structures. However, the PMMA degradation appears to proceed by side-group depolymerization and random-chain scission depolymerization along with the diffusion of gas-phase nitrogen⁴³. It degrades to tertiary alkyl free radical or secondary alkyl free radical, and the methyl methacrylate monomer or tertiary free radical. A char formation occurs after 400°C, and was decomposed at about 450°C leaving residue of about 1.6% w/w at the final temperature 700°C.

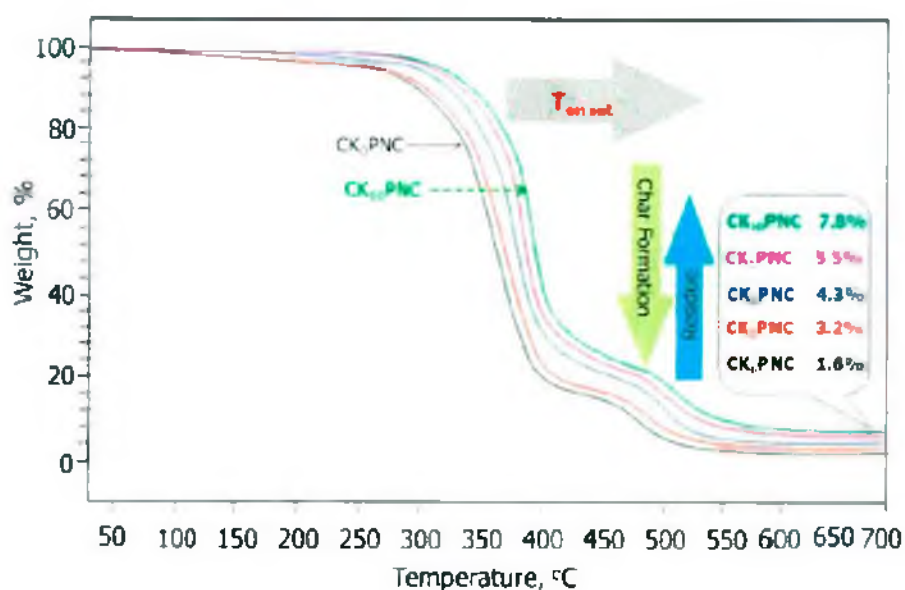


Figure 4.6: Thermograms of neat PMMA film and nanocomposite films.

The thermal degradation of nanocomposites films fabricated using 1, 3, 5, and w/CCMK, denoted as CK₁PNC, CK₃PNC, CK₅PNC and CK₁₀PNC films, showed almost similar patterns of weight loss, with higher thermal stabilities, as shown in Table 4.2. There was a progressive

increase of the thermal stability of nanocomposites with the increase of CCMK amount in the nanocomposite films. The neat PMMA film was least thermally stable and CK₁₀PNC was the most thermally stable. As the CCMK content increased, the nanocomposites film exhibited a significant delay in weight loss at temperatures greater than 300°C. The temperature at 50% weight loss increased from 370°C to 385°C, with an increase in CCMK content from 0 to 10%. Interestingly, after decomposition, the nanocomposites films yielded charred residue proportional to their CCMK content. The yield of polymeric charred residue along with bone dried kaolinite at 700°C increased from 1.6% to 3.2%, 4.3%, 5.5% and 7.8% w/w with an increase in CCMK content from 0% to 1%, 3%, 5% and 10% w/w respectively.

Table 4.2: Thermogravimetric profile of pure PMMA and composite films recorded from thermographs

Composites	Decomposition Starts at °C	Char Formation at °C	Decomposition Ends at °C	Residue% (w/w), at 700 °C
CK ₀ PNC	280	450	562	1.6
CK ₁ PNC	288	460	565	3.2
CK ₃ PNC	300	470	570	4.3
CK ₅ PNC	312	482	585	5.5
CK ₁₀ PNC	315	487	590	7.8

3.5. Scanning Electron Microscope (SEM) Morphological Studies of Nanocomposites Films

SEM micrographs have been used to investigate the morphologies of kaolinite, virgin PMMA film and the films fabricated from self-assembled modified kaolinite into PMMA matrix.

Fabrication of PMMA/CCMK nanocomposites brought significant variation in the morphologies. The nanocomposites revealed uniform and smooth appearances with small irregularities and smaller or larger bumps with varying degrees of roughness. **Figure 4.7A–E** shows SEM images of the pure PMMA films and the nanocomposite films produced from 1, 3, 5, and 10% w/w modified kaolinite and PMMA matrix. It is obvious that the pure PMMA film surface is very smooth. The composite film CK1PNC showed that few particles are scattered within the film but CK3PNC film appeared to be along with some bulk structure; that could be due to the entropic effect and the change of dielectric constant of the medium. The variation of the dispersion medium (PMMA) and dispersed phase (CCMK) creates a new environment within the composite in terms of energy distribution within the particles which dominate the self-assembly

phenomena. Furthermore, increased modified kaolinite in CK₅PNC films leads to their homogeneous dispersion within the matrix, because an adequate interaction occurs between solid CCMK and PMMA phases, due to the uniform mixing of the system. An agglomeration of modified kaolinite particles in CK₁₀PNC film which was suffering from lack of matrix came out of the film surface with sharp edges.

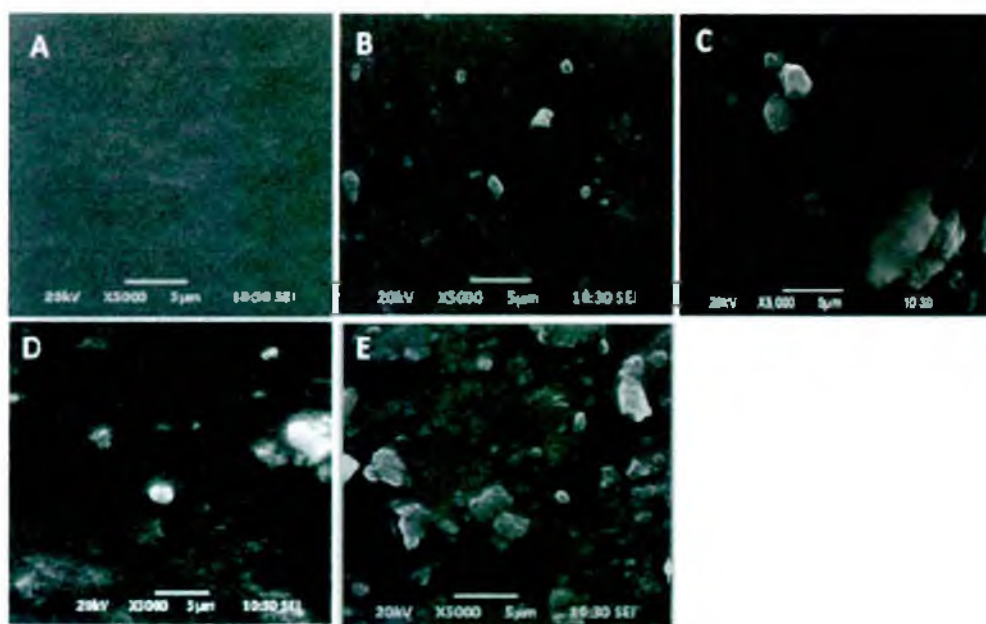


Figure 4.7: SEM images of virgin PMMA film (A) and the composites CK₁PNC (B), CK₃PNC (C), CK₅PNC (D), and CK₁₀PNC (E) films.

Conclusion: In the present study, self-assembled choline chloride modified kaolinite (CCMK) and polymethyl methacrylate (PMMA) nanocomposite films were fabricated by a simple casting method. Nanocomposites showed higher thermal stability, tensile strength and reduced elongation percentages at breaking points compared to those of neat PMMA film. Among the films, CK₅PNC showed the best mechanical properties. The film of CK₅PNC showed an optimum tensile strength of 31 N/mm² and about 0.60% strain at yield, which indicates, the film exhibited maximum elasticity with remarkable load bearing capacity. Although CK₁₀PNC film showed the highest tensile strength (33 N/mm²), the film also exhibited the lowest strain (0.20%). The percentage of elongation at break of nanocomposite films decreased with the increase of CCMK. Furthermore, thermal stability of CK₅PNC film was found almost similar to that of CK₁₀PNC film. Scanning electron microscopy images of CK₅PNC film showed a homogeneously distributed kaolinite smooth surface. The nanocomposite films created from modified indigenously layered material and lipophilic synthetic polymer could play important role in the field of packaging industry, and would be economical if applied in nanoscience and nanotechnology

References

1. Cavallaro, Giuseppe, Giuseppe Lazzara, Marina Massaro, Stefana Milioto, Renato Noto, Filippo Parisi, and Serena RIELA. "Biocompatible poly (N-isopropylacrylamide)-halloysite nanotubes for thermoresponsive curcumin release." *The Journal of Physical Chemistry C* 119, no. 16 (2015): 8944-8951.
2. Fakhrullina, GÖlnur I., Farida S. Akhatova, Yuri M. Lvov, and Rawil F. Fakhrullin. "Toxicity of halloysite clay nanotubes in vivo: a *Caenorhabditis elegans* study." *Environmental Science: Nano* 2, no. 1 (2015): 54-59.
3. Cavallaro, Giuseppe, Giuseppe Lazzara, Svetlana Konnova, Rawil Fakhrullin, and Yuri Lvov. "Composite films of natural clay nanotubes with cellulose and chitosan." *Green Materials* 2, no. 4 (2014): 232-242.
4. Costache, Marius C., M. J. Heidecker, Evangelos Manias, and Charles A. Wilkie. "Preparation and characterization of poly (ethylene terephthalate)/clay nanocomposites by melt blending using thermally stable surfactants." *Polymers for Advanced Technologies* 17, no. 9-10 (2006): 764-771.
5. Ghasemi, Hesam, Pierre J. Carreau, Musa R. Kamal, and Jorge Uribe-Calderon. "Preparation and characterization of PET/clay nanocomposites by melt compounding." *Polymer Engineering & Science* 51, no. 6 (2011): 1178-1187.
6. Pantani, Roberto, Giuliana Gorrasi, Giovanni Vigliotta, Marius Murariu, and Philippe Dubois. "PLA-ZnO nanocomposite films: Water vapor barrier properties and specific end-use characteristics." *European Polymer Journal* 49, no. 11 (2013): 3471-3482.
7. Pegoretti, A., J. Kolarik, C. Peroni, and C. Migliaresi. "Recycled poly (ethylene terephthalate)/layered silicate nanocomposites: morphology and tensile mechanical properties." *Polymer* 45, no. 8 (2004): 2751-2759.
8. Wang, Yimin, Junpeng Gao, Yunqian Ma, and Uday S. Agarwal. "Study on mechanical properties, thermal stability and crystallization behavior of PET/MMT nanocomposites." *Composites part B: engineering* 37, no. 6 (2006): 399-407.
9. Ghasemi, Hesam, Pierre J. Carreau, Musa R. Kamal, and Seyed H. Tabatabaei. "Properties of PET/clay nanocomposite films." *Polymer Engineering & Science* 52, no. 2 (2012): 420-430.
10. Ghanbari, Abbas, Marie-Claude Heuzey, Pierre J. Carreau, and Minh-Tan Ton-That. "Morphology and properties of polymer/organoclay nanocomposites based on poly (ethylene terephthalate) and sulfopolyester blends." *Polymer International* 62, no. 3 (2013): 439-448.
11. Shnean, Zanaib Y. "Effect of Grain and Calcinations Kaolin Additives on Some Mechanical and Physical properties on Low Density Polyethylene Composites." *Al-Khwarizmi Engineering Journal* 4, no. 4 (2008): 37-44.
12. Bergaya, F., B. K. G. Theng, and G. Lagaly. "Handbook of clay science. Elsevier, Amsterdam." *Handbook of clay science. Elsevier, Amsterdam.* (2006).
13. Zhao, Jie, Maria Milanova, Marijn MCG Warmoeskerken, and Victoria Dutschk. "Surface modification of TiO₂ nanoparticles with silane coupling agents." *Colloids and surfaces A: Physicochemical and engineering aspects* 413 (2012): 273-279.
14. Wen, Bin, Xinfeng Xu, Xiaowei Gao, Yanfen Ding, Feng Wang, Shimin Zhang, and Mingshu Yang. "Highly exfoliated poly (ethylene terephthalate)/clay nanocomposites via melt compounding: Effects of silane grafting." *Polymer-Plastics Technology and*

- Engineering* 50, no. 4 (2011): 362-371.
- 15 Spencer, Matthew W., D. L. Hunter, B. W. Knesek, and Donald R. Paul. "Morphology and properties of polypropylene nanocomposites based on a silanized organoclay." *Polymer* 52, no. 23 (2011): 5369-5377.
 - 16 Kim, Eung Soo, Jae Hun Shim, Ji Yoon Woo, Kwang Sik Yoo, and Jin San Yoon. "Effect of the silane modification of clay on the tensile properties of nylon 6/clay nanocomposites." *Journal of Applied Polymer Science* 117, no. 2 (2010): 809-816.
 - 17 Lazzara, Giuseppe, Giuseppe Cavallaro, Abhishek Panchal, Rawil Fakhruddin, Anna Stavitskaya, Vladimir Vinokurov, and Yuri Lvov. "An assembly of organic-inorganic composites using halloysite clay nanotubes." *Current Opinion in Colloid & Interface Science* 35 (2018): 42-50.
 - 18 Mohan, Turup Pandurangan, and Krishnan Kanny. "Effects of synthetic and processing methods on dispersion characteristics of nanoclay in polypropylene polymer matrix composites." *Materials Sciences and Applications* 2, no. 07 (2011): 785.
 - 19 Cavallaro, Giuseppe, Anna Danilushkina, Vladimir Evtugyn, Giuseppe Lazzara, Stefana Milioto, Filippo Parisi, Elvira Rozhina, and Rawil Fakhruddin. "Halloysite nanotubes: Controlled access and release by smart gates." *Nanomaterials* 7, no. 8 (2017): 199.
 - 20 Okada, A., M. Kawasumi, A. Usuki, Y. Kojima, T. Kurauchi, and O. Kamigaito. "Synthesis and properties of nylon-6/clay hybrids." *Polymer based molecular composites* 171 (1990): 45-50.
 - 21 Pegoretti, Alessandro, A. Dorigato, and A. Penati. "Tensile mechanical response of polyethylene-clay nanocomposites." *Express Polym Lett* 1, no. 3 (2007): 123-131.
 - 22 Agubra, Victor, Peter Owuor, and Mahesh Hosur. "Influence of nanoclay dispersion methods on the mechanical behavior of E-glass/epoxy nanocomposites." *Nanomaterials* 3, no. 3 (2013): 550-563.
 - 23 George, TresaSunitha, K. Asha Krishnan, R. Anjana, and K. E. George. "Studies on nano kaolin clay reinforced PS-HDPE nanocomposites." *Indian Journal of Advances in Chemical Science* 1, no. 4 (2013): 201-206.
 - 24 Anjana, R., and K. E. George. "Reinforcing effect of nano kaolin clay on PP/HDPE blends." *International journal of engineering research and applications* 2, no. 4 (2012): 868-872.
 - 25 Mustafa, Samir Nassaf. "Effect of kaolin on the mechanical properties of polypropylene/polyethylene composite material." *Diyala Journal of Engineering Sciences* 5, no. 2 (2012): 162-178.
 - 26 Ghosh, A. "Nano-clay particle as textile coating." *International Journal of Engineering & Technology IJET-IJENS* 11, no. 5 (2011).
 - 27 Srinivasan, Rajani. "Advances in application of natural clay and its composites in removal of biological, organic, and inorganic contaminants from drinking water." *Advances in Materials Science and Engineering* 2011 (2011).
 - 28 El-Bashir, S. M., M. S. AlSalhi, F. Al-Faifi, and W. K. Alenazi. "Spectral Properties of PMMA Films Doped by Perylene Dye-stuffs for Photosensitive Greenhouse Cladding Applications." *Polymers* 11, no. 3 (2019): 494.
 - 29 Huang, Xinyu, and William J. Brittain. "Synthesis and characterization of PMMA nanocomposites by suspension and emulsion polymerization." *Macromolecules* 34, no.

- 10 (2001): 3255-3260.
- 30 Su, Shengpei, and Charles A. Wilkie. "Exfoliated poly (methyl methacrylate) and polystyrene nanocomposites occur when the clay cation contains a vinyl monomer." *Journal of Polymer Science Part A: Polymer Chemistry* 41, no. 8 (2003): 1124-1135.
 - 31 Yeh, Jui-Ming, Shir-Joe Liou, Ching-Yi Lin, Chiao-Yu Cheng, Ya-Wen Chang, and Kueir-Rarn Lee. "Anticorrosively enhanced PMMA– clay nanocomposite materials with quaternary alkylphosphonium salt as an intercalating agent." *Chemistry of Materials* 14, no. 1 (2002): 154-161.
 - 32 Kumar, Manish, S. Arun, Pradeep Upadhyaya, and G. Pugazhenth. "Properties of PMMA/clay nanocomposites prepared using various compatibilizers." *International Journal of Mechanical and Materials Engineering* 10, no. 1 (2015): 7.
 - 33 Nabirqudri, Syed Abusale Mhamad, Aashis S. Roy, and MVN Ambika Prasad. "Electrical and mechanical properties of free-standing PMMA–MMT clay composites." *Journal of Materials Research* 29, no. 24 (2014): 2957-2964.
 - 34 Jo, Choonghee, Jin Fu, and Hani E. Naguib. "Constitutive modeling for intercalated PMMA/clay nanocomposite foams." *Polymer Engineering & Science* 46, no. 12 (2006): 1787-1796.
 - 35 Modak, Sadhan Kumar, Arup Mandal, and Debabrata Chakrabarty. "Studies on synthesis and characterization of poly (methyl methacrylate)-bentonite clay composite by emulsion polymerization and simultaneous in situ clay incorporation." *Polymer Composites* 34, no. 1 (2013): 32-40.
 - 36 Mittal, Vikas. "Polymer layered silicate nanocomposites: a review." *Materials* 2, no. 3 (2009): 992-1057.
 - 37 Katz, H.S.; Milewki, J.V. *Handbook of Fillers and Reinforcements for Plastics*; Van Nostrand Reinhold: New York, NY, USA, 1978.
 - 38 Duan, Guorong, Chunxiang Zhang, Aimei Li, Xujie Yang, Lude Lu, and Xin Wang. "Preparation and characterization of mesoporous zirconia made by using a poly (methyl methacrylate) template." *Nanoscale research letters* 3, no. 3 (2008): 118.
 - 39 Youssef, Ahmed M., F. M. Malhat, AA Abdel Hakim, and Imre Dekany. "Synthesis and utilization of poly (methylmethacrylate) nanocomposites based on modified montmorillonite." *Arabian Journal of Chemistry* 10, no. 5 (2017): 631-642.
 - 40 Mitchell, James Kenneth, and Kenichi Soga. *Fundamentals of soil behavior*. Vol. 3. Hoboken, NJ: John Wiley & Sons, 2005.
 - 41 Adeyemo, Aderonke Ajibola, Idowu Olatunbosun Adeoye, and Olugbenga Solomon Bello. "Adsorption of dyes using different types of clay: a review." *Applied Water Science* 7, no. 2 (2017): 543-568.
 - 42 Ferriol, M., A. Gentilhomme, M. Cochez, N. Oget, and J. L. Mieloszynski. "Thermal degradation of poly (methyl methacrylate)(PMMA): modelling of DTG and TG curves." *Polymer degradation and stability* 79, no. 2 (2003): 271-281.
 - 43 Lee, Yi-Mu, and Dabir S. Viswanath. "Degradation of poly (methyl methacrylate)(PMMA) with aluminum nitride and alumina." *Polymer Engineering & Science* 40, no. 11 (2000): 2332-2341.

Chapter: Five

Fabrication of Kaolinite/Metal Oxides Nanocomposites and Their Biological Applications

Chapter Five

Abstract: Indigenous layered nanostructured materials are ultimate choice due to their viability, environment adaptability, thermal stability and surface characteristic in the fields of biological and pharmaceuticals sciences. Nano-engineering of layered materials incorporates their enhanced inherent properties. Here, we have fabricated composite nanostructure of metal oxides (ZnO and Fe₂O₃) anchored kaolinite surface by a simple method. ATR-IR, EDX, XRD and SEM were used to characterize kaolinite and the nanocomposites in terms of functional groups, elements, crystallinity and morphological change. Hybrid nanocomposites of kaolinite-metal oxides were prepared after calcination at 680°C of adsorbed salts onto kaolinite surface from respective saturated aqueous salts solutions. Nanocomposites were subjected to apply against selective bacteria (*Salmonella pullorum*, *Escherichia coli*, *Pseudomonas aeruginosa*) and cancer cells (c.f. Hela and BHK-21). It is revealed that the fabricated nanocomposites showed better antimicrobial activity than virgin kaolinite whereas only kaolinite-Fe₂O₃ nanocomposites showed the highest toxic effect against both cells. The synergistic effect of nanocomposites would offer the modulation of enhanced electronic and physical properties from a simple technology to improve inherent antimicrobial activity and cell toxicity of kaolinite for targeted assay.

1. Introduction

Nano-sized metal oxide such as ZnO, TiO₂, and CuO nanoparticles¹⁻³ have received great attention as a candidate for biomedical implants⁴, medical devices⁵ and biological applications such as cytotoxicity, antimicrobial activity and photocatalysis due to a strong resistance to chemical and photocorrosion, high efficiency, lack of toxicity, and low cost. In particular, Fe₂O₃ nanoparticles, with a band gap of ~2.2 eV, have received increasing attention for bacterial inhibition in recent years, due to its visible light absorption properties (~564 nm), unique magnetic properties and biocompatibility.⁶⁻⁸ By evaluating against ten pathogenic bacteria, Behera et al. have found that iron oxide nanoparticles have moderate antibacterial activity against both Gram positive and Gram negative pathogenic bacteria.⁹ However, the antibacterial mechanism of Fe₂O₃ nanoparticles is not clear, and still greater efforts should be made to improve the antibacterial activity. In previous studies, the antibacterial activity was strongly dependent on the particle size. Nanometer-scale metal oxides like ZnO, MgO and CuO exhibited higher antibacterial activity than micrometer scale particles due to the increased surface defects, higher surface area or the ability to penetrate bacterial cells, and the antibacterial activity increased sharply when the particle size of metal oxide was less than 50 nm.¹⁰⁻¹² However, the small nanoparticles are easy to aggregate into bigger clusters resulting from their high surface energy, which restricts the antibacterial activity. To address this problem, suitable matrix should be used to disperse and stabilize nanoparticles. The use of silicon nanowires,¹³ nanoplatelets,¹⁴ and graphene oxide¹⁵ could promote activity, nanoparticles have been proved to enhance antibacterial performance. Generally, monodispersed nanostructures exhibited distinctive functions.¹⁶⁻¹⁸ However, there are few works about the nanoparticles dispersion state in the composites which has great influence on antibacterial activity. To control the dispersion state of antibacterial nanoparticles in matrix is useful for enhancing the antibacterial activity of Fe₂O₃ nanoparticles. Clay minerals such as kaolinite, montmorillonite and halloysite have attracted specific research attentions as promising supporting materials for assembling functional nanoparticles in catalytic and antibacterial, owing to their abundant source, special shape and excellent surface properties.¹⁹⁻²¹ Kaolinite (Kln, Al₂Si₂O₅(OH)₄) is a 1:1 type layer silicate mineral composed of an octahedral (Al-OH) sheet stacked on top of a tetrahedral (Si-O) sheet. Kln has showed excellent adsorbability, good stability and biocompatibility in our previous

studies.²²⁻²³ The abundant hydroxyl groups of Kln could provide active sites for anchoring antibacterial metal oxide. The negative charge and hydrophilicity of Kln may enhance the direct contact and interaction between Kln and bacterial cells through electrostatic interactions. These properties enable Kln to become a promising matrix in the synthesis of antibacterial composites.

One of the possibilities regarding how to increase its activity is the introduction of metal oxide nanoparticles into the clay mineral structure²⁴. Preparation, characterization and biological activity of kaolinite/metal oxide nanocomposite has been set as the present work²⁵. Significantly ZnO nanoparticles³ and nanohoney combs shows promising results, therefore we decided to provide the detailed study of an effect of kaolinite/TiO₂ composite preparation conditions on physicochemical and biological activities. The produced saponin inspired ZnO nanohoney (SiZnO NHs) combs as potential antifungal and antibacterial agents have been studied on *Sclerotium rolfsii* (*S. rolfsii*), *Pythium debarynum* (*P. debarynum*) and *Escherichia coli* (*E. coli*), *Staphylococcus aureus* (*S. aureus*), respectively. SiZnO NHs exhibited the highest antibacterial (~50%) and antifungal (~40%) activity against Gram-negative bacteria (*E. coli*) and fungus (*P. debarynum*), respectively at concentration of 0.1 mol.²⁶

Katerina et al.²⁷ have reported a composite of kaolinite-TiO₂ and its activity against *Staphylococcus aureus*, *Escherichia coli*, *Enterococcus faecalis*, *Pseudomonas aeruginosa*. They found that non-calcinated composite showed higher activity than calcinated composite. The highest antibacterial activity was obtained for the KATI14 sample. The determined MIC values of 3.3 mg/L for *S. aureus* and *E. coli*, and 10 mg/L for *E. faecalis* and *P. aeruginosa* confirmed best potential of the KATI14 in term of growth inhibition of all bacterial strains used. The other KATI samples caused growth inhibition (10 mg/L) of *S. aureus* and *E. coli* only. The MIC values for *E. faecalis* and *P. aeruginosa* was not determined, which can be caused by the MIC value being higher than 10 mg/L, and thus above the highest concentration of the composite applied in the growth media.

Very recently, in 2017 Lefei et al.²⁸ have reported on preparation, characterization, antimicrobial and cytotoxicity studies of copper/zinc loaded montmorillonite. In the modified montmorillonite, hydrated Cu ions and Zn ions were exchanged in the interlayer space of montmorillonite and the particles were irregular shapes. The results showed that Cu/Zn- montmorillonite enhanced

antibacterial and antifungal activity compared with Zn- montmorillonite and Cu- montmorillonite possibly due to the synergistic effect between Cu and Zn. Among the Cu/Zn- montmorillonite with different Cu/Zn ratios, Cu/Zn- montmorillonite with a Cu/Zn ratio of 0.98 or 0.51 showed higher antimicrobial activity against gram-negative bacteria (*Escherichia coli*), gram-positive bacteria (*Staphylococcus aureus*), fungi (*Candida albicans*). Moreover, the antimicrobial activity of Cu/Zn- montmorillonite was correlated with its specific surface area. Cytotoxicity studies on IPEC-J2 cell showed a slight cytotoxicity of Cu/Zn- montmorillonite.

In this study, a facile technique only a concentrated aqueous salt solutions for respective Fe_2O_3 and ZnO nanoparticles were blended with two dimensional (2D) kaolinite nanosheets collected from Bijoypur. The deposited polyhydroxycations of (Fe(III) or Zn(II)) onto the surface of kaolinite with a negative charge -2.1 to -29.1 mV via electrostatic attraction were calcinated at 680°C to fabricate hybride nanostructure. Antibacterial properties of nanocomposites against selective micro-organisms and cells have been evaluated.

2. Experimental

2.1. Materials

Kaolinite known as china clay was collected from Bijoypur. It was used after purification (washing with dilute HCl aqueous solution) and drying at 105°C under atmospheric pressure. Zinc sulphate heptahydrate ($\text{ZnSO}_4 \cdot 7\text{H}_2\text{O}$) and Ferrous sulphate heptahydrate ($\text{FeSO}_4 \cdot 7\text{H}_2\text{O}$) were purchased from Aldrich-Sigma, India and were used without further purification. Dimethyl sulfoxide (DMSO) was purchased from Aldrich-Sigma, India. Laboratory prepared demineralized water was used in all purposes of work throughout the experiments.

2.2. Methods

Powdered Zinc sulphate heptahydrate ($\text{ZnSO}_4 \cdot 7\text{H}_2\text{O}$)/Ferrous sulphate heptahydrate ($\text{FeSO}_4 \cdot 7\text{H}_2\text{O}$) was used as ZnO/ Fe_2O_3 precursor for the preparation of the composites. The initial kaolinite was mixed with respective salt of zinc sulphate/ferrous sulphate in water solution and stirred for 30 minutes. Distilled water was then added to the mixture in 1:1 volume ratio to salt sulphate solution. Afterwards, the temperature of the dispersion was raised to 100°C and kept for 60 minutes. The dispersion was left to cool down to the laboratory temperature and filtrated using the Büchner funnel. The solid content separated from the dispersion was rinsed with distilled water severaltimes. The solid content was dried at 105°C and calcined at 680°C . Thus

the metaloxides nanoparticles anchored with kaolinite matrix were obtained. The illustration of the whole synthetic route has been depicted schematically in the **Figure 5.1**. This procedure was followed for synthesis of both kaolinite-metaloxides ($\text{ZnO}/\text{Fe}_2\text{O}_3$) nanocomposites. Later these samples were used for further characterization and assessment.

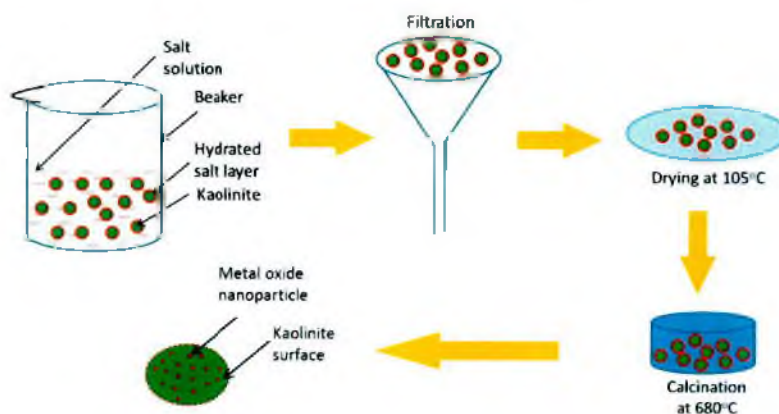


Figure 5.1: Schematic presentation of the synthetic route of metal oxide nanoparticles embedded kaolinite nanocomposites.

2.3 Characterization

The elemental composition of raw clay and modified kaolinite with ZnSO_4 before and after calcination were checked by EDS spectra (EDAX) analysis. ATR-IR spectra were measured on a FT-IR 8400S spectrophotometer (Shimadzu Corporation, Japan) in the range of $4000\text{--}400\text{ cm}^{-1}$, resolution: 4 cm^{-1} ; no. of scans: 16 times. The x-ray powder diffraction (XRPD) patterns of the samples were recorded by an x-ray diffractometer (Ultima IV, Rigaku Corporation, Japan) at room temperature. Prior to XRD analysis the samples were ground into fine powders using mortar-pestle. Nickel (Ni) filtered $\text{Cu K}\alpha$ radiation ($\lambda=0.154\text{nm}$), from a broad focus Cu tube operated at 40kV and 40 mA, was applied to the samples for measurement. The XRD patterns of the samples were measured in the continuous scanning mode with scan speed of $3^\circ/\text{min}$ and in the scan range of 5 to 100° . Bragg's law was used to compute the basal spacing (d_{001}) of the crystalline samples. The morphology of the samples were analyzed by an analytical scanning electron microscope (JEOL JSM-6490LA, Tokyo, Japan) operated at an accelerating voltage of 20 kV in the back-scattered electron mode.

2.4 Antimicrobial activity

In this research work, we followed agar diffusion method by Kirby-Bauer. Several attempts were made for scrutinizing antimicrobial activity of the particle focusing different microorganisms such as *Escherihia coli*, *Salmonella pullorum*, and *Pseudomonas aeruginosa*. Following the conventional way to check activity, first suspension of kaolinite-ZnO nanocomposites with demineralized water and DMSO with demineralized water was added to the organism. The samples were prepared by taking 5 (five) mg of synthesized composites in 5 ml DMSO, with 2.5 ml demineralized water and subjected to sonication for 10 minutes. Then the samples were used for antimicrobial analysis. It is worthy to mention that prior to the use every time the vials were vortex to keep the suspension homogeneous. 25 μ l of prepared solution was added to the each well and kept those petridishes containing microorganism in the incubator where temperature maintain 37°C for 24 hours. The synthesized metaloxides nanocomposites were added onto the culture medium containing microorganism as powder and allowed to expose in sunlight for 5 hours with continuous aeration.

2.5 Cytotoxic effect:

This experiment was carried out at cytotoxicity lab in Centre for Advanced Research in Science. In brief, HeLa a human cervical carcinoma cell line and BHK-21 a baby hamster kidney fibroblast cell line were maintained in DMEM (Dulbecco's Modified Eagles' Medium) containing 1% penicillin- streptomycin (1:1) and 0.2% gentamycin and 10% fetal bovine Serum (FBS). Hela cells ($5 \times 10^4/250 \mu$ l) and BHK-21 cells ($3.7 \times 10^4/250 \mu$ l) were seeded onto 48-well plate and incubated at 37°C + 5% CO₂. After 24 hours 50 μ l of sample was added each well. Cytotoxicity was examined under an inverted light microscope after 24 hour of incubation. Duplicated wells were used for each sample.

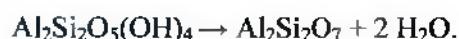
3. Results and Discussion

3.1 Preparation of kaolinite-metal oxides hybrid nanocomposites

Kaolinite- metal oxides nanocomposites were synthesized via a simple blending method in an aqueous solution. After heating the solution becomes concentrated and the interaction between negatively charged surface of kaolinite and the polyhydroxylation of the salts was increased, results an electrostatically adhered composites. Later upon heat at 680°C, the cationic part oxidized and the kaolinite dehydrated to a new crystallinity of layered structure known as metakaolinite. The electrostatically distributed cation onto the surface of kaolinite produced nanodot after thermal treatment at 680°C. The fabricated composites produced from nano-interaction of kaolinite and cation were characterized using EDS, ATR-IR spectroscopy, and XRD. The morphology of the composites was also investigated using SEM.

3.2 Energy Dispersive X-Ray spectrophotometer (EDS)

The elemental composition of raw clay and modified kaolinite with ZnSO₄ and FeSO₄ before and after calcination were checked by EDS spectral (EDAX) analysis. In the **Figure 5.2**, the spectra A, C, E and B, D, F represent the elemental peaks for neat kaolinite and modified kaolinite with ZnSO₄ and FeSO₄ before and after calcinations at 680°C. It is evident that the neat kaolinite gave the highest intensity of O, Al, and Si peaks, compared to the peaks recorded after calcination. The following **Table 5.1**, shows the percentage compositions of the raw material and products in the different forms. The weight percentage of O, Al and Si in neat kaolinite is around the theoretical value, c.f. 60.4, 18.5 and 21. The Al and Si values are slightly increased (23.7, 25) and O value is decreased (51.2) since kaolinite was subjected to dehydrate at 680°C which results two molecules of water ejection.



The spectra in the **Figure 5.2C** and **Figure 5.2D** shows after modification of ZnSO₄ salt before and after calcination as both of the Zn and sulfur are observed in **Figure 5.2C** and after calcination the sulfur was combusted as SO_{x(2-3)} after calcinations at 680°C, as a results the

weight percentage of Zn in the finished product was increased from 2.5 to 6.9. Similarly, the weight percentage of Fe was also increased from 4 to 7.3 after heating at 680°C the saturated kaolinite surface with FeSO₄.

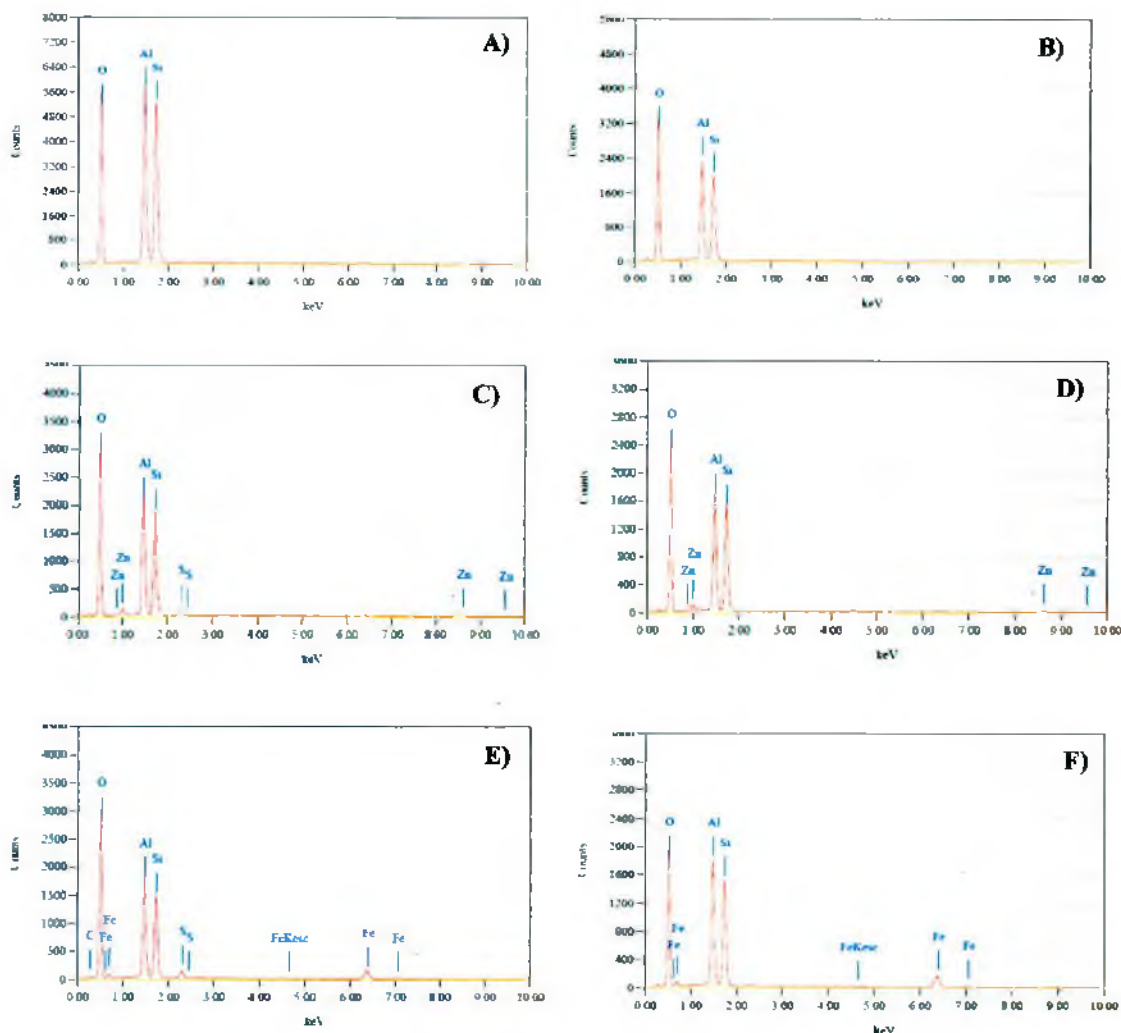


Figure 5.2: shows the EDS spectral (EDAX) analysis of pure kaolinite and modified kaolinite with ZnSO₄ and FeSO₄ salts before (A, C, E) and after (B, D, F) calcination at 680°C respectively.

Table 5.1: Elemental analysis of neat kaolinite and the modified kaolinite prepared at different conditions

Figure	Name	O	Al	Si	Zn	Fe	S
A	Kaolinite, 105°C	60.42	18.47	21.11	--	--	--
B	Kaolinite, 680°C	51.16	23.68	25.16			
C	Kaolinite-ZnSO ₄ , 105°C	64.96	15.73	15.79	2.49	--	1.03
D	Kaolinite-ZnO, 680°C	58.62	17.53	16.97	6.88	--	
E	Kaolinite-FeSO ₄ , 105°C	63.78	11.70	11.19	--	4.06	1.14
F	Kaolinite-Fe ₂ O ₃ , 680°C	57.10	17.74	17.87	--	7.29	--

3.3 Characterization of nanocomposites by spectral means

The neat kaolinite and modified kaolinite before and after calcination were subjected to analyze by different spectral analysis. The functional groups and interaction of clay/cation self-assembled nanocomposites were analyzed by ATR-IR spectroscopy. The **Figure 5.3** shows ATR-IR spectra of neat kaolinite and the hybrid composites. The spectra in the **Figure 5.3 (A,B), (C,D) and (E,F)** represents the raw kaolinite, kaolinite with zinc sulphate and kaolinite with Ferrous sulphate modified composites before and after calcinations at 680°C respectively. The characteristic absorption bands of the inorganic moiety at 1,036.8 cm⁻¹ (ν Si-O), 913.1 cm⁻¹ (ν Al-OH), 819.5 cm⁻¹ (ν Al-O), and 523.4 cm⁻¹ (ν Al-O-Si)²⁹ of kaolinite were found in all spectra of A, C, and E obtained before calcination. The band at 3,600-3700 cm⁻¹ relates to free OH stretching. The sharp peaks present in the neat kaolinite were destroyed due to the loss of some water molecules at higher temperature. Before calcination, the peaks pattern remains same for the kaolinite even after modification except a little shift towards lower field. Whereas, in the **Figure 5.3 (B, D, F)** the spectra produced after calcinations, shows different peaks from one another which could be due to the present of nanoparticles formed after interaction of polyhydroxy cation.

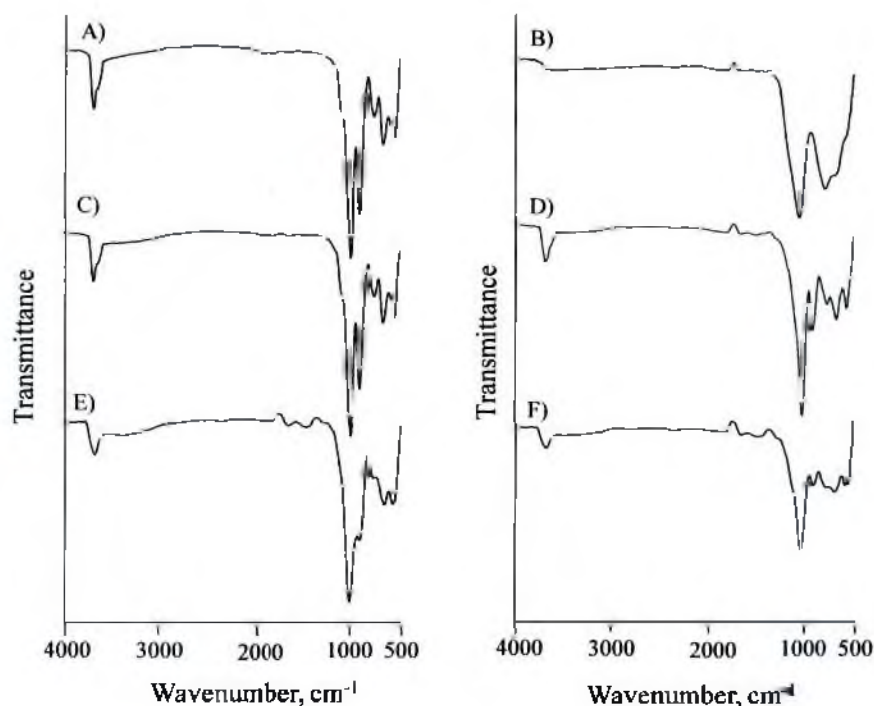


Figure 5.3: ATR-IR spectral analysis of pure kaolinite and modified kaolinite with ZnSO_4 and FeSO_4 salts before (A, C, E) and after (B, D, F) calcination at $680\text{ }^\circ\text{C}$ respectively.

3.4 XRD analysis

Fig. 4 shows the XRD pattern of the studied kaolinite and composites. The following mineralogical phases were identified: kaolinite (K), quartz (Q), and anatase (A). XRD is used to characterize kaolinite and to determine it in hydrated or dehydrated form. The plot shown in **Figure 5.4A** shows the basal spacing reflections indicating a sharp peak at 12.2° (2θ) which translate to a (001) basal interlayer spacing of 7.18 \AA which is characteristic for pure kaolinite.³⁰

To clarify whether the silicate layers of kaolinite were intercalated by cations, powdered XRD analysis was performed on pure kaolinite and kaolinite-cations ($\text{Zn}^{+2}/\text{Fe}^{+3}$) complex and the resulting diffraction patterns presented in **Figure 5.4 (A, C, E)**. The diffraction patterns are characterized by a strong narrow peak at $2\theta = 12.2^\circ$, corresponding to a d-spacing [$d_{(001)}$] value of 7.1 \AA . This suggests that cations did not penetrate kaolinite and that adsorption occur only on the external surfaces of mineral.³⁰

Besides, the calcined pure kaolinite and the modified kaolinite gave similar pattern of XRD which reflect the loss of crystallinity of kaolinite structure with remaining quartz entities. The amorphous moieties gave a slight curvature with 18-28° (2θ).

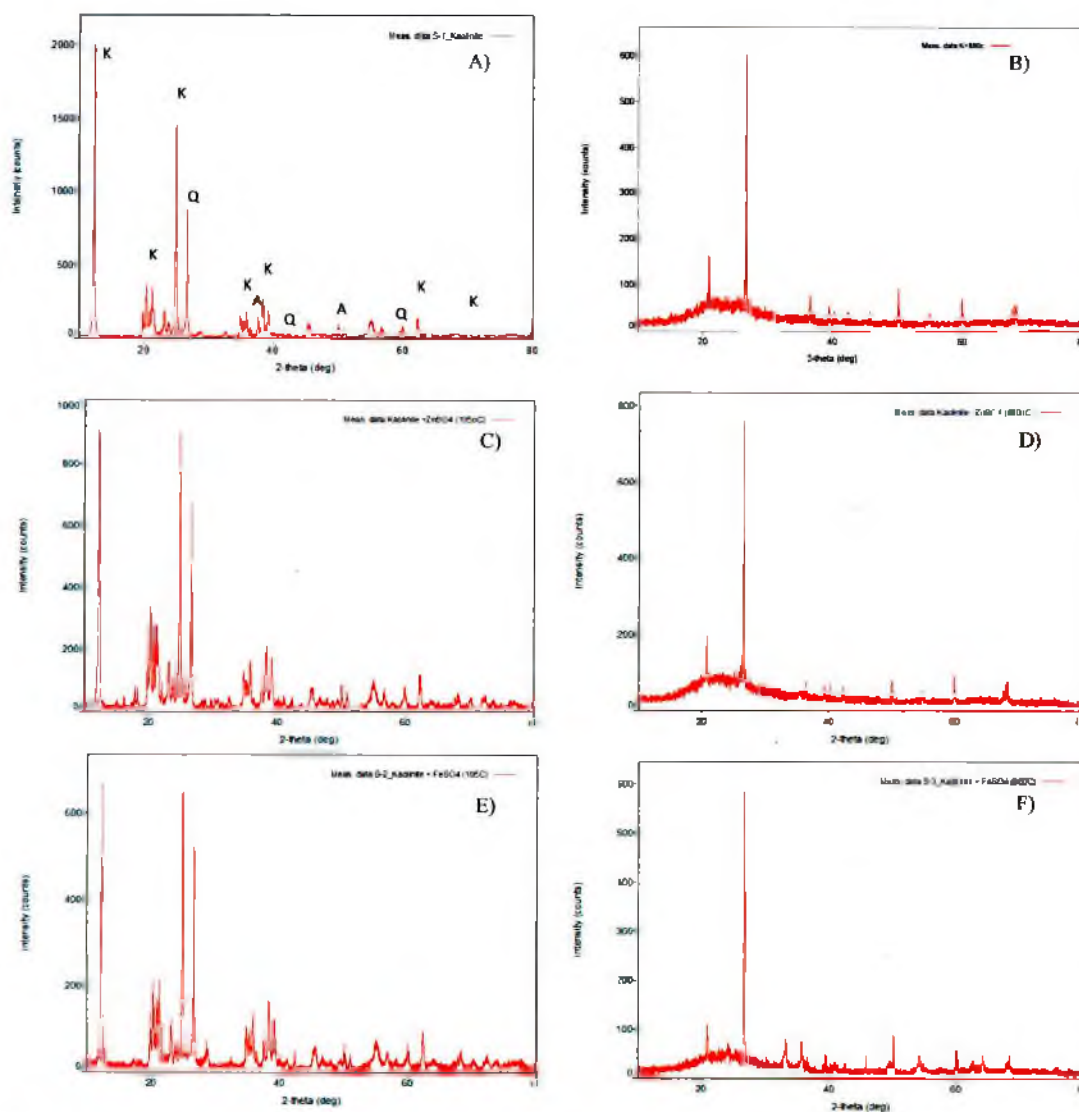


Figure 5.4: XRD pattern of pure kaolinite and modified kaolinite with ZnSO₄ and FeSO₄ salts before (A, C, E) and after (B, D, F) calcination at 680 °C respectively.

3.5 Observation of Morphological by SEM

Morphologies of kaolinite and modified kaolinites before and after calcination were observed using scanning electron microscopy. The **Figure 5.5(A,B), (C,D)** and **(E, F)** represent the images of neat kaolinite, kaolinite modified with FeSO_4 and kaolinite modified with ZnSO_4 after treating with corresponding saturated aqueous salt solutions and calcinated at 680°C respectively. It is revealed that a granular sharp particle (**Figure 5.5A**) was observed from neat kaolinite and a noncrystalline amorphous powdery mass (**Figure 5.5B**) was found after calcinations. Interestingly, when kaolinite was blended with saturated solution of FeSO_4 , the particles were observed clearly (**Figure 5.5C**), this could be due to the environment created by the distribution of Fe^{2+} on the surface of kaolinite. After calcination, the image does not appear with any significant change, although the smaller particles stacked together (**Figure 5.5D**). A little change was found when ZnSO_4 was used to treat kaolinite. Before calcination, the cationically modified kaolinite shows a bulky aggregate mass but after calcinations, a homogeneously distributed very fine powdery smooth surface was found. Insert of all images, represent 16 folds magnified appearance, help us to understand more closely.

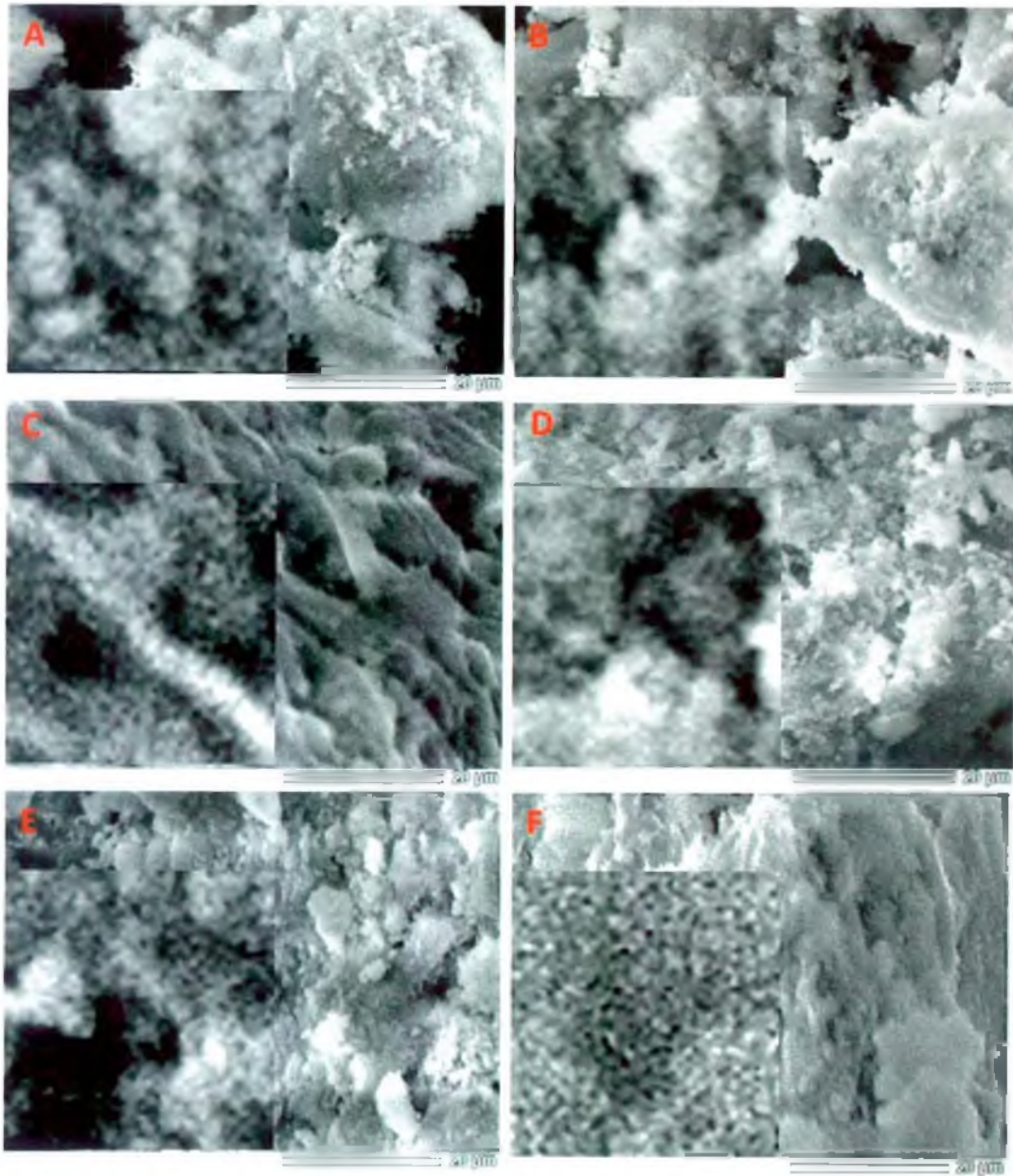


Figure 5.5: Shows scanning electron microscope images of pure kaolinite and modified kaolinite with $ZnSO_4$ and $FeSO_4$ salts before and after calcination at $680^\circ C$.

3.6 Antibacterial activity

The antibacterial activities of pure kaolinite and modified kaolinite with different conditions were subjected to disperse (200µg/mL) against *E. coli*, *P. aeruginosa*, *S. pullorum* cells and incubated for 24 hours at 37°C. As shown in Fig.5.6, in order to compare the efficiency of the samples, a moderate concentration (200µg/mL) was arbitrarily selected to work. The **Figure 5.6** shows three bar chart (A, B and C) with different bacterial growth with respect to their control experiments.

It is revealed that kaolinite with Zn^{+2} (KZ₁₀₅) prevents *E. coli* growth more efficiently than other samples used. Only about 5×10^5 cells were survived after 48 h incubation at 37°C. It is remarkably mentionable that all the cationically modified kaolinite even before and after calcination the samples kill more bacterial cell than pure kaolinite. From this phenomenon one can easily understand that the synergistic cationic effect of kaolinite in presence of Zn^{+2}/Fe^{+3} destroys *E. coli* cell wall easily due to rapid production of reactive oxygen species (ROS) in the interface which is elaborately discussed later.

In **Figure 5.6B**, it is evident that except the calcinated kaolinite- Fe_2O_3 nanocomposites, all the other composites show about twice efficiency (survive $2.2-2.4 \times 10^5$ *P. aeruginosa* cells) than pure kaolinite (survive 4.8×10^5 *P. aeruginosa* cells) after 48 h incubation at 37 °C.

Similarly, in **Figure 5.6C**, it is observed that the kaolinite with Zn^{+2} (KZ₁₀₅) prevents the maximum growth of (survive 2.5×10^5 cells) *S. pullorum*. Interestingly, Zn^{+2} modified kaolinite nanocomposites showed higher efficiency than Fe^{+3} modified kaolinite nanocomposites. In order to explore the reasons behind the discrepancies of the efficiency we need more study.

The **Table 5.2** shows the survival percentage of different microorganisms against the pure kaolinite and the modified kaolinite with cations (Zn^{+2}/Fe^{+3}) and the calcinated nanocomposites.

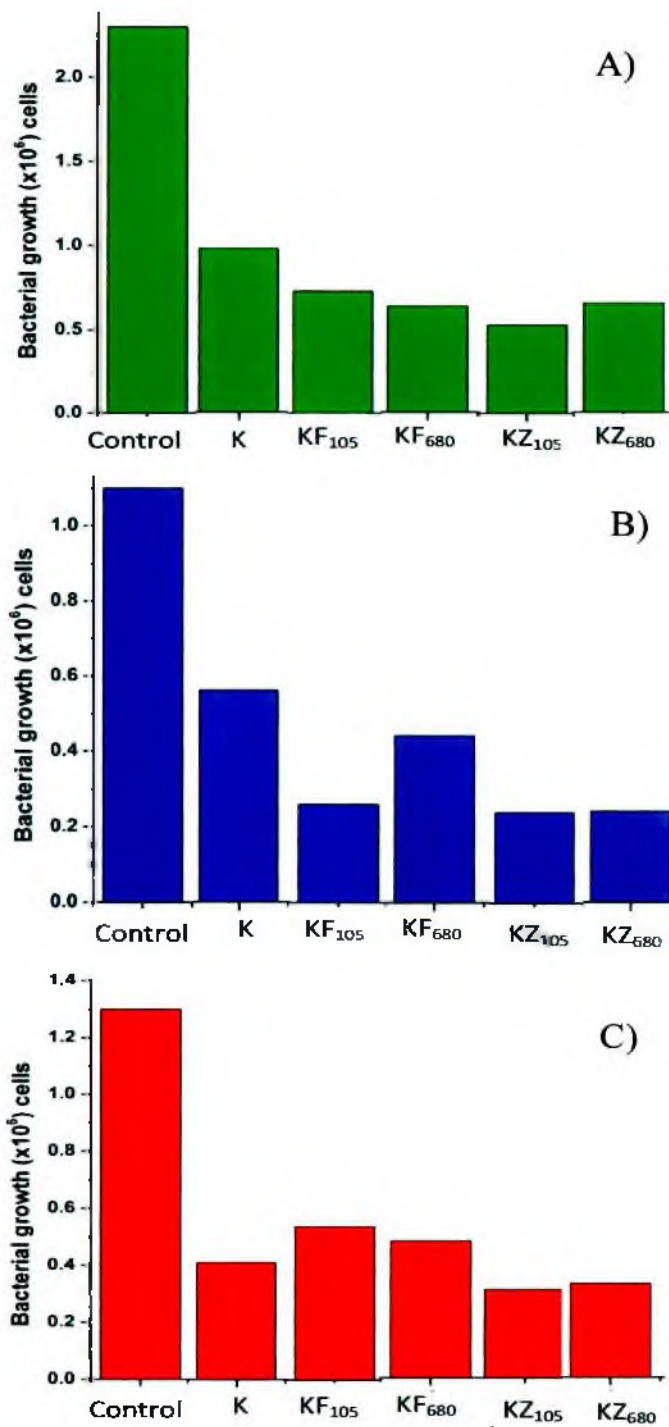


Figure 5.6: Bar chart for the anti-microbial activity of pure kaolinite and modified kaolinite with ZnSO₄ and FeSO₄ salts before and after calcination at 680 °C against *E. coli*, *P. aeruginosa*, *S. pullorum* cells.

Table 5.2: survival percentage of different microorganisms against the pure kaolinite and the modified kaolinite.

Nanocomposites	Control	% Survival		
		<i>Escherichia coli</i> (A)	<i>Pseudomonas aeruginosa</i> (B)	<i>Salmonella pullorum</i> (C)
K	100	44	51	32
KF105		33	24	42
KF680		29	41	37
KZ105		23	21	23
KZ680		30	21	25

3.7 Proposed mechanism for ROS generation

Oxidative stress is a highly recognized mechanism of various nanoparticles. A systematic study was performed to evaluate the toxicity/biocompatibility of pure kaolinite and its modified form for toxicity studies. It is widely known that kaolinite is highly biocompatible. Liu et al³¹ concluded that based on XTT (sodium 2,3,-bis[2-methoxy-4-nitro-5-sulfophenyl]5-[phenylamino-carbonyl]-2H tetrazolium inner salt) results, graphene-based materials mediate a little superoxide anion production and a trace amount of ROS may be produced; this plays a minor role in the antibacterial activity of graphene based materials. To investigate ROS production as one of the key factors for cell death, here we did not measure ROS quantitatively. The levels of ROS in pure kaolinite and modified kaolinite nanocomposites cells were around 2.5-3.0 folds higher, respectively, compared to the level of ROS in control cells throughout the experiment (Figure 5.6 (A, B and C)). These results indicate that cell death is mediated by ROS production, which might alter the cellular redox status. Liu et al³¹ further demonstrated that most *E. coli* cells were individually wrapped with thin layers of GO nanosheets. In contrast, *E. coli* cells were usually embedded in large rGO aggregates. The different behavior of GO and rGO suggests the aggregation/dispersion of graphene-based materials may play an important role in their antibacterial activities. Akhavan and Ghaderi³² suggest that that the direct-contact interaction of the bacteria with the very sharp edge of the nanowalls resulted in more damage to the cell membrane of the Gram-positive *Staphylococcus aureus* bacteria lacking the outer membrane compared to the Gram-negative *E. coli* ones owning the outer membrane.

Intracellular oxidative stress could be hastened by nanoparticles by disturbing the equilibrium between the oxidant and antioxidant processes.^{33,34} ROS typically include the superoxide radical (O^{2-}), hydrogen peroxide (H_2O_2), and hydroxyl radical (OH), which cause damage to cellular components, including DNA and proteins.^{35,36} ROS generation is also an important factor in the apoptosis process, and the excess generation of ROS induces mitochondrial membrane permeability and damages the respiratory chain to trigger the apoptotic process.^{37,38}

From the antibacterial activity results, we concluded that the antibacterial activity of kaolinite and modified kaolinite with metals oxide nanoparticles not only depends on density of functional groups, size, conductivity, and the amount of cells deposited on modified kaolinite materials but also membrane oxidative stress caused by direct contact with sharp nanosheets, and the generation of ROS and DNA fragmentation consequently leads to cell death as shown in **Figure 5.7 A, B**.

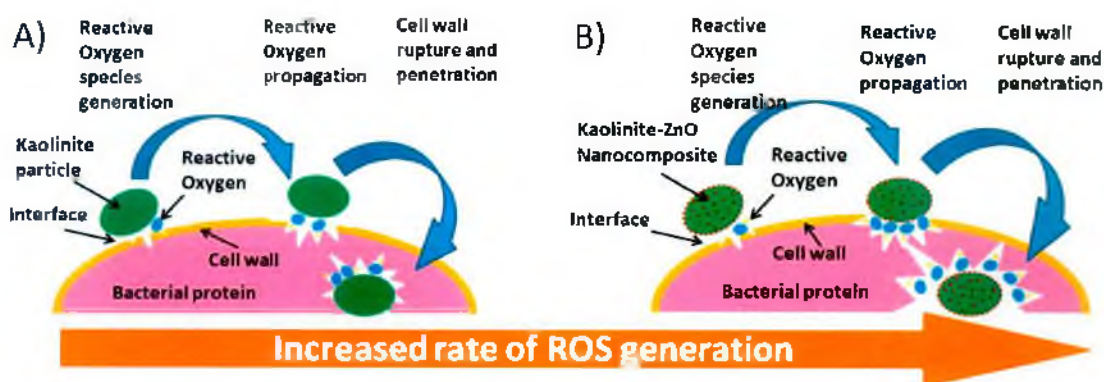


Figure 5.7: Schematic representation of the ROS generation, propagation and cell wall penetration of bacteria during interaction of pure kaolinite (A) and modified kaolinite (B).

3.8 Cytotoxic effect against HeLa cells

Kaolinite and modified kaolinite with salts of iron and zinc at 105 and 680°C were subjected to apply against cancer cells c.f. Hela and BHK-21. In order to investigate the effect of concentration on the survival of the targeted cells, we have empirically selected three different amounts of samples, e.g. 125, 250 and 500 mg. Table 5.3 Shows the percentage survival of Hela cell. It is very important to mention that neat kaolinite shows highest activity among the samples in case of all variable sample amounts. When 125 mg of pure kaolinite was added then only 10-20 % Hela cell was survived. This survival percentage was remained same until the kaolinite quantity reached upto 250 mg. When more kaolinite was added (c.f. 500 mg) then less than 5% of cell survival was found. This activity was as same as (less than 5% and 10-20% survival of cell) the activity obtained from calcinated (at 680°C) kaolinite at the amount of 250 mg and 500 mg respectively. It is revealed that the percentage cell survival (80-90) was remarkably high when 125 mg of calcinated (at 680°C) kaolinite was applied which indicates that the kaolinite morphology has been changed at 680°C. As a result, this leads for formation of smaller particle size becoming more negatively charged entities. Among the modified kaolinite only the particles obtained from ferrous sulphate modified and calcinated at 680°C showed excellent cytotoxicity effect against hela cell. When 125 mg was used then 40% cell was survived but less than 5% cell was found after using 250 mg of the particles. It is notable that Fe₂O₃ particle onto kaolinite surface boost up the activity due to their electronic and physical properties change. Poor cytotoxic performance was observed from modified kaolinite prepared from zinc salts at 105 and 680°C for all ranges of the particles quantity used for the experiments.

Table 5.3: Effect of concentration of kaolinite and modified kaolinite on percentage Hela Cell survival

Name	Amount of sample		
	125 mg	250 mg	500 mg
	% Hela Cell survival		
Kaolinite/105°C	10-20	10-20	<5
Kaolinite 680°C	80-90	10-20	<5
Kaolinite +Fe ²⁺ /105°C	80-90	80-85	70-80
Kaolinite+Fe ₂ O ₃ /680°C	>40	<5	<5
Kaolinite +Zn ²⁺ /105°C	>90	>95	>90
Kaolinite+ZnO/680°C	>90	80-90	>90

Figure 5.8 and **Figure 5.9** show the images originated under an inverted light microscope when the HeLa cell was treated with solvent (+) and 500 mg of the particles with two different magnifications respectively. When the cell was washed with solvent, the growth of cell and survival was nearly 100% which was considered as controlled experiment. As the cell treated with 500 mg pure kaolinite, the survival was almost zero which is reflected from the clear images recorded from microscope. Interestingly, calcinated particles produced from modified kaolinite with iron salt showed excellent performance even for 250 mg results a clear picture.

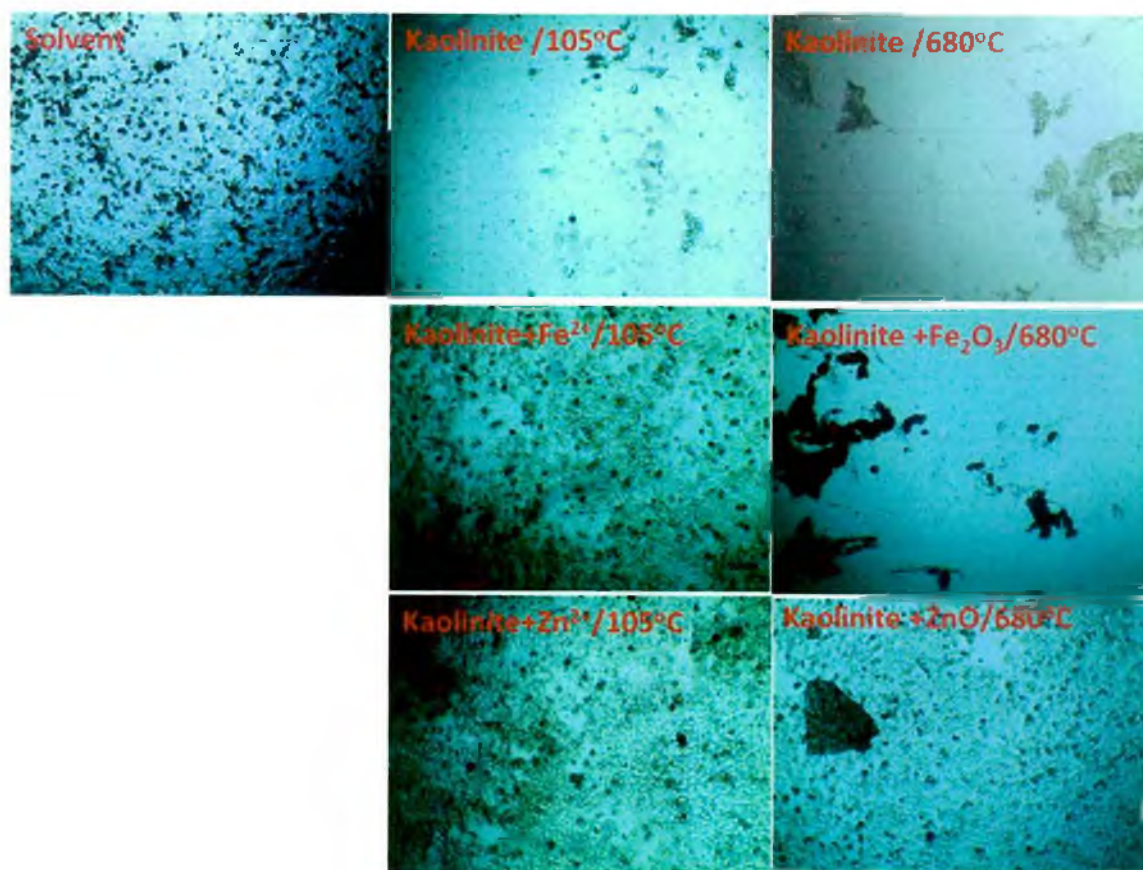


Figure 5.8: Images recorded from an inverted light microscope after 24 hours of incubation for cytotoxicity test of cancer cell HeLa in presence of pure kaolinite, and modified kaolinite with ZnSO₄ and FeSO₄ salts before and after calcination at 680°C.

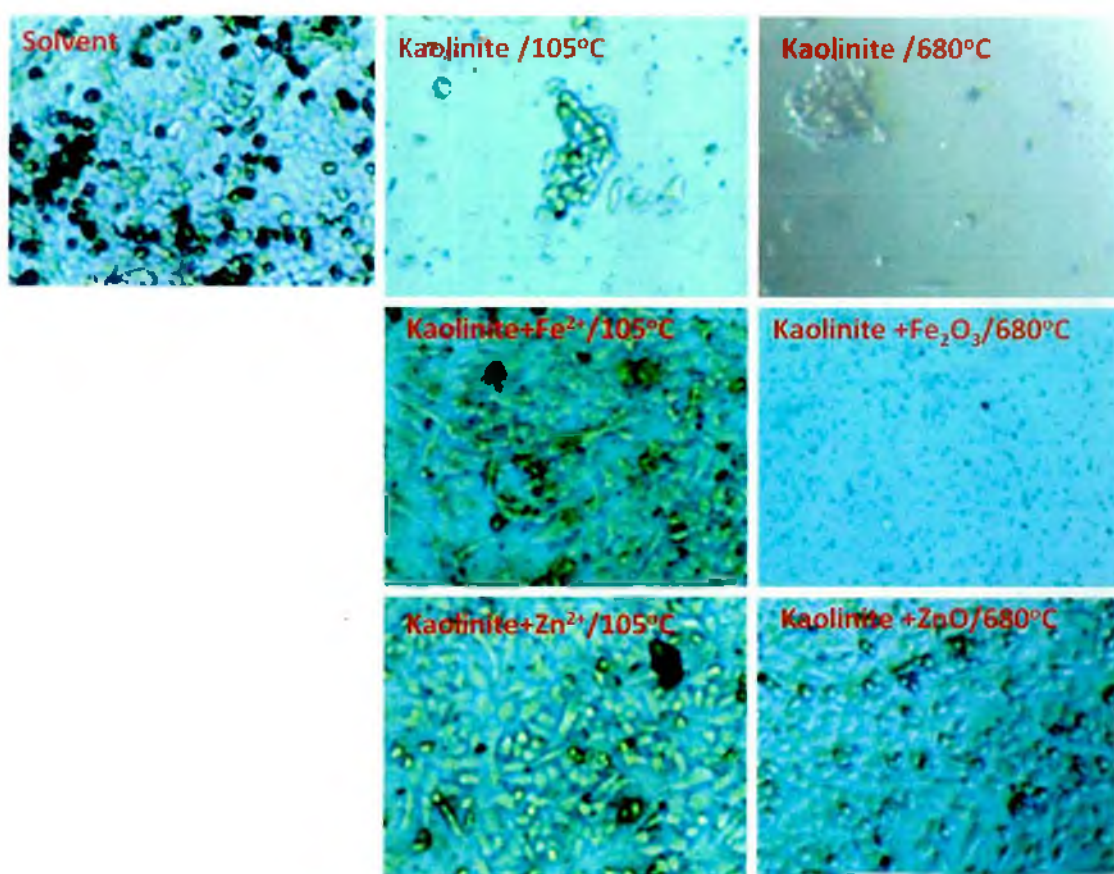


Figure 5.9: magnified images produced from the images originated from an inverted light microscope after 24 hours of incubation for cytotoxicity test of cancer cells HeLa in presence of pure kaolinite, and modified kaolinite with $ZnSO_4$ and $FeSO_4$ salts before and after calcination at $680^\circ C$.

3.9 Cytotoxic effect against BHK-21 cells

Similarly, Cytotoxic effects of kaolinite and modified kaolinite with two different salts of iron and zinc before and after calcination at $680^\circ C$ were investigated with varying the doses of particles. The **Table 5.4** shows that at low dose (125 mg) of unmodified (pure kaolinite) and modified kaolinite were not sufficient to inhibit the survival of BHK-21 cell. Only about 20-30% cell was destroyed, when pure kaolinite and zinc salt modified kaolinite was used. As the quantity of particles increased, the percentage survival of cell was decreased significantly, especially for pure kaolinite and iron salt modified kaolinite after calcination. When 250 mg of

particles was applied only 70-80% of cell was destroyed but about 90% cell was destroyed for 500 mg which indicates the critical concentration of particles to prevent the growth of BHK-21 cell. It is evident that the particles produced from modified kaolinite with iron salt at 680°C calcination showed the highest toxicity against BHK-21 when 500 mg was used.

Table 5.4: Effect of concentration of kaolinite and modified kaolinite on percentage of BHK-21 Cell survival.

Name	Amount of sample		
	125 mg	250 mg	500 mg
	% BHK-21 Cell survival		
Kaolinite/105°C	60-70	20	10-20
Kaolinite 680°C	>90	60-70	10-20
Kaolinite +Fe ²⁺ /105°C	>90	70-80	70
Kaolinite+Fe ₂ O ₃ /680°C	>90	20-30	10
Kaolinite +Zn ²⁺ /105°C	70-80	>95	70
Kaolinite+ZnO/680°C	70-80	>95	70

Figure 5.10 and **Figure 5.11** show the images originated under an inverted light microscope when the BHK-21 cell was treated with solvent (+) and 500 mg of the particles with two different magnifications respectively. When the cell was washed with solvent, the growth of cell and survival was nearly 100% which was considered as controlled experiment. As the cell treated with 500 mg pure kaolinite, the survival was 10-20% which is reflected from the nearly rough images recorded from microscope. Interestingly, calcinated particles produced from modified kaolinite with iron salt showed excellent performance for 500 mg results an almost destroyed and rough picture.

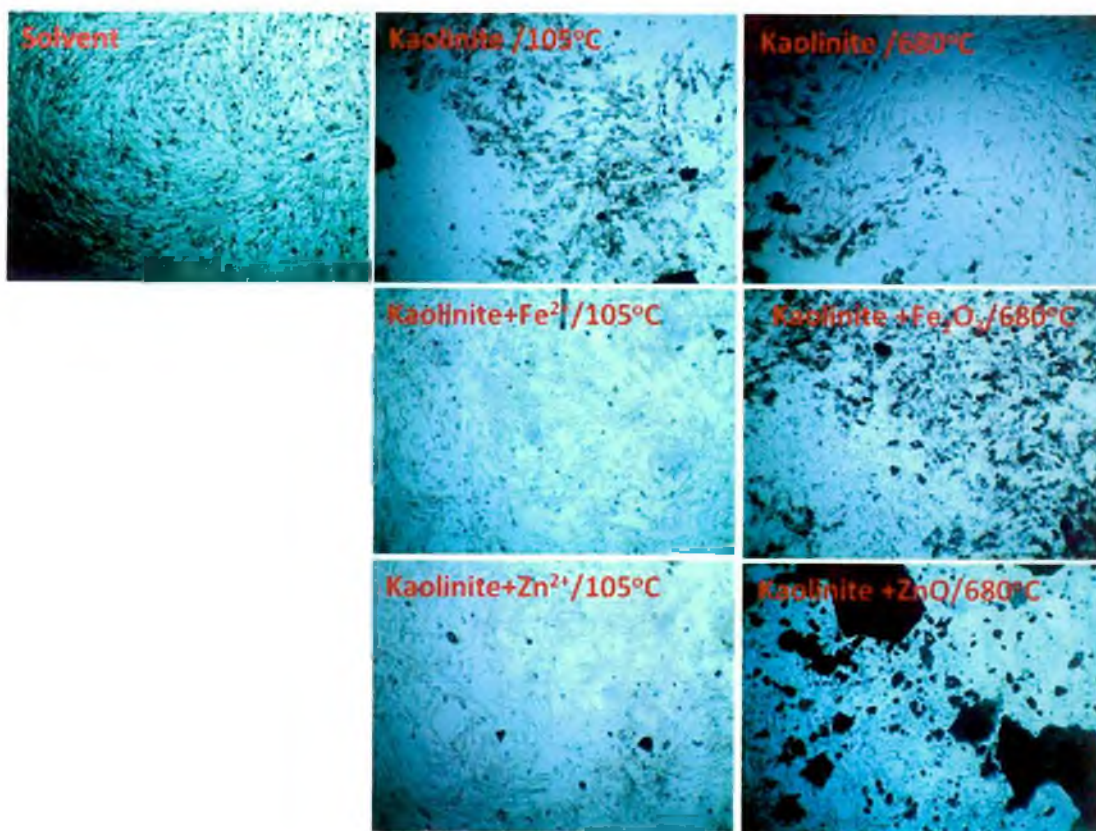


Figure 5.10: Images recorded from an inverted light microscope after 24 hours of incubation for cytotoxicity test of cancer cell BHK-21 in presence of pure kaolinite, and modified kaolinite with ZnSO_4 and FeSO_4 salts before and after calcination at 680°C .

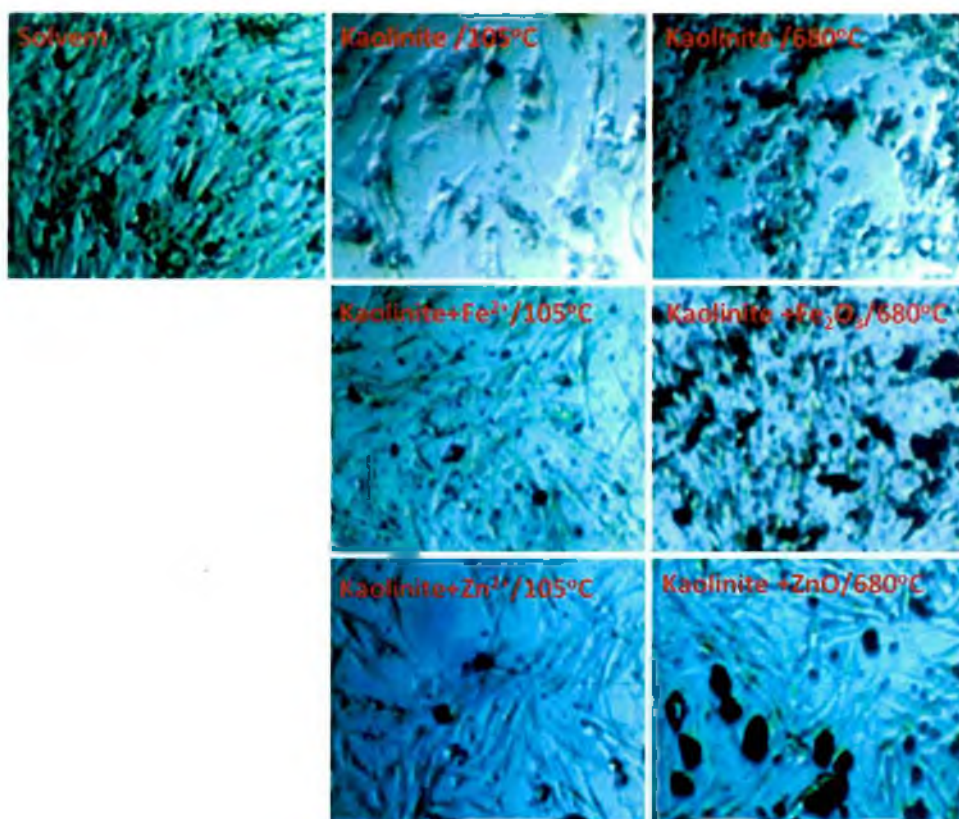


Figure 5.11: Magnified images produced from the images originated from an inverted light microscope after 24 hours of incubation for cytotoxicity test of cancer cell BHK-21 in presence of pure kaolinite, and modified kaolinite with $ZnSO_4$ and $FeSO_4$ salts before and after calcination at $680^\circ C$.

Conclusion: A very simple blending method with saturated salt solution and kaolinite has been developed to prepare cationically (Zn^{++} and Fe^{++}) modified kaolinite composites (CMKC). Calcination of CMKC at $680^{\circ}C$ produced metal oxides (ZnO and Fe_2O_3) doped kaolinite nanocomposites. Energy Dispersive X-Ray spectrophotometer (EDS) reveals the presence of metal oxides on the surface of kaolinite moieties. XRD pattern reflects there was little intercalation between cations and the kaolinite sheets. All fabricated particles showed better antimicrobial activity against *Escherichia coli* (gram negative bacteria) than virgin kaolinite. The activity 2-2.5 folds higher of synthesized particles against *Pseudomonas aeruginosa* offers in the real life application. Kaolinite would be a promising candidate to destroy the HeLa and BHK-21 cells, which would be more effective after treating iron salt. This simple technology would play a vital role to bring a breakthrough in nano medication in the field of nanoscience and technology.

References

1. Cai, Qian, Yangyang Gao, Tianyi Gao, Shi Lan, Oudjaniyobi Simalou, Xinyue Zhou, Yanling Zhang, Chokto Harnood, Ge Gao, and Alideertu Dong. "Insight into biological effects of zinc oxide nanoflowers on bacteria: why morphology matters." *ACS applied materials & interfaces* 8, no. 16 (2016): 10109-10120.
2. Applerot, Guy, Jonathan Lellouche, Anat Lipovsky, Yeshayahu Nitzan, Rachel Lubart, Aharon Gedanken, and Ehud Banin. "Understanding the antibacterial mechanism of CuO nanoparticles: revealing the route of induced oxidative stress." *Small* 8, no. 21 (2012): 3326-3337.
3. Sun, Liang, Ying Qin, Qingqing Cao, Bingqing Hu, Zhiwei Huang, Ling Ye, and Xingfu Tang. "Novel photocatalytic antibacterial activity of TiO₂ microspheres exposing 100% reactive {111} facets." *Chemical Communications* 47, no. 47 (2011): 12628-12630.
4. Campoccia, Davide, Lucio Montanaro, and Carla Renata Arciola. "A review of the biomaterials technologies for infection-resistant surfaces." *Biomaterials* 34, no. 34 (2013): 8533-8554.
5. Wang, Linlin, Chen Hu, and Longquan Shao. "The antimicrobial activity of nanoparticles: present situation and prospects for the future." *International journal of nanomedicine* 12 (2017): 1227.
6. Durmus, Naside G., Erik N. Taylor, Kim M. Kummer, and Thomas J. Webster. "Enhanced efficacy of superparamagnetic iron oxide nanoparticles against antibiotic-resistant biofilms in the presence of metabolites." *Advanced Materials* 25, no. 40 (2013): 5706-5713.
7. Deng, Can-Hui, Ji-Lai Gong, Guang-Ming Zeng, Cheng-Gang Niu, Qiu-Ya Niu, Wei Zhang, and Hong-Yu Liu. "Inactivation performance and mechanism of *Escherichia coli* in aqueous system exposed to iron oxide loaded graphene nanocomposites." *Journal of hazardous materials* 276 (2014): 66-76.
8. Yang, Ce, Jiajia Wu, and Yanglong Hou. "Fe₃O₄ nanostructures: synthesis, growth mechanism, properties and applications." *Chemical Communications* 47, no. 18 (2011): 5130-5141.
9. Behera, Sudhanshu Shekhar, Jayanta Kumar Patra, Krishna Pramanik, Niladri Panda, and Hrudayanath Thatoi. "Characterization and evaluation of antibacterial activities of chemically synthesized iron oxide nanoparticles." (2012).
10. Raghupathi, Krishna R., Ranjit T. Koodali, and Adhar C. Manna. "Size-dependent bacterial growth inhibition and mechanism of antibacterial activity of zinc oxide nanoparticles." *Langmuir* 27, no. 7 (2011): 4020-4028.
11. Simon-Deckers, Angelique, Sylvain Loo, Martine Mayne-L'hermite, Nathalie Herlin-Boime, Nicolas Menguy, Cecile Reynaud, Barbara Gouget, and Marie Carriere. "Size-, composition- and shape-dependent toxicological impact of metal oxide nanoparticles and carbon nanotubes toward bacteria." *Environmental science & technology* 43, no. 21 (2009): 8423-8429.
12. Li, Yang, Wen Zhang, Junfeng Niu, and Yongsheng Chen. "Mechanism of photogenerated reactive oxygen species and correlation with the antibacterial

- properties of engineered metal-oxide nanoparticles." *ACS nano* 6, no. 6 (2012): 5164-5173.
- 13 Lv, Min, Shao Su, Yao He, Qing Huang, Wenbing Hu, Di Li, Chunhai Fan, and Shuitong Lee. "Long-Term Antimicrobial Effect of Silicon Nanowires Decorated with Silver Nanoparticles." *Advanced Materials* 22, no. 48 (2010): 5463-5467.
 - 14 Y. Zhou, X. Jiang, T. Jia, Y. Su, P. Fei, Y. Lu, P. Rui and H. Yao, *J. Phy. Chem. B*, 2014, 2, 691-697.
 - 15 Gao, Nan, Yingjie Chen, and Jiang Jiang. "Ag@ Fe₂O₃-GO nanocomposites prepared by a phase transfer method with long-term antibacterial property." *ACS applied materials & interfaces* 5, no. 21 (2013): 11307-11314.
 - 16 Lin, Jiang-Jen, Wen-Chun Lin, Shing-Da Li, Cheng-Yen Lin, and Shan-hui Hsu. "Evaluation of the antibacterial activity and biocompatibility for silver nanoparticles immobilized on nano silicate platelets." *ACS applied materials & interfaces* 5, no. 2 (2013): 433-443.
 - 17 Li, Xiaoyu, Jing Ouyang, Huaming Yang, and Shi Chang. "Chitosan modified halloysite nanotubes as emerging porous microspheres for drug carrier." *Applied Clay Science* 126 (2016): 306-312.
 - 18 Peng, Kang, Liangjie Fu, Huaming Yang, and Jing Ouyang. "Perovskite LaFeO₃/montmorillonite nanocomposites: synthesis, interface characteristics and enhanced photocatalytic activity." *Scientific reports* 6 (2016): 19723.
 - 19 Peng, Kang, Liangjie Fu, Jing Ouyang, and Huaming Yang. "Emerging parallel dual 2D composites: natural clay mineral hybridizing MoS₂ and interfacial structure." *Advanced Functional Materials* 26, no. 16 (2016): 2666-2675.
 - 20 Zhang, Yi, Aidong Tang, Huaming Yang, and Jing Ouyang. "Applications and interfaces of halloysite nanocomposites." *Applied Clay Science* 119 (2016): 8-17.
 - 21 Huo, Chengli, and Huaming Yang. "Synthesis and characterization of ZnO/palygorskite." *Applied Clay Science* 50, no. 3 (2010): 362-366.
 - 22 Hu, Peiwei, and Huaming Yang. "Insight into the physicochemical aspects of kaolins with different morphologies." *Applied Clay Science* 74 (2013): 58-65.
 - 23 Y. Zhang, M. Long, P. Huang, H. Yang, S. Chang, Y. Hu, A. Tang and L. Mao, *Sci. Rep.*, 2016, 6, 3335.
 - 24 Kibanova, Daria, Martin Trejo, Hugo Destailhats, and Javiera Cervini-Silva. "Synthesis of hectorite-TiO₂ and kaolinite-TiO₂ nanocomposites with photocatalytic activity for the degradation of model air pollutants." *Applied Clay Science* 42, no. 3-4 (2009): 563-568.
 - 25 Koči, Kamila, Vlastimil Matějka, Pavel Kovář, Zdenek Lacný, and Lucie Obalová. "Comparison of the pure TiO₂ and kaolinite/TiO₂ composite as catalyst for CO₂ photocatalytic reduction." *Catalysis Today* 161, no. 1 (2011): 105-109.
 - 26 Sharma, Deepali, Md Ashaduzzaman, Mohsen Golabi, Amritanshu Shrivastav, Krishna Bisetty, and Ashutosh Tiwari. "Studies on bacterial proteins corona interaction with saponin imprinted ZnO nanohoneycombs and their toxic responses." *ACS applied materials & interfaces* 7, no. 43 (2015): 23848-23856.
 - 27 DĚDKOVÁ, Kateřina, Pavlína PEIKERTOVÁ, Kateřina MATĚJOVÁ, Jaroslav LANG, and Jana KUKUTSCHOVÁ. "STUDY OF THE ANTIBACTERIAL ACTIVITY OF COMPOSITES KAOLINITE/TiO₂." *Nanocon 2012*.

- 28 Jiao, Lefei, Fanghui Lin, Shuting Cao, Chunchun Wang, Huan Wu, Miaoan Shu, and Caihong Hu. "Preparation, characterization, antimicrobial and cytotoxicity studies of copper/zinc-loaded montmorillonite." *Journal of animal science and biotechnology* 8, no. 1 (2017): 27.
- 29 Liao, Hsin-Tzu, and Chin-San Wu. "Synthesis and characterization of polyethylene-octene elastomer/clay/biodegradable starch nanocomposites." *Journal of applied polymer science* 97, no. 1 (2005): 397-404.
- 30 Holešová, Sylva, Marianna Hundáková, and Erich Pazdziora. "Antibacterial kaolinite based nanocomposites." *Procedia Materials Science* 12 (2016): 124-129.
- 31 Liu, Shaobin, Tingying Helen Zeng, Mario Hofmann, Ehdi Burcombe, Jun Wei, Rongrong Jiang, Jing Kong, and Yuan Chen. "Antibacterial activity of graphite, graphite oxide, graphene oxide, and reduced graphene oxide: membrane and oxidative stress." *ACS nano* 5, no. 9 (2011): 6971-6980.
- 32 Akhavan, Omid, and Elham Ghaderi. "Toxicity of graphene and graphene oxide nanowalls against bacteria." *ACS nano* 4, no. 10 (2010): 5731-5736.
- 33 Kang, Seoktae, Moshe Herzberg, Debora F. Rodrigues, and Menachem Elimelech. "Antibacterial effects of carbon nanotubes: size does matter!" *Langmuir* 24, no. 13 (2008): 6409-6413.
- 34 Nel, Andre, Tian Xia, Lutz Madler, and Ning Li. "Toxic potential of materials at the nanolevel." *science* 311, no. 5761 (2006): 622-627.
- 35 Park, Eun-Jung, Jinhee Choi, Young-Kwon Park, and Kwangsik Park. "Oxidative stress induced by cerium oxide nanoparticles in cultured BEAS-2B cells." *Toxicology* 245, no. 1-2 (2008): 90-100.
- 36 Foster, K. A. "Galeffi F, Gerich FJ, Turner DA, Müller M." *Optical and pharmacological tools to investigate the role of mitochondria during oxidative stress and neurodegeneration. Prog Neurobiol* 79 (2006): 136-171.
- 37 Ott, Martin, Vladimir Gogvadze, Sten Orrenius, and Boris Zhivotovsky. "Mitochondria, oxidative stress and cell death." *Apoptosis* 12, no. 5 (2007): 913-922.
- 38 Valko, Marian, CJB Rhodes, Jan Moncol, M. M. Izakovic, and Milan Mazur. "Free radicals, metals and antioxidants in oxidative stress-induced cancer." *Chemico-biological interactions* 160, no. 1 (2006): 1-40.

Conclusion

This research strongly demonstrates technological features of nanostructured layered kaolinite for fabricating valuable industrial composite materials using very simple and cost-effective techniques.

1. At first, we have successfully prepared nano-composite films of kaolinite dispersed and self-assembled into starch biopolymer. ATR-IR spectrum shows the presence of the functional groups of starch and kaolinite in the nanocomposite films. The self-assembled nanocomposite film produced from 15% w/w kaolinite and starch exhibited moderate mechanical strength (stress 6.3 MPa) at break but showed the highest workable mechanical strength (stress 4.3 MPa) within the area of modulus of resilience. Thermal stability of composites were increased with the addition of kaolinite but the optimum stability was found for K₁₅SNC film with $T_{Onset} = 280^{\circ}\text{C}$, maximum rate of decomposition $R_{max} = 30 (\mu\text{g}/^{\circ}\text{C})$ and $T_{peak} = 314^{\circ}\text{C}$. Contraction of all K₍₅₋₂₀₎SNC nanocomposite films at around 95°C were found lower in magnitude compared to K₀SNC film. SEM images proved that the nanofiller kaolin reduces the porosity of the film and the minimum number of pore was envisaged in the K₁₅SNC film. Such nanocomposite advanced materials produced from starch biopolymer and indigenous layered materials would play crucial role in the field of nanoscience and technology.
2. Secondly, a self-standing and porous composite bed of kaolinite and choline chloride was synthesized with 1:1 w/w ratio of the constituents. Choline chloride and kaolinite had a chemical interaction with each other as determined through XRD and FTIR. The bed was highly efficient in removing RR dye from its aqueous solution. A 20 ppm aqueous solution at pH 11.7 was treated with the composite bed and the efficiency of dye removal was measured. It was found that the bed removed the dye from its solution with 100% efficiency. Due to the readiness of the dye removal at 20 ppm concentration by the composite bed, all the dye was removed by the surface of the bed and the bulk of the bed

was not required to participate in the process. Hence, we found that the dye removal for this particular concentration was independent of bed thickness. Thus, we believe a competent bed for dye removal such as this would go a long way in answering the long lasting issues of water pollution due to textile industrial waste effluents.

3. Later, self-assembled choline chloride modified kaolinite (CCMK) and polymethyl methacrylate (PMMA) nanocomposite films were fabricated by a simple casting method. Nanocomposites showed higher thermal stability, tensile strength and reduced elongation percentages at breaking points compared to those of neat PMMA film. Among the films, CK₅PNC showed the best mechanical properties. The film of CK₅PNC showed an optimum tensile strength of 31 N/mm² and about 0.60% strain at yield, which indicates, the film exhibited maximum elasticity with remarkable load bearing capacity. Although CK₁₀PNC film showed the highest tensile strength (33 N/mm²), the film also exhibited the lowest strain (0.20%). The percentage of elongation at break of nanocomposite films decreased with the increase of CCMK. Furthermore, thermal stability of CK₅PNC film was found almost similar to that of CK₁₀PNC film. Scanning electron microscopy images of CK₅PNC film showed a homogeneously distributed kaolinite smooth surface. The nanocomposite films created from modified indigenously layered material and lipophilic synthetic polymer could play important role in the field of packaging industry, and would be economical if applied in nanoscience and nanotechnology.
4. Finally, a very simple blending method with saturated salt solution and kaolinite has been developed to prepare cationically (Zn⁺⁺ and Fe⁺⁺) modified kaolinite composites (CMKC). Calcination of CMKC at 680°C produced metal oxides (ZnO and Fe₂O₃) doped kaolinite nanocomposites. Energy Dispersive X-Ray spectrophotometer (EDS) reveals the presence of metal oxides on the surface of kaolinite moieties. XRD pattern reflects there was little intercalation between cations and the kaolinite sheets. All fabricated particles showed better antimicrobial activity against *Escherichia coli* (gram negative bacteria) than virgin kaolinite. The activity 2-2.5 folds higher of synthesized particles against *Pseudomonas aeruginosa* offers in the real life application. Kaolinite would be a promising candidate to destroy the HeLa and BHK-21 cells, which would be more

effective after treating iron salt. This simple technology would play a vital role to bring a breakthrough in nano medication in the field of nanoscience and technology.

After thorough research with indigenous nanostructured layered kaolinite (Bijoypur clay), we come to conclude that these materials offer several technological advantages over other available synthetic nanoparticles and therefore should receive more attention from material scientist throughout the globe for designing environment friendly composite materials for ensuring sustainable and green environment.

List of Publications from This Research

Journal Publications

1. **Dipti Saha**, Mithun Kumar Majumdar, Ajoy Kumar Das, A. M. Chowdhury, Md Ashaduzzaman*. Structural Nanocomposite Fabrication from Self-Assembled Choline Chloride Modified Kaolinite into Poly (Methylmethacrylate). *Journal of Composites Science*, 3 (3) 2019, 83.
2. Afroza Alam, **Dipti Saha**, Muhammad Mominur Rahman, Shaikat Chandra Dey, Md. Ashaduzzaman*, A Novel Self-Standing Porous Composite Bed of Kaolinite-Choline Chloride for Efficient Removal of Anionic Azo Dyes from Aqueous Solutions (Submitted).

Conference Presentations

1. **Dipti Saha**, Mithun Kumar Majumder, Ajoy Kumar Das, A. M. Sarwaruddin Chowdhury, Md. Ashaduzzaman*, Fabrication of Nanocomposites Film from Choline Chloride Modified Kaolinite and Poly(methylmethacrylate), *International Conference on Material Science and Semiconductor Devices*, September (07-08), 2018, University of Dhaka, Bangladesh.
2. **Dipti Saha**, A. M. Sarwaruddin Chowdhury, Ajoy Kumar Das, Md. Ashaduzzaman*, Mechanical Properties Exploration of Fabricated Environment Friendly Starch-Kaolinite Self-Assembled Nanocomposite Films, *1st International Conference on Innovation in Engineering and Technology*, December (27-28), University of Dhaka, Bangladesh.

Biography



Professor Dipti Saha

Dipti Saha is a full-time professor and researcher in the Department of Applied Chemistry and Chemical Engineering at University of Dhaka, the most prestigious academic institution in Bangladesh. She was born in 1966 in Narayangongj. Dipti Saha passed secondary school certificate (SSC) examination from Narayangonj Govt. Girls' High School in 1981 and higher secondary certificate (HSC) examination from Narayangonj Govt. Tolarum College in 1983. She successfully completed her B.Sc. in 1990 and M.Sc. in 1992 in Applied Chemistry and Chemical Technology, obtaining **first class first position** in both. After finishing her M.Sc., she joined the department as a lecturer the following year, in 1993. Since then she has been actively involved in teaching and research. After being appointed as department chair in February, 2019, she has been making countless effort to improve the academic, research, and extracurricular standard of her institution. Under her prudent leadership, the department has been making rapid success.

Professor Saha has been an active and prominent researcher in the field of nanocomposites and petrochemical synthesis. She has published **63** research papers in various peer-reviewed national and international journals to date. Her current work mainly focuses on nanocomposite synthesis and their biological and environmental application. She has also done a vast amount research on the synthesis of some industrially important petrochemicals by the alkylolation process and has developed various mathematical models.

Professor Saha has successfully defended her PhD thesis on **Composites of Indigenous Nanostructured Layered Materials** under the supervision of Professor Dr. Md. Ashaduzzaman. She has presented the output of this research in two international conferences. Besides, she has published on article from this research in **Journal of Composites Science** as a first author.

Professor Dipti Saha now looks forward to excelling further in relevant research fields.